

**USE OF SNPS WITH CONTROLLED SIZE &
SHAPE FOR ENHANCED SURFACE
HYDROPHOBICITY & HARDNESS FOR COIL
COATING APPLICATIONS**

**A Thesis Submitted to
the Graduate School
İzmir Institute of Technology
in Partial Fulfillment of the Requirements for the Degree of**

MASTER OF SCIENCE

in Chemical Engineering

**by
Şevval SULUBAŞ**

**June 2023
İZMİR**

We approve the thesis of **Şevval SULUBAŞ**

Examining Committee Members:

Prof. Dr. Mehmet POLAT

Department of Chemical Engineering, Izmir Institute of Technology

Assoc. Prof. Dr. Canan URAZ

Department of Chemical Engineering, Ege University

Assoc. Prof. Nermin Seda KEHR

Department of Chemistry, Izmir Institute of Technology

21 June 2023

Prof. Dr. Mehmet POLAT

Supervisor, Department of Chemical
Engineering, Izmir Institute of Technology

Prof. Dr. Hürriyet POLAT

Co-Supervisor, Department of
Chemistry, Izmir Institute of
Technology

Prof. Dr. Erol ŞEKER

Head of the Department of Chemical
Engineering, Izmir Institute of Technology

Prof. Dr. Mustafa DEMİR

Dean of Graduate School of
Engineering and Sciences

ACKNOWLEDGEMENT

First and foremost, I would like to express my deepest gratitude to my advisors, *Prof. Dr. Mehmet POLAT* and *Prof. Dr. Hürriyet POLAT*, for their support, guidance, motivation, patience, confidence and encouragement throughout my thesis study. Your unique outlook on life has enriched my research and allowed me to explore new dimensions of knowledge. I could not have imagined having better mentors.

Secondly, I would like to express my sincere gratitude to AkzoNobel Kemipol for their invaluable support and resources throughout this project. I am deeply grateful for their collaboration and partnership, which significantly enhanced the quality and impact of my work. I warmly express my special thanks to my dear colleagues *İlkin Ece ALTAŞ*, *Cemre KOCAHAKİMOĞLU*, *Yağız UYSAL*, *Hakan AYYILDIZ*, and *Ecem TARANCI* for their endless friendship, motivation, and support during writing of my thesis. They really became very close to my heart by their love and care. Also, I am really thankful to my coil labmates, especially to *Ender KARA* and *Gülçin KOŞAN* for their support and contributions during my experiments.

I should open a special parenthesis for my IZTECH labmates; *Cansu ÜNLÜ*, *Hazal PAKER*, *Tuğçe GÜLİYEV* and *Esra Sıla GÜNDÜZ* for their valuable contributions. Also, I also thank to my dear friends *Anıl KAHVECİOĞLU*, *Cansu GÜLER*, and *SU ERSÖZ* for being part of LCDP. I would like to thank to *Mutlu Devran YAMAN*, *Zehra Sinem YILMAZ*, *Adem YAVUZ* and *Mine BAHÇECİ* for endless diligent hours they spent for me for the SEM, AFM analyses carried out in the Material Research and Development Center of IZTECH.

I am deeply grateful to my friend *Simge BAHÇEVANCI* for her support, despite being 4000 km away. Your constant presence and unwavering understanding have been invaluable to me. I sincerely appreciate the unconditional support you have provided in every aspect of my life. Your friendship means the world to me, and I am truly thankful for it.

My deepest gratefulness goes to my family; *Meltem SULUBAŞ*, *Vasfi SULUBAŞ* and *Murat SULUBAŞ* for their endless support, limitless love and motivation during my educational life. I feel very lucky to have you.

ABSTRACT

USE OF SNPs WITH CONTROLLED SIZE & SHAPE FOR ENHANCED SURFACE HYDROPHOBICITY & HARDNESS FOR COIL COATING APPLICATIONS

Increasing the hardness of surface while improving hydrophobicity simultaneously has important implications in coating applications. The use of nano sized particles for this purpose is an interesting area of research. SNPs with mono and multi size distributions in a wide size range were successfully synthesized using the Stöber Method directly or after proper modifications such as utilizing seed particles as in Stöber growth solutions.

The synthesized monosize and bi-modal silica particles were then employed in coating studies. The silica nanoparticles were added to a clear coat without pigments and fillers, followed by the introduction of a pigmented topcoat. The addition of 25% monosize silica nanoparticles led to a contact angle (CA) of 92°, while an equal amount of bi-modal silica particles increased the CA to 106°. Notably, the highest CA value of 116.7° was achieved with a 40% addition of bi-modal silica particles. When measured CA was converted to actual CA by incorporating the roughness parameter, the maximum effective CA was calculated as 140°.

In terms of mechanical properties, loading monosize silica nanoparticles up to 35% resulted in a surface hardness of 2H. Further increasing the loading to 45% improved the surface hardness to 3H. While a 40% addition of monosize silica was necessary to achieve a pencil hardness of 3H, 20% addition of bi-modal sample was sufficient. The findings above demonstrate that addition of nanosized silica particles simultaneously improve hardness and surface hydrophobicity and that a bi-modal particle size distribution results in a superior performance compared to mono-modal particle size distribution.

ÖZET

BOBİN BOYA UYGULAMALARINDA YÜZEY HİDROFOBİKLIĞI VE SERTLİĞİNİ ARTTIRMAK İÇİN KONTROLLÜ BOYUT VE ŞEKİLLERDEKİ SİLİKA NANO PARÇACIKLARIN KULLANILMASI

Hidrofobikliği geliştirirken aynı anda yüzeyin sertliğini arttırmanın boya uygulamalarında önemli etkileri vardır. Bu amaçla nano boyutlu parçacıkların kullanılması ilginç bir araştırma alanıdır. Geniş bir boyut aralığında tek ve çok boyutlu dağılımlara sahip SNP'ler, doğrudan Stöber Metodu kullanılarak veya Stöber büyüme solüsyonlarında olduğu gibi tohum partiküllerinin kullanılması gibi uygun modifikasyonlardan sonra başarıyla sentezlendi.

Sentezlenen tek boyutlu ve iki boyutlu silika parçacıkları daha sonra boya çalışmalarında kullanılmıştır. Silika nanopartiküller, pigmentler ve dolgu maddeleri içermeyen vernik boyasına ilave edildi, ardından pigmentli bir sonkat boyaya eklendi. %25 tek boyutlu silika nanoparçacıklarının eklenmesi, 92°'lik bir temas açısı verirken, eşit miktarda iki boyutlu silika parçacıklarının eklenmesi, temas açısını 106°'ye yükseltti. Özellikle, en yüksek temas açısı değeri olan 116.7°'ye, %40 iki boyutlu silika parçacıklarının eklenmesiyle ulaşılmıştır. Ölçülen temas açısı pürüzlülük parametresi dahil ederek gerçek temas açısına dönüştürüldüğünde, maksimum etkili temas açısı 140° olarak hesaplandı.

Mekanik özellikler açısından, tek boyutlu silika nanoparçacıklarının %35'e kadar yüklenmesi, 2H'lik bir yüzey sertliği ile sonuçlandı. Yüklemeyi %45'e daha da artırılması, yüzey sertliğini 3H'ye çıkardı. 3H kalem sertliği elde etmek için %40 tek boyutlu silika ilavesi gerekiyken, %20 iki boyutlu silika parçacık ilavesi yeterliydi. Yukarıdaki bulgular, nano boyutlu silika parçacıklarının eklenmesinin aynı anda sertliği ve yüzey hidrofobikliğini iyileştirdiğini ve iki boyutlu tane dağılımının, tek boyutlu tane dağılımına kıyasla üstün bir performansla sonuçlandığını göstermektedir.

TABLE OF CONTENTS

LIST OF FIGURES	viii
CHAPTER 1. INTRODUCTION	1
CHAPTER 2. LITERATURE SURVEY	4
2.1 Coatings/Coil Coatings	4
2.2 Surface Energy	7
2.2.1 Wettability & Hydrophobicity.....	9
2.2.2 Hydrophobicity in Nature.....	14
2.2.3 Fabrication of Hydrophobic Surfaces.....	16
2.3 Sol-Gel Synthesis of Silica-Stöber Method	17
2.3.1 Growth Mechanism of SNPs	20
2.3.2 Effect of Process Parameters on Stöber Synthesis	23
2.3.2.1 Precursors	23
2.3.3 Effect of Presence of Seed Particles	30
CHAPTER 3. MATERIALS AND METHOD.....	31
3.1 Materials.....	31
3.1.1 Synthesis of SNPs.....	31
3.1.2 Silica Added Coatings Studies	31
3.2 Methods.....	32
3.2.1 SNP Synthesis Using Stöber Method	33
3.2.2 SNP Synthesis by Seed Addition (Seeded Growth)	35
3.2.3 Coating Studies.....	42

CHAPTER 4. RESULT AND DISCUSSION	48
4.1 Characterization of Stöber Silica SNPs.....	48
4.1.1 Effect of TEOS Concentration	51
4.1.2 Effect of TEOS & Other Components Concentrations	54
4.1.3 Seed Addition (Seeded Growth).....	58
4.2 Coating Studies	84
4.2.1 Monosize Silica-Added Coating Studies.....	84
4.2.2 Bi-modal Silica-Added Coating Studies	100
CHAPTER 5. CONCLUSION	109
REFERENCES	112

LIST OF FIGURES

<u>Figure</u>	<u>Page</u>
Figure 1. Curing methods in convective & NIR ovens (Tunçgenç, 2004)	6
Figure 2. Schematic diagram of coil coating line (Tunçgenç, 2004).....	6
Figure 3. Schematic diagram of interfacial tension in vapor/liquid/solid system (Wang et al. 2020).....	8
Figure 4. Schematic of the shape of a water drop and the water contact angle (WCA) for solid surfaces along a hydrophobicity-hydrophilicity gradient (Krasowska et al., 2009)	8
Figure 5. Good wettability (hydrophilic) (Yıldır et al., 2016)	9
Figure 6. Normal wettability (Yıldır et al., 2016).....	10
Figure 7. Poor wettability (hydrophobic) (Yıldır et al., 2016).....	10
Figure 8. Extremely poor wettability (super-hydrophobic) (Yıldır et al., 2016)	10
Figure 9. Different wetting states (Tunçgenç, 2004)	11
Figure 10. Schematic diagram of the relationship between equilibrium contact angle and interfacial tension in gas/liquid/solid system. (a) Young contact angle ($^{\circ}$), (b) Wenzel contact angle ($^{\circ}$), and (c) Cassie contact angle ($^{\circ}$), (Wang et al., 2020).....	12
Figure 11. Slowly pumping a liquid into or out of sessile droplet (Yıldır et al., 2016)	13
Figure 12. SEM images of superhydrophobic surfaces at low and high magnifications.... (a) and (b) lotus leaf with a 162° water contact angle; (c) and (d) rose petal with a 152.4° water contact angle (Krasowska et al., 2009)	15
Figure 13. Silica networking (Innocenzi, 2016)	19
Figure 14. Monomer addition and aggregation models (Hyde et al., 2016).....	22
Figure 15. Relative reaction rate vs pH (Rout, 2013).....	28
Figure 16. Flowsheet for the different seed and their growth solution, pulse addition ..	36
Figure 17. Flowsheet for the different seed and their growth solution, continuous addition	37
Figure 18. Flowsheet for the effect of TEOS amounts on growth solution.....	38
Figure 19. Flowsheet for effect of different seed amount and TEOS addition ratio	42
Figure 20. MEK test (Tunçgenç, 2004)	44

Figure 21. Impact Resistance Test (Tunçgenç, 2004)	44
Figure 22. T Bent Test, OT image (Tunçgenç, 2004)	45
Figure 23. Pencil Hardness Test (Tunçgenç, 2004).....	45
Figure 24. Adhesion Test Evaluation Specs (Tunçgenç, 2004).....	46
Figure 25. Particle Size Distribution of Stöber Silica Particles	49
Figure 26. Cumulative Volume (%) vs Size Classes (μm).....	50
Figure 27. The zeta potential of Stöber Silica Particles.....	51
Figure 28. Particle Size Distribution of bi-modal silica particles.....	81
Figure 29. Cumulative Volume (%) vs Size Classes (μm).....	81
Figure 30. The zeta potential of Bi-Modal Silica Particles.....	82
Figure 31. Cumulative Volume (%) vs Size Classes (μm) (Blue: monosize silica; green: bi-modal silica particles)Cumulative Volume (%) vs Size Classes (μm) (Blue: monosize silica; green: bi-modal silica particles)	83
Figure 32. FTIR spectrum of monosize and bi-modal silica particles (transmittance vs wavelength).....	83
Figure 33. Viscosity vs Shear Rate Graph (Black: Standard Clear Coat, Grey: 5% SNP added coating, red: 5% commercial silica added coating).....	85
Figure 34. Viscosity vs Shear Rate Graph (Black: Standard Clear Coat, Grey: 5% SNP added coating, red: 5% commercial silica added coating).....	86
Figure 35. Standard clear coat system (1), commercial silica added coating (2) and nanosilica added coating (3)	87
Figure 36. Viscosity vs Time Graph (Black: Standard Clear Coat, Grey: 1.2 % SNP	91
Figure 27. Standard clear coat system (1), commercial silica added coating (2) and nanosilica added coating (3)	92
Figure 38. Comparison of measured vs actual CA with respect to silica loading amount	98
Figure 39. Scratch resistance results of 25 % and 30 % monosize silica added sample	99
Figure 40. Standard clear coat (1), commercial silica added (2) and NSP added (3)...	101
Figure 41. Comparison of measured vs actual CA with respect to silica loading amount	104
Figure 42. Test sample of 5% commercial silica added	107

LIST OF TABLES

<u>Table</u>	<u>Page</u>
Table 1. Different properties of solvents (Malay et al., 2013).....	26
Table 2. Wet coating properties of polyester topcoat (Akzonobel Kemipol).....	32
Table 3. Effect of TEOS concentrations experimental values.....	34
Table 4. Effect of TEOS & Other Components Concentrations for Silica C.....	34
Table 5. Effect of TEOS & Other Components Concentrations for Silica D.....	35
Table 6. Different Seed Formulas.....	36
Table 7. Silica D and growth solution study.....	39
Table 8. Modified Silica D and growth solution study.....	39
Table 9. Seed: Silica C (Classic Stöber Method) and different growth solution studies	40
Table 10. Seed: Modified Silica C and different growth solution studies.....	40
Table 11. Seed from Stöber Method and its growth solution.....	41
Table 12. Coating application values.....	43
Table 13. SEM images of SNPs with different batches after 2 and 24 hours of synthesis	48
Table 14. Particle Size Distribution and Specific Surface Area of SPNs.....	50
Table 15. SEM images of SNPs with different TEOS amounts (M) after 2 and 24 h....	52
Table 16. SEM images of SNPs with different concentration (M) combinations after 2 h	55
Table 17. SEM images of SNPs with different concentration (M) combinations after 2 h	57
Table 18. Effect of using silica D as seed and their different growth solutions.....	60
Table 19. Seed synthesis by using 1 M TEOS & 1.75 M TEOS in growth solutions	61
Table 20. Seed synthesis by using 0.5 M TEOS and their different growth solutions ...	63
Table 21. Seed Silica D and covering with same formula, pulse TEOS 0.5 M addition	65
Table 22. Seed: doubled amount of TEOS and EtOH in Silica D and covering with	66
Table 23. Seed: Silica C and their different growth solutions.....	68
Table 24. Doubled amount of TEOS and water in Silica C and their different growths	70
Table 25. Seed Stock Stability Control SEM images.....	73

Table 26. Using 150 mg seed and 0.25 M TEOS added at a rate of 0.7 ml/min for growth solution	75
Table 27. After 4h and 24h of started reaction SEM images of silica particles by using 75 mg seed with different TEOS &EtOH (1/10) addition rates	77
Table 28. After 24h of started reaction SEM images of silica particles by using 150 mg seed with different TEOS &EtOH (1/10) addition rates	79
Table 29. SEM images of 100 ml and 1.5 L total solution with 150 mg seed and 8 ml/min TEOS & EtOH addition rate	80
Table 30. Particle Size Distribution and Specific Surface Area of SPNs.....	82
Table 31. AFM results of 5% of commercial and 5% of SNP added coated film.....	88
Table 32. SEM Images of 5% commercial and SNPs added samples.....	89
Table 33. Roughness parameters and Contact Angle Measurements for blank, 5% commercial silica and 5% SNPs added coating	90
Table 34. AFM results of 1.2 % monosize SNP and 1.2 % commercial silica added coating	93
Table 35. SEM images different % of monosize SNPs added coating film.....	94
Table 36. Contact Angle value of monosize SNPs added both 10 μm and 20 μm films	96
Table 37. Roughness parameter, Measured and Actual Contact Angle	97
Table 38. Results of pencil hardness of monosize SNPs added coating.....	99
Table 39. AFM and SEM images different % of bi-modal SNPs added coating film..	101
Table 40. Contact Angle value of bi-modal SNPs added both 20 μm and 10 μm films	102
Table 41. Roughness parameter, Measured and Actual Contact Angle	103
Table 42. Results of pencil hardness of bi-modal SNPs added coating	105
Table 43. Results of MEK test of monosize SNPs added coating both 10 μm and 20 μm	106
Table 44. Result of scratch test for standard and 40% bi-modal silica added samples	108

CHAPTER 1

INTRODUCTION

Coil coated metal sheets are commonly used in construction, transportation, automotive, roofing, and domestic appliances owing to their superior corrosion resistance, weatherability, ductility and mechanical strengths compared to other materials such as ceramics and plastics. In addition to these advantages, the coil coating applications also offer decorative surfaces. The total film thickness in such coatings is generally 25 microns, leading fast curing times in the order of 20-40 seconds. Due to such advantages combined with significant energy saving, easy processability, and rapid production time, the coil coating has started to expand to diverse application areas in recent years. Such expansion, which was followed by increased competition, automatically necessitated a wider range of colours, surface textures and innovative functional properties. As a results, anti-bacterial and anti-microbial, digital printable, easy-to-slip, hard surface and self-cleaning coatings have been an intensive area of research and development (Sorce et al., 2019; Tunçgenç, 2004).

Surface hardness is an important property for many applications because it affects the coating's ability to resist wear, abrasion, and deformation. The hardness of a coating determines its ability to resist scratches, and other types of physical damage, which can compromise the integrity and longevity of the coating (Momber et al., 2020).

Hydrophobic coatings are also at the center of increasing interest. A hydrophobic coating can be defined as that leading to a surface with an effective contact angle (CA) value of greater than 90° . This is because hydrophobic surfaces possess unique self-cleaning and easy cleaning abilities as a result of their water repellent characteristics.

Self-cleaning coatings are typically super-hydrophobic, with a water contact angle greater than 150° . However, superhydrophobic (self-cleaning) coil coatings do not conform to the proper coil coating test standards due to curing conditions. The contact angle value, hence, the effectiveness and applicability of self-cleaning or easy-to-clean coatings, also depends on the roughness of the surface in addition to its chemical composition. Such surfaces with nano or micro scale protrusions exhibit high water repellence, causing water to form spherical droplets that roll away from the surface,

carrying dirt along with them. Consequently, there is a growing interest in such coating technologies due to their high potential in commercial products and their ability to reduce cleaning labour costs (Liu et al., 2017).

In addition to the easy-to-clean property, another major benefit of synthesizing a hydrophobic surface is the reduction in the corrosion rate of the metal substrate. This ability is crucial, similar to other self-cleaning properties, as metal corrosion is one of the most serious problems in current industrial development, causing significant economic losses and environmental pollution every year. Through surface modification, the contact area and exposure between the corrosive medium and the coating surface can be reduced, resulting in a decreased corrosion rate. Therefore, there is a growing demand for hydrophobic coatings that possess easy-to-clean ability and strong corrosion resistance by repelling water droplets (Liang et al., 2021; Tunçgenç, 2004).

Combining high hydrophobicity with improved surface hardness can have practical implications in various industries where both surface hardness and hydrophobicity are desirable. As stated, improving surface hydrophobicity offers the advantages with respect to water repellence, easy-to-clean properties, and decreased corrosion rate as summarized in the above paragraphs. Enhancing the surface hardness of coatings further results in increased resistance to wear, abrasion, and physical damage, thereby improving their overall durability. To investigate the overall performance of the coated surfaces with respect to surface hydrophobicity and hardness, as well as the relationship between these two properties, researchers employ various characterization techniques such as measuring contact angles and carrying out hardness tests.

This thesis aims to understand the impact of introducing mono and multisize (bimodal) silica particles on the hydrophobicity and surface hardness of coil coatings. The particles were manufactured using classic Stöber Method and its modified version where seed particles were added to the growth solution. Varying amounts of tetraethyl orthosilicate (TEOS) were used to determine optimal conditions for producing larger, well-formed spherical particles. Subsequently, the thesis explored the effect of introducing pre-manufactured Stöber seed particles to create larger or multi-sized silica particles at different seed particle sizes and amounts. TEOS amounts in the growth solution, and the rate of TEOS addition on the morphology and size of the resulting silica particles were also studied.

The silica particles synthesized was characterized using particle size distribution and zeta potential analysis. The findings of these analyses were checked using SEM

observations. The formed silica particles were incorporated into coil coatings, and the coated panels underwent into characterization test using SEM, AFM as well as contact angle measurements with water and mechanical tests such as scratch resistance, pencil hardness.

This thesis consists of 5 main chapters. In the first chapter, general information on coil coatings and the effect of hydrophobicity and surface hardness on coil coating properties is presented. Importance of integrating hydrophobicity and surface hardness in a coil coating application is also described. In the second chapter, a literature review is presented on hydrophobicity and sol gel synthesis (Stöber Method). Third chapter describes the materials, methods and experimental procedures employed in the studies. The fourth chapter presents the synthesis and characterization details of the manufactured particles along with the effect of addition of these particles into the recipe with respect to hydrophobicity and hardness. The final chapter gives summary conclusions based on the presented data.

CHAPTER 2

LITERATURE SURVEY

2.1 Coatings/Coil Coatings

Coatings are favourable substitutes for covering various materials such as plastics, metals, glass, and wood, primarily for decoration and protection purposes. They can be divided into two groups: organic and inorganic coatings, based on the chemical structure of the binder (Zeno et al.,2007). Organic coatings are the oldest and most preferred used method mainly for energy saving, reduced downtime, increased lifetime, capital saving, and materials substitution (Marrion, 2004). Organic coating formulas include a mixture of four chemical substances: resin (binder), volatile components, additives, and pigments. The basic mixing process occurs during the production of the organic coating. The first component, resin, binds the other substances together in the coating mixture to form a continuous film and adhere to the substrate. Secondly, volatile components (mostly water or solvent) adjust the viscosity of the coating and dissolve the binder and other additive components. When water is used as the volatile component, the coating is called waterborne, while if a solvent is used, the coating is called solvent-borne. In order to reduce volatile organic compound (VOC) emissions, waterborne coatings have become more preferable as higher-solids coatings to eliminate the use of solvents. The third component, additives, includes catalysts for polymerization reactions, dispersion stabilizers for long-term pigment stability, and anti-corrosion additives for corrosion protection. These additives are used in small quantities to develop specific properties in the coating. If a coating contains only binder, volatile components, and additives, it can be called clear coats or just clears. Since clear coats do not include pigments, they are examples of transparent varnishes and clear coats used in automobiles (Zeno et al.,2007). Lastly, pigments are insoluble particulate solids that are dispersed in the medium of the coating and remain suspended in the resin after film formation. In addition to providing color and opacity, pigments have a significant effect on film properties, such as durability, mechanical strength, and corrosion protection (Völz, 2001).

Coil coating is a method where metal sheets, usually made of steel or aluminium, are coated in a long and continuous process before being formed into the desired shape of the product. After being coated in high-speed lines, the metals are wrapped as a coil. Therefore, the method takes its name from the storage of the metal sheet in coils, both before and after the application of the coating. Coil-coated metal sheets have applications in almost every area of daily life, including industrial facilities, construction and buildings, domestic appliances, and more. Coil coating has become popular due to its flexible and broad application areas, offering several advantages, such as optimized efficient processes and cost reduction, in recent years (Tunçgenç, 2004).

Additionally, the ability to resist corrosion is necessary to protect metal facilities. With an understanding of the second law of thermodynamics, it is known that corrosion cannot be prevented, but the corrosion rate can be decreased according to the entropic principle. Furthermore, metal corrosion is one of the most serious problems during current industrial development, leading to significant economic losses every year. It has become a common concern for researchers to explore environmentally friendly methods to reduce metal corrosion. The corrosion process is typically caused by the contact between the substrate and the corrosive medium. Hydrophobic coatings have garnered worldwide attention due to their special characteristics, such as self-cleaning, easy-to-clean, anti-fogging, and anti-corrosion properties, suitable for various applications including paints, optical devices, windshields, and interior fabrics. By enhancing the hydrophobicity of the coil coating, the contact area between the matrix and the corrosive medium can be reduced, effectively preventing corrosion. Additionally, the self-cleaning and easy cleaning abilities of the metal surface can be improved (Liang et al., 2021).

The coil coating process includes curing and quenching processes. Coil coaters have two options: conventional and infrared ovens, for curing the coating to be applied to the metal. The preferred oven type varies according to the geopolitical region, taking into consideration electricity and natural gas consumption. The main difference between conventional and infrared ovens lies in the curing process. In the convection oven, heating starts from the metal, and curing continues from the metal to the outer surface. On the other hand, in an infrared oven, curing starts from the surface and continues towards the metal surface, as shown in Figure 1.

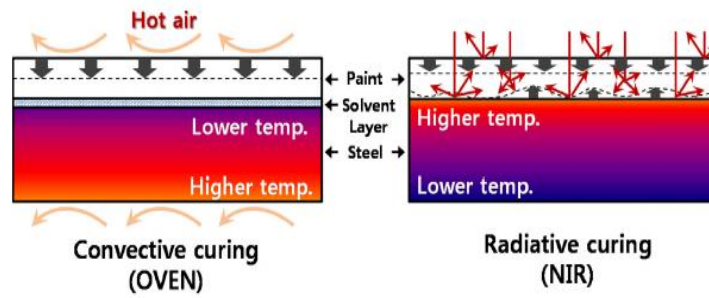


Figure 1. Curing methods in convective & NIR ovens (Tunçgenç, 2004)

Generally, a conventional oven is used in the coil coating sector since it allows for the production of a wider range of colour products. The conventional oven typically operates at temperatures between 300 and 500 °C, while line speeds vary between 20 and 200 m/min. Depending on the oven temperature and line speeds, the coated metals are exposed to heat. The coil coating process has a very fast curing time (20-30 seconds) and a thin coating layer, typically around 25 microns. In contrast to other coating sectors where options like brushing, spraying, and electrodeposition are used to apply the coating, rollers are utilized in the coil coating process. Figure 2 shows a schematic diagram of a coil-coating line, where it can be observed that the cleaning and surface treatment of the metal panel are also included within the continuous coil-coating process (Tunçgenç, 2004).

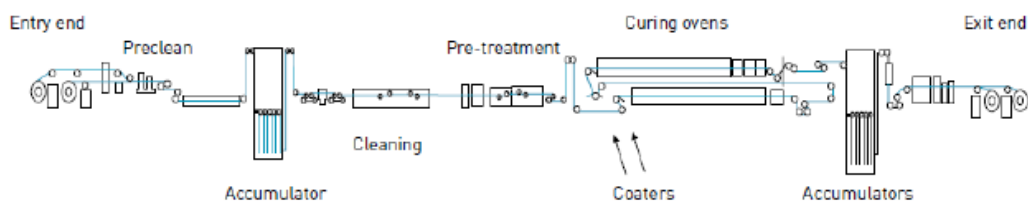


Figure 2. Schematic diagram of coil coating line (Tunçgenç, 2004)

Metals react with oxygen and moisture in the atmosphere, which can lead to the formation of rust on the surface. Therefore, metal surfaces are covered with oil, particulates, and oxide layers before the coating process. The cleaning and rinsing steps are the first ones in preparing the metals for coating, as they remove organic soil, particulates, oil, and oxide layers (Saarimaa et al., 2015). Afterward, the metals are ready

for the application of a conversion coating, which prevents the formation of oxide layers and provides an inert surface. This step is also known as the pre-treatment process. The chemical pre-treatment of the substrate plays an essential role in ensuring compatibility between the substrate and the applied organic coating, resulting in optimum adhesion and overall corrosion resistance (Hörnström et al., 1992).

2.2 Surface Energy

The bulk and surface properties of polymer materials determine their overall performance and potential applications. While bulk properties are important for structural applications, mainly concerning mechanical integrity and strength, surface properties play a critical role in determining overall performance, such as durability and application feasibility. This vital position is primarily due to the direct contact or interaction of the material surface with the surroundings. These interactions can involve physical and/or chemical processes, such as oxidation, degradation, corrosion, friction, abrasion, and wetting. Additionally, the surface of materials is particularly significant in many end-use applications, especially in the coating sector, in terms of touch, feel, shine, colour, and gloss differences (Yılıgör et al., 2016).

One of the most significant properties of solid surfaces in describing surface behaviour is the "surface energy" or "surface tension," which indicates the strength of intermolecular forces between polymer chains (van der Waals forces). Polar groups in the polymer chains lead to strong intermolecular forces and result in high surface energy. The polarity of these groups in the polymer chains can be optimized based on their size, electronic structure, and polarity. Surface energy is also one of the most useful parameters used to predict the wettability of polymer surfaces, which plays an important role in a wide range of practical applications in daily life, industry, and agriculture. Generally, the static contact angle between a polymer surface and a fluid droplet is measured to better understand the wetting behaviour of a polymer surface. It is known that polar fluids wet polar surfaces better than non-polar solvents and vice versa. A lower surface energy results in poor wetting and higher contact angle values (Nguyen-Tri et al., 2019). It is a strong indicator for describing the interfacial relationships between solid, liquid and gas phases as shown in Figure 3 (Wang et al., 2020).

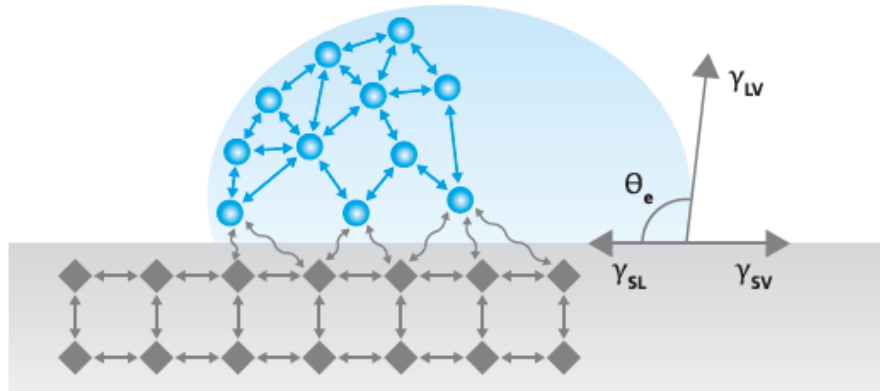


Figure 3. Schematic diagram of interfacial tension in vapor/liquid/solid system (Wang et al., 2020)

In other words, the contact angle depends on the cohesive forces, which are the liquid-liquid intermolecular forces, and the adhesive forces, which are the liquid-solid intermolecular forces, as shown in Figure 3 (Nguyen-Tri et al., 2019) (Wang et al., 2020) (Tunçgenç, 2004) If the cohesive forces are much stronger than the adhesive forces, the liquid will not wet the solid surface, and the contact angle measurement will be greater than 90° . If the adhesive forces are stronger, then the liquid droplet will interact strongly with the solid surface, leading to wetting and a contact angle less than 90° , as shown in Figure 4 (Tunçgenç, 2004; Krasowska et al., 2009).

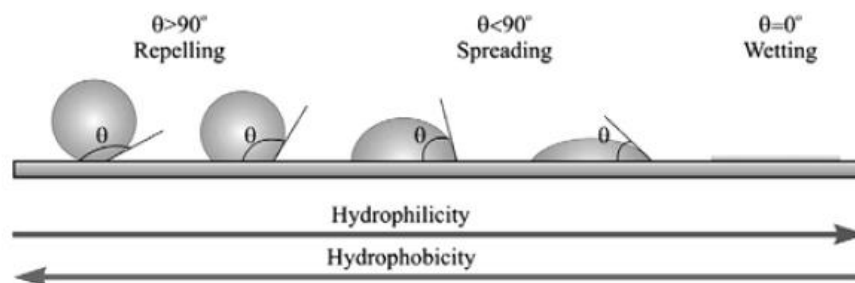


Figure 4. Schematic of shape of a water drop and the water contact angle (WCA) for solid surfaces along a hydrophobicity-hydrophilicity gradient (Krasowska et al., 2009)

When water is used as the fluid to determine the contact angle, the measured value equals the water contact angle (WCA) (Krasowska et al., 2009). The WCA is also explained as the angle at which a liquid-vapor interface meets a solid surface. Hydrophilicity and hydrophobicity are the most common terms used to describe the relative affinity of water droplets on solid surfaces. If the WCA is higher than 90° , the surface repels water, and a higher hydrophobic surface is obtained. When the WCA is lower than 90° , better wetting occurs, and the hydrophobicity of the surface decreases with the decreasing WCA, as shown in Figure 4 (Nguyen-Tri et al., 2019; Tunçgenç, 2004). A detailed description of wetting phenomena, wetting types and models, and their theoretical foundations are provided in section 2.2.1.

2.2.1 Wettability & Hydrophobicity

As mentioned in the previous section, the contact angle is defined as the angle between the tangent of the liquid droplet at the contact point between the solid, liquid, and gas phases and the solid phase surface at the three-phase boundaries. The solid (S), liquid (L), and gas (G) often referred to as the vapor phase (V) form three separate interfaces, namely S-L, S-G, and L-G.

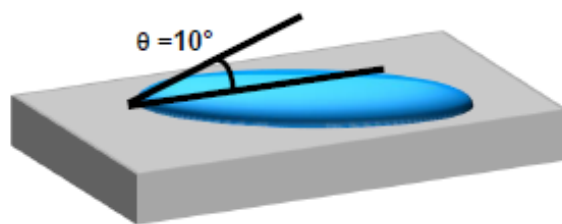


Figure 5. Good wettability (hydrophilic) (Yıldır et al., 2016)

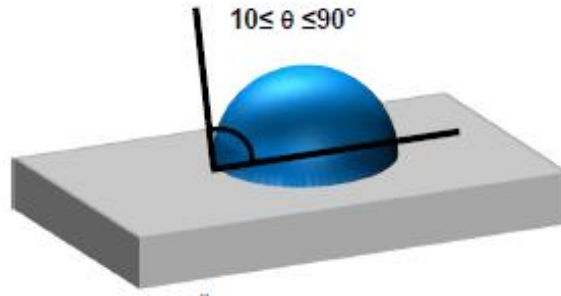


Figure 6. Normal wettability (Yılıgör et al., 2016)

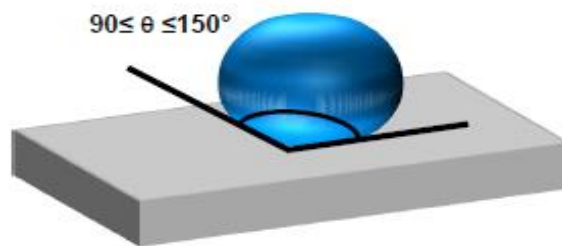


Figure 7. Poor wettability (hydrophobic) (Yılıgör et al., 2016)

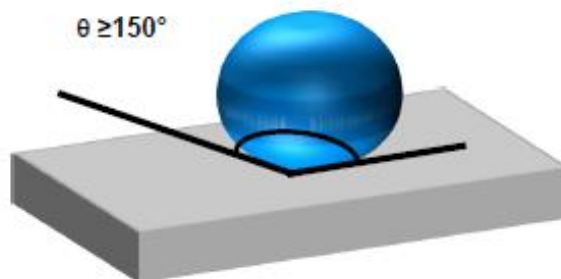


Figure 8. Extremely poor wettability (super-hydrophobic) (Yılıgör et al., 2016)

According to these contact angle values, wetting levels and surface characteristics can be altered as seen in Figure 5, Figure 6, Figure 7 and Figure 8. As the contact angle values increase, the hydrophobicity of the surface increases while the hydrophilic behaviour decreases.

In 1805, Thomas Young explained the contact angle based on the mechanical force equilibrium of three interfacial tensions at the three-phase contact line, and their relationship can be described as seen in Equation 1:

$$\gamma_{sv} = \gamma_{sl} + \gamma_{lv} \cos \theta_Y \quad \text{Eq. 1}$$

Young's Equation contains γ_{sv} , γ_{sl} and γ_{lv} terms represent the interfacial tensions between the solid-vapor interface, solid-liquid interface, and vapor-liquid interface, respectively. θ_Y refers to Young contact angle, which is equal to the equilibrium contact angle (θ_e) obtained based on thermodynamic principles in ideal wetting system. An ideal system is described as flat, smooth, and chemically homogeneous. However, these perfect surface properties cannot be found in real life. Surfaces in reality are non-ideal due to fabrication processes that may generate defects, resulting in surfaces that are not perfectly smooth or homogeneous. Therefore, the surfaces of materials are heterogeneous due to the presence of pores and roughness (Nguyen-Tri et al., 2019; Yılmaz et al., 2016).

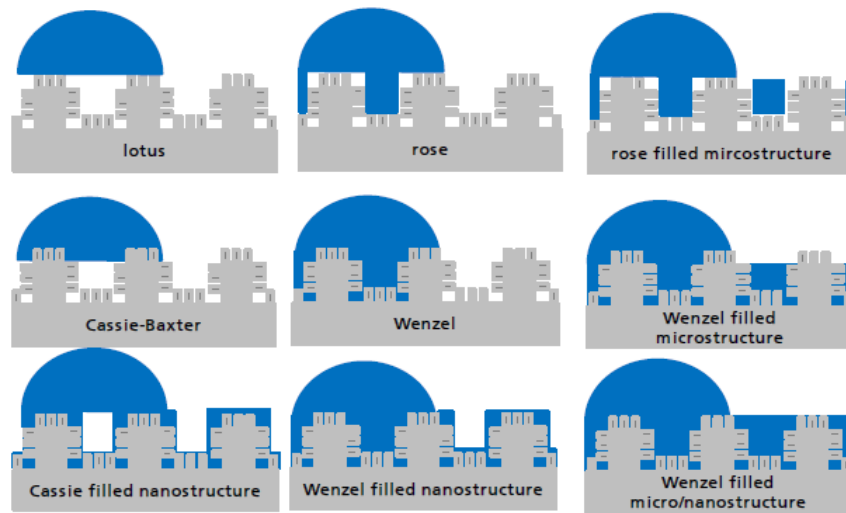


Figure 9. Different wetting states (Tunçgenç, 2004)

According to the surface topography, which includes micro/nano structures and their arrays, there can be different surface wetting states, as shown in Figure 9. The proper wetting state is selected to determine the actual contact angle values. Commonly, the Wenzel and Cassie-Baxter models are used for non-ideal surfaces.

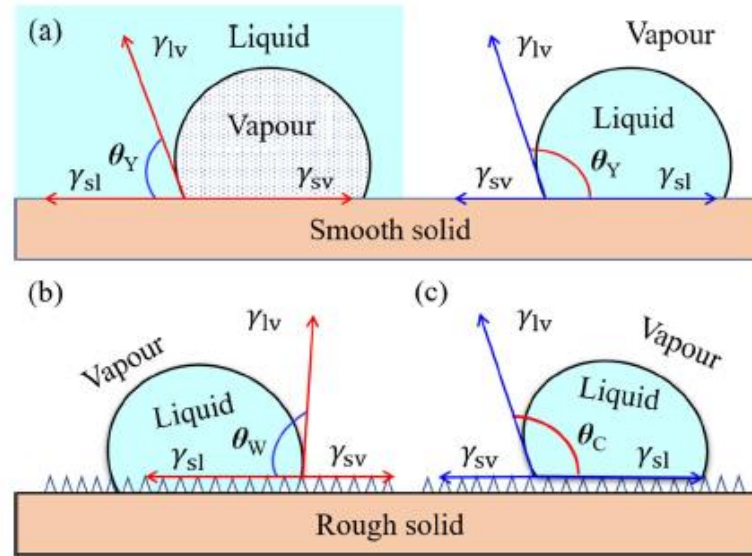


Figure 10. Schematic diagram of the relationship between equilibrium contact angle and interfacial tension in gas/liquid/solid system. (a) Young contact angle (θ_Y), (b) Wenzel contact angle (θ_W), and (c) Cassie contact angle (θ_C), (Wang et al., 2020)

In 1936, Wenzel studied the effect of roughness on the contact angle by assuming complete wetting of a rough surface by the liquid droplet. He defined the roughness factor (r) as the ratio of the actual area (A_{actual}) of a rough surface to its projected geometric area ($A_{projected}$) [$r = A_{actual}/A_{projected}$]. According to this definition, the roughness parameter equals 1 for ideal, flat, and smooth surfaces, while r is higher than 1 for rough surfaces. In the Wenzel state, it is assumed that the roughness scale is much smaller than the size of the liquid droplet. On the other hand, the Cassie-Baxter model assumes that droplets 'sit' on a composite surface of solid and air. According to Cassie-Baxter's law, water droplets form spheres and reside on the top of the fibrous surface without filling in the nanoholes, thus maintaining hydrophobicity (Nguyen-Tri et al., 2019; Koch et al., 2014; Yilgör et al., 2016; Wang et al., 2020).

Increasing surface roughness leads to a larger solid-liquid interface and a higher contact angle, resulting in a more hydrophobic surface, as seen in Figure 11. In the Wenzel state, it is assumed that the liquid completely penetrates the roughness on the surface. The relationship between roughness and the measured contact angle (θ_W) can be

explained as follows (Nguyen-Tri et al., 2019; Yılmaz et al., 2016; Wang et al., 2020; Nguyen-Tri et al., 2019; Koch et al., 2014).

$$\cos \theta_W = r \cos \theta_Y \quad \text{Eq. 2}$$

Many researchers stated the importance of using this equation to present actual contact angle (Nguyen-Tri et al., 2019; Yılmaz et al., 2016; Wang et al., 2020; Nguyen-Tri et al., 2019; Koch et al., 2014). In 2005, Suh et al. analysed the effect of roughness of the substrate on the final wetting properties by studying both Wenzel and Cassie models (Suh & Jon, 2005). In 2012, Chakraborty et al., stated that roughness and wetting characteristics have a significant impact on the dynamics of the contact line and provide insights for improving the design and performance of microfluidic systems. Also, contact angle measurements on both smooth and rough surfaces were investigated (Chakraborty et al., 2012). In 2014, Koch et al. aimed to investigate how surface roughness affects wetting and contact angle measurements. They explained that two different Wenzel and Cassie contact angle measurements by calculating the roughness value for both (Koch et al., 2014).

However, the static contact angle alone is not sufficient to understand wettability phenomena. In addition to measuring the roughness parameter and static contact angle, the dynamic contact angle, which includes the advancing and receding angles, can help us better understand the concept. This is also referred to as contact angle hysteresis (CAH).

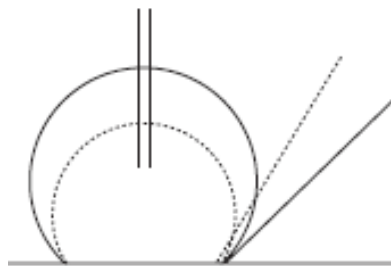


Figure 11. Slowly pumping a liquid into or out of a sessile droplet (Yılmaz et al., 2016)

It has become a popular topic due to the recent interest in superhydrophobic and self-cleaning surfaces. When a liquid drop is subjected to gravity or shear force, its movement is hindered by the retention force generated from contact angle hysteresis (CAH). CAH can be explained by the difference in contact angles at the advancing contact line and the receding contact line. One of the most common and simple methods of measuring CAH is through an embedded needle. In the advancing contact angle measurement, a fixed volume of the liquid is pumped through an orifice in the solid substrate, and the maximum contact angle is obtained during this process. Conversely, the liquid is slowly drawn through the same orifice, and the lowest contact angle is observed in this step. The advancing contact angle can be considered to facilitate the flow of the droplet, while the receding contact angle resists the flow, as seen in Figure 12.

All of these static, dynamic contact angles, and contact angle hysteresis are useful for understanding and analysing the surface heterogeneity (Yıldır et al., 2016; Nguyen-Tri et al., 2019; Koch et al., 2014).

2.2.2 Hydrophobicity in Nature

A wide variety of superhydrophobic surfaces can be found in nature. There are many examples in plants and animals that demonstrate excellent water repellence capacity, such as lotus leaves, taro leaves, rice leaves, rose petals, water strider legs, butterfly wings, and penguin body feathers (Krasowska et al., 2009; Nguyen-Tri et al., 2019; Bai et al., 2021). The lotus leaf is the most popular and well-known example of a superhydrophobic surface (with a contact angle greater than 150°) and has been set as a benchmark for scientists studying hydrophobic surface properties. With a contact angle higher than 160° , dirt easily rolls off the lotus leaf surface. As a result, the lotus leaf acts as self-cleaning, as water droplets bead up and take on a spherical form. This effect has made the lotus leaf a symbol of purity.

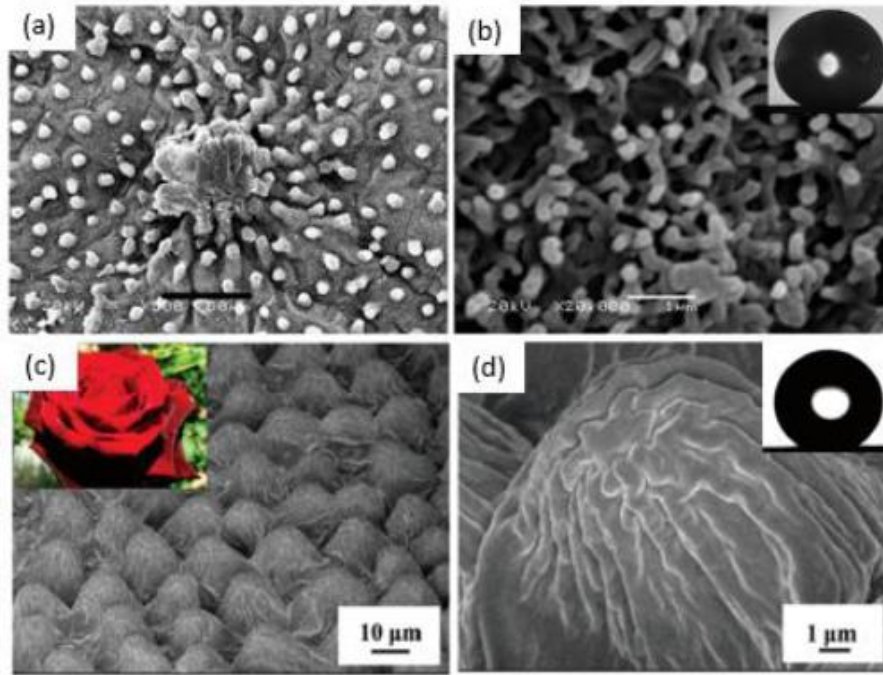


Figure 12. SEM images of superhydrophobic surfaces at low and high magnifications. (a) and (b) lotus leaf with a 162° water contact angle; (c) and (d) rose petal with a 152.4° water contact angle (Krasowska et al., 2009)

As shown in Figure 12, electron microscopy images indicate that a combination of hierarchical surface roughness and low surface energy wax-like materials is the principal reason for this super hydrophobicity. The SEM image of the lotus leaf reveals the presence of two levels of roughness. These structures are formed by hydrophobic crystalloids with a nano-sized range (10-100 nm) located on top of the micro-sized roughness (3-10 μm) on the surface. In addition to the "lotus effect," there is a "petal effect" observed in rose petal surfaces, which exhibit a high contact angle of 152.4° . The rose petal surfaces have micro-sized roughness with an average diameter of 16 μm . Unlike the lotus leaf, the rose petal surface lacks nano-scale roughness, resulting in a water droplet's inability to roll or slide even when the surface is turned upside down due to high adhesion. This difference is primarily attributed to the presence of micro and nano structures on the surface. These structures also influence the dynamic wetting behaviour, which was explained in the previous section (Krasowska et al., 2009; Nguyen-Tri et al., 2019; Bai et al., 2021).

2.2.3 Fabrication of Hydrophobic Surfaces

Nguyen-Tri et al. focus on nano-based approaches for the preparation of these coatings and discusses their properties and applications. Hydrophobic and self-cleaning surfaces are significant class of smart coatings that create interest among the researchers in the scientific world. Tailoring the chemical composition (chemical method) and creating roughness (physical method) are two general methods to produce water repellence surface. One of them is related with chemical modifications such as sol-gel, chemical etching, dip coating and chemical deposition while another method is based on physical etching and electrical deposition (Nguyen-Tri et al., 2019).

The etching technique in this study is primarily inspired by the natural structure of ribbed hair arrays. The primary goal of this approach is to enhance the surface roughness of the substrate. Wang and his co-workers utilized a combination of micro/nanosphere lithography and plasma etching techniques to fabricate the ribbed hair arrays. These rib structures are crucial for promoting air trapping and reducing solid-liquid contact, leading to enhanced super hydrophobicity (Wang et al., 2015). Also, chemical etching can include grafting hydrophobic molecules or polymers onto the surface or treating the surface with hydrophobic agents through chemical reactions or physical adsorption. Addition to etching technique, electrical deposition is another important way to create hydrophobic surface with physical modification. In 2005, Yang et al. studied deposition fabrication method by incorporating CNTs into the Ni-P matrix. They aimed to enhance the corrosion resistance and mechanical properties by creating hydrophobic surfaces that provide a degree of protection against corrosion by preventing or reducing the contact between the corrosive medium and substrate (Yang et al., 2005).

The sol-gel method involves the synthesis of a colloidal solution (sol) that undergoes a gelation process to form a solid network (gel). By incorporating hydrophobic additives or modifying the surface chemistry, superhydrophobic nanocoating can be achieved through the sol-gel process (Wang et al., 2020).

In this study, it was aimed to fabricate hydrophobic surface by using sol-gel process. After obtaining silica nanoparticles (SNPs), it added to coil coating to create nano roughness on the surface of coating film. As it can be seen in the above discussion, the surface hydrophobicity is a function of two important parameters. One of them is the

actual contact angle of the surface which is caused by the interaction between the surface and the liquid atoms, and it is thermodynamic quantity. Another parameter is roughness value of the projected area as seen in equation 2. Therefore, the purpose of the study is to gain benefit from both sides of obtained thermodynamic contact angle and surface roughness for the projected area.

In the following part, sol-gel fabrication method for creating hydrophobic surface was explained in detail.

2.3 Sol-Gel Synthesis of Silica-Stöber Method

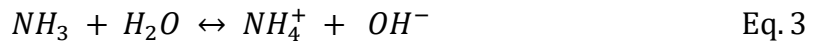
Silicates (silica) or silicon oxides have a general chemical formula of SiO_2 and are composed of silicon and oxygen, which are the most abundant elements in Earth's crust. They have a wide range of applications in industries such as construction, concrete production, glass manufacturing, ceramics, silicones, and various end-use applications. In addition to these different application areas, colloidal silica has been extensively studied at the nano and micro scales, especially in recent years, due to its unique properties, including a large surface area, relative chemical and thermal stability under various conditions, high colloidal stability, low toxicity, and optical transparency. These attractive properties have led to an increased application field, resulting in the development of synthesis methods to produce silica with different properties (Hyde et al., 2016).

Although the components of silicates are abundant in nature and they have a wide range of applications, controlling the size, shape, and impurity levels during particle production through crushing and grinding processes is nearly impossible. This uncontrolled situation limits the use of natural silicates for specific and specialized purposes. Therefore, synthetic silica production methods are preferred to achieve specific morphological properties such as spherical, solid, mesoporous, and hollow structures. The most preferred synthesis method for silicates is the sol-gel method, which offers potential control over the entire reaction during synthesis. This method allows for the production of particles with controlled size, shape, and size distribution through a low-cost process. The chemistry of the sol-gel process is based on hydrolysis and polycondensation

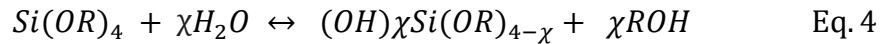
reactions, where monomers are converted into a colloidal solution that serves as a precursor to network polymers. The sol-gel method can be tailored according to the desired particles to be synthesized (Hyde et al., 2016; Tunçgenç, 2004).

In 1968, Stöber et al. introduced a new method for synthesizing silica nanoparticles with sizes ranging from 20 to 800 nm. This technique involves the preparation of monodisperse spherical nanoparticles with controlled size (Ghimire & Jaroniec, 2021; Meier et al., 2018). The Stöber method includes the hydrolysis of a silica source, usually TEOS, in a mixture of solvent, typically alcohol, and water, followed by the condensation of the resulting silanols. To adjust the pH of the reaction medium (usually around 11-13) and catalyse the reaction, ammonia or NH₄OH is commonly used. The reactions that occur in the Stöber method can be described as follows (Innocenzi, 2016):

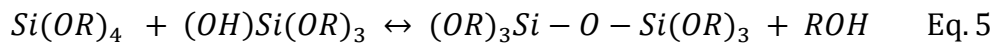
Ionization of ammonia:



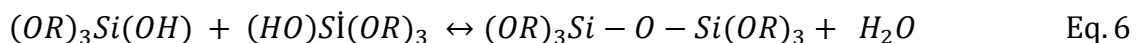
Hydrolysis:



Alcohol condensation:



Water condensation:



where R is C₂H₅ for TEOS.

Since the TEOS–water system exhibits an immiscibility condition, alcohol is frequently used as a homogenizing medium in the synthesis. Ammonia is used to adjust the pH of the reaction and catalyse it. In the ionization of ammonia step, water dissociates to produce nucleophilic hydroxyl anions (OH⁻) in a fast first step.

Additionally, the hydrolysis of TEOS occurs to form hydrolysed monomers. These monomers then condense to form the initial nanostructures. The hydrolysis and condensation reactions produce the initial particles, known as nuclei, and the period of formation of these nuclei is referred to as the "induction period." After the hydrolysis

reaction, the condensation reaction occurs instantaneously, where the hydroxyl group of the intermediate $[(\text{SiOC}_2\text{H}_5)_{4-x}(\text{OH})_x]$ reacts with either the ethoxy group of other TEOS molecules through "alcohol condensation (alcoxolation)" (Equation 5) or the hydroxyl group of another hydrolysis intermediate through "water condensation (oxolation)" (Equation 6) to form Si-O-Si bridges, which contribute to the formation of the silica network. Alcoxolation is the preferred condensation reaction between partially hydrolysed titanate precursors to establish a stronger silica network, while oxolation is favoured over alcoxolation for silicates when partially hydrolysed monomers are involved. A schematic diagram of each step of the Stöber reaction can be seen below:

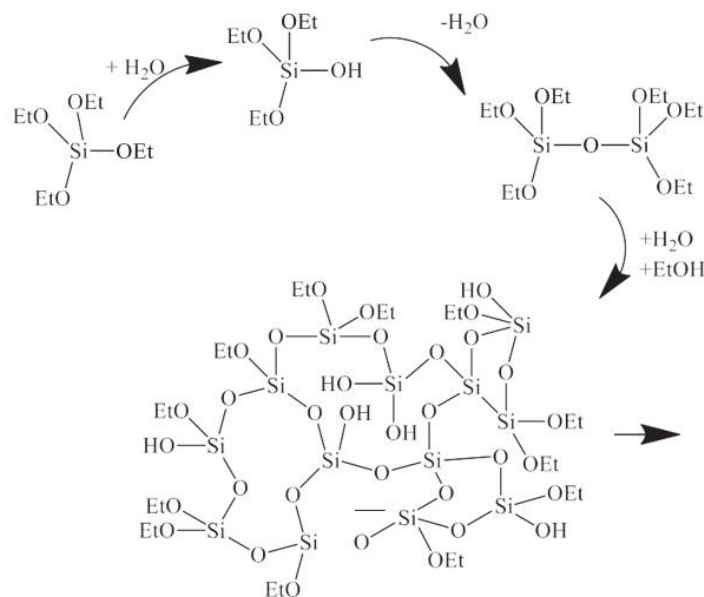


Figure 13. Silica networking (Innocenzi, 2016)

After the hydrolysis reaction of alkoxide molecules, reactive monomers such as dimers, trimers, linear and cyclic species (silica rings and cages) can develop in the array during the reactions, as shown in the Figure 13. However, in general, only structures with at least 4 silicon tetrahedra are stable. The rings act as nucleation points, and the addition of monomers and other species leads to the formation of three-dimensional particles. Two different condensation reactions can occur within the same molecule or mostly between different molecules, which is also known as intermolecular cyclization. While cyclic silica structures are less stable than chain silica structures, structures with 3 or 4 tetrahedra

generate the cyclic structures, and initial particles with a size of 1–2 nm are formed (Innocenzi, 2016).

2.3.1 Growth Mechanism of SNPs

The mechanism of how initial colloidal structures grow to form the final particles in Stöber reaction is a controversial topic in the literature. Two extreme models, "monomer addition" and "controlled aggregation", have been proposed and validated for various conditions. Both models start with the generation of nuclei and continue to increase in size over time. However, the differences between the models lie in the definition of nuclei and the growth mechanism.

2.3.1.1 Monomer Addition Model

The monomer addition model proposes that the growth of silica particles occurs by the addition of monomers to the existing particles. This model, also known as the nucleation and growth model, proposes that the nanoparticles are formed through the following steps: nucleation of small clusters of atoms or molecules, followed by growth of these clusters through the addition of monomers (building blocks) until they reach the desired size. This model assumes that the size distribution of nanoparticles is determined by the rate of monomer addition and the rate of growth.

The monomer addition model was first proposed by LaMer and Dinegar in 1950 based on the formation of monodispersed sulfur hydrosols. In this model, nucleation is limited to the early stages of the reaction, after which growth is based on the deposition of monomers on the particle surface without additional nucleation (LaMer et al, 1950). In 1968, Stöber et al. first proposed the monomer addition model to describe the growth mechanism of silica particles during the Stöber process. They suggested that the growth occurs by the addition of TEOS monomers to the silica nuclei, which leads to the formation of larger particles (Stöber et al, 1968). In 1990, Brinker et al. performed a detailed investigation of the growth mechanism of silica particles during the Stöber

reaction. They observed that the growth of silica particles occurs by the addition of TEOS monomers to the existing particles, which supports the monomer addition model (Busquets et al., 2016). Matsoukas and Gulari also proposed a similar model for silica particle growth in 1988, where nucleation is restricted to the initial stages of the reaction and growth is proportional to the hydrolysis constant (Matsoukas et al., 1988). Bailey and Mecartney proposed a model in 1992 where silica atoms appear in a random expanded polymeric ring and grow through the monomer addition pathway (Bailey & Mecartney, 1992). In 2001, Jana et al. studied the growth mechanism of gold nanoparticles in the presence of silica spheres synthesized using the Stöber process. They observed that the growth of gold nanoparticles occurs by the addition of gold precursor to the silica spheres, which supports the monomer addition model for the growth of silica particles as well (Jana et al., 2001). In 2019 which found that Si(OH)_4 acted as the nucleus of nanoparticles and increased in size through the addition of hydrolysed monomer (Si(OH)_4). Overall, the article provides a comprehensive review of colloidal silica particle synthesis and the various models proposed to explain the process (Jiang et al., 2019).

2.3.1.2 Aggregation Growth Model

The aggregation growth model proposes that silica particles are formed through a two-step process: nucleation and growth. In this model, the reaction starts with the formation of small silica nuclei by hydrolysis of TEOS in the presence of water and acid catalyst. These nuclei can then aggregate together to form larger particles, followed by further growth through the addition of monomers. The differences between monomer addition and aggregation growth models were explained by Hyde et al. as shown in Figure 14 (Hyde et al., 2016).

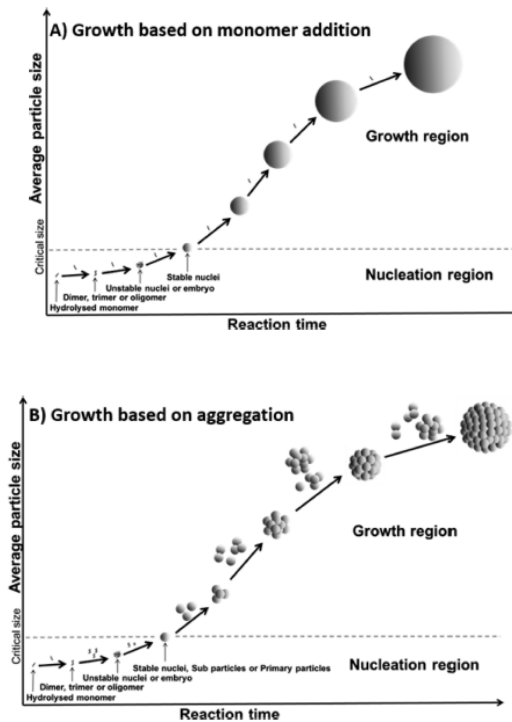


Figure 14. Monomer addition and aggregation models (Hyde et al., 2016)

In 1988, Bogush et al. conducted a study to investigate the growth mechanism of silica particles during the Stöber process over a range of temperatures. They proposed that the growth of particles occurs by the aggregation of smaller particles, which supports the aggregation growth model. (Bogush et al, 1988). In 1991, Bogush and Zukoski used the Smoluchowski equation to characterize the growth of SNPs assuming a solely aggregative mechanism. They considered the development of the particle number density function with time to be equal to the net summation of an aggregative birth, an aggregative death, and a nucleation term. They proposed a model that included van der Waals, electrostatic, and solvation interactions in the kernels for both birth and death terms to incorporate particle-particle interactions. They found that the particle diameter and size distribution could be predicted correctly using the aggregation mechanism. This model is still commonly used to investigate particle formation and growth. Many studies support the view that aggregation is the dominant growth mechanism and that final SNPs characteristics are influenced by experimental parameters such as ionic strength, pH, and solvent properties (Bogush et al, 1991). In the recent studies by, Branda et al. (2007), and

Zeng et al. (2015) provide evidence in favor of aggregation as the primary growth mechanism (Branda et al., 2007; Zhang et al., 2015).

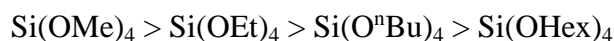
The final characteristics of SNPs are influenced by experimental parameters such as ionic strength, pH, and solvent properties. Many studies support the idea that aggregation is the dominant growth mechanism, with the rates of nucleation and aggregation controlling the final particle size (Bogush et al, 1991; Stöber et al, 1968).

2.3.2 Effect of Process Parameters on Stöber Synthesis

The Stöber process is a widely used method for the synthesis of silica particles with controlled size and morphology. The process parameters, such as the type and concentration of the precursor, solvent type and its pH, temperature, and reaction time, have a significant effect on the size, morphology, and properties of the synthesized silica particles.

2.3.2.1 Precursors

Alkoxysilanes (silicon alkoxides) are the most used precursors for sol-gel silica production. The presence of strong covalent Si-O bonds within the molecules leads to hydrophobicity and immiscibility properties with water. However, an increase in the molecular weight of the alkoxysilane molecules causes an increase in the boiling point. This increase in size of the alkoxy groups decreases the reactivity of the molecules due to steric hindrance.



TEOS, or Tetraethyl orthosilicate, is a commonly used alkoxide in the series of silica-based material precursors. Its popularity is attributed to its high purity, optimum reactivity, versatility, ease of use, and relatively low toxicity compared to other chemicals used in materials synthesis. While tetramethyl orthosilicate (TMOS) is another commonly

used precursor, it is less stable due to the bulky ethoxide group, causing it to hydrolyse more than four times faster than TEOS. However, research suggests that TMOS may be preferred for drug encapsulation due to its enhanced hydrolysis rates under acidic and basic conditions (Ghimire & Jaroniec, 2021; Finnie et al., 2007; Stöber et al, 1968; Innocenzi, 2016).

In 1968, Stöber observed that the mean size of the final silica particles decreased as the alkyl-chain length of the alkoxy silane precursor increased. This is because longer alkyl chains slow down the condensation reaction rate (Stöber et al, 1968). In 2004, Kim et al. found that increasing the TEOS concentration in the Stöber reaction led to an increase in the size of the synthesized SNPs. They also noted that the pH of the reaction mixture had an effect on the size of the SNPs (Kim et al., 2004). In 2010, Ibrahim et al. studied the effect of TEOS concentration on the nucleation and growth of SNPs and were able to explain the reasons for the increase in particle size with the increase in TEOS concentration. They found that increasing the TEOS concentration resulted in a shorter nucleation period and an increased growth rate, which led to the formation of larger silica particles (Ibrahim et al., 2010). In 2019, Jiang et al. studied the effect of TEOS concentration on the size of the synthesized SNPs using a modified Stöber process. They found that increasing the TEOS concentration resulted in a larger particle size, but only up to a certain concentration. Beyond that concentration, the particle size decreased due to increased particle aggregation (Jiang et al., 2019).

2.3.2.2 Solvents

Solvent selection is an important factor in the Stöber reaction because the solvent can influence the rate of the hydrolysis and condensation reactions that take place, as well as the size, shape, and structure of the resulting silica particles. The Stöber synthesis involves the hydrolysis and condensation of silicon alkoxide precursors in the presence of an alcohol solvent, which produces a silica sol that can be further processed to form solid silica particles. The choice of solvent can affect the reaction kinetics and thermodynamics, which in turn affect the particle size, shape, and structure (Malay et al., 2013).

Solvent used in the Stöber reaction should be able to dissolve TEOS and be miscible with water, which is often used as a co-solvent. Water can hydrolyse the alkoxy silane precursor and promote the formation of silica particles. Higher water contents generally result in smaller particle sizes due to faster hydrolysis rates, while lower water contents lead to larger particle sizes due to slower hydrolysis rates. In addition, the solvent should have a high boiling point to ensure that the reaction proceeds at a moderate temperature and that the solvent does not evaporate during the reaction (Malay et al., 2013; Bari et al., 2020).

Ethanol, isopropanol, and n-butanol are commonly used alcohols in Stöber reaction. If TEOS is used as a silica source in the reaction, ethanol is often considered the best solvent for the Stöber reaction due to its high boiling point, low toxicity, and ability to solubilize TEOS effectively.

There are some important parameters for selection of solvent. The polarity of the solvent can affect the rate of hydrolysis and condensation reactions that occur during the Stöber synthesis, as well as the size and morphology of the resulting particles. When highly polar solvents such as ethanol or water are used, they tend to produce smaller and more uniform particles than non-polar solvents like toluene or hexane. This is because the higher polarity solvents facilitate the nucleation and growth of silica particles by promoting the hydrolysis and condensation of the silica precursors (Malay et al., 2013).

The viscosity of the solvent can also affect the particle size and shape in the Stöber synthesis. High-viscosity solvents like glycerol or PEG can lead to larger and more irregularly shaped particles, while low-viscosity solvents like ethanol or methanol tend to produce smaller and more spherical particles. This is because the solvent viscosity can affect the diffusion rate of the reactants and the rate of particle growth, with slower diffusion and growth rates resulting in larger and more irregular particles.

The dielectric constant (ϵ) is a common way to indicate solvent polarity. When the molecular weight (MW) of the alcohol increases and the dielectric constant decreases, the size of silica nanoparticles (SNPs) tends to increase, and the particle size distribution (PSD) becomes narrower (Malay et al., 2013; Bari et al., 2020).

Steric effect, which is related to the structure of a molecule, can be represented by a topological index called the Wiener index. The Wiener index is defined as the sum of the lengths of the shortest paths between all pairs of vertices in the chemical graph representing the non-hydrogen atoms as shown in below. An increase in steric effect has a positive effect on the rate of reaction, indicating that solvation resistances due to steric

effect are not sufficient to reduce the rate of reaction significantly. This finding contradicts earlier literature that suggested that the steric effect of solvent reduces the rate of reaction (Bari et al., 2020).

Table 1. Different properties of solvents (Malay et al., 2013)

Solvent	ϵ	Wiener Index	$\mu, \text{mPa}\cdot\text{sec}$ (at 35°C)
Ethanol	24.6	9	1.074
Propanol	20.1	20	1.959
Isopropanol	18.3	18	2.040
Butanol	17.8	35	2.572

Stöber's study in 1968 showed that using methanol, a short-chain alcohol with a faster reaction rate, resulted in wider particle size distributions compared to using longer chain length alcohols such as butanol (Stöber et al, 1968). In their 2005 study, Mine et al. found that the average particle sizes resulting from the Stöber reaction were in the order of 1-butanol > 1-propanol > ethanol. They also observed that interparticle repulsion was the strongest for ethanol and the weakest for 1-butanol (Mine et al., 2005). Bari et al. stated that due to its higher viscosity compared to methanol, particles tend to grow to a larger size when synthesized in ethanol (Bari et al., 2020). In short, solvents with low polarity, low hydrogen bonding ability, and high viscosity may result in an increase in the size of silica nanoparticles (SNPs) (Stöber et al, 1968; Malay et al., 2013; Bari et al., 2020; Mine et al., 2005).

2.3.2.3 pH

The pH of the reaction mixture is an important parameter in the Stöber reaction, as it can influence the degree of hydrolysis and condensation of the silicon alkoxide precursors, as well as the size, shape, and structure of the resulting silica particles.

In the Stöber reaction, the hydrolysis of the silicon alkoxide precursors is initiated by the addition of water to the reaction mixture. The hydrolysis reaction involves the breaking of the silicon-oxygen bonds in the precursor molecule and the formation of silanol (-Si-OH) groups. The silanol groups can then undergo condensation reactions to form siloxane (-Si-O-Si-) bonds and create a three-dimensional silica network. (Stöber et al, 1968).

The degree of hydrolysis and condensation reactions can be influenced by the pH of the reaction mixture. At low pH (acidic conditions), the concentration of hydronium ions (H_3O^+) is high, which can accelerate the hydrolysis reaction by protonating the oxygen atoms in the precursor molecule and making them more susceptible to nucleophilic attack by water. However, at very low pH values, the acid-catalysed hydrolysis can lead to the formation of larger and more irregular silica particles, as the rapid hydrolysis and condensation reactions can create a high degree of supersaturation in the reaction mixture, which can favour the formation of larger particles. On the other hand, at higher pH values (basic conditions), the concentration of hydroxide ions (OH^-) is high, which can also accelerate the hydrolysis reaction by deprotonating the precursor molecule and making it more susceptible to nucleophilic attack by water. Therefore, there is not universally "best" pH value for the Stöber reaction, as the optimal pH can vary depending on the specific experimental conditions and the desired particle properties.

Another crucial characteristic is stability of the silica particles, as the degree of protonation of the silanol groups can influence the surface charge and colloidal stability of the particles. For example, at low pH values, the surface charge of the silica particles may become more positive, which can promote particle aggregation and reduce the colloidal stability (Stöber et al, 1968; Rout, 2013; Alessi et al., 2013).

The hydrolysis and condensation rates of alkoxy silanes are shown in Figure 15, which illustrates that the rates of hydrolysis and condensation decreased similarly up to pH 6, after which their behaviours changed in an opposite manner in alkaline pH. The study also demonstrated that the availability of OH^- ion significantly drives the condensation reaction (Rout, 2013).

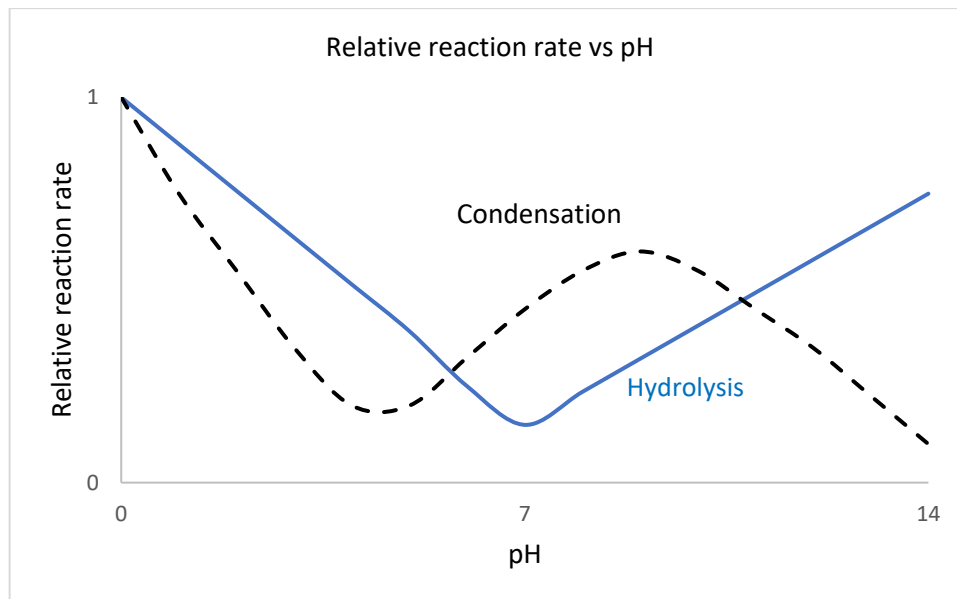


Figure 15. Relative reaction rate vs pH (Rout, 2013)

Since Stöber reaction is typically a base-catalysed hydrolysis and condensation reaction of alkoxy silanes, ammonia, ammonium hydroxide, sodium hydroxide, potassium hydroxide, and other strong bases are commonly used to catalyze the reaction. Other catalysts, such as acids, can also be used for Stöber reaction under acidic conditions. Additionally, surfactants and polymers can be used as templates or structure-directing agents to influence the morphology and size of the resulting silica particles.

Ammonia is most frequently used base-catalyst in the Stöber method because it increases the rate of hydrolysis and condensation reactions. Ammonium ions can also increase the pH of the reaction mixture, which can have an impact on the kinetics of the reaction. In addition, ammonium ions can interact with the silica particles during the growth stage, leading to changes in particle morphology and size distribution. The addition of ammonium to the reaction mixture can lead to the formation of ammonium hydroxide (NH_4OH), which can increase the pH of the solution. A higher pH can lead to faster hydrolysis and condensation reactions, resulting in the formation of larger silica particles. Ammonium can also act as a buffer, helping to maintain a stable pH throughout the reaction. During the growth stage, the presence of ammonium ions can lead to the formation of complex silica-ammonium species, which can affect the size and shape of the silica particles. This can result in a shift towards larger particles, or in the formation of more spherical particles. The specific effect of ammonium on the Stöber reaction can depend on a variety of factors, including the concentration of ammonium ions, the

reaction conditions (such as temperature and pH), and the specific silica precursor used (Alessi et al., 2013; Matsoukas & Gulari, 1988).

2.3.2.4 Temperature

Temperature is an important parameter in the Stöber reaction as it affects the rate of hydrolysis and condensation reactions. Increase in temperature leads formation of smaller particles due to two reasons. Firstly, the equilibrium solubility of $\text{Si}(\text{OH})_4$ intermediate product, obtained by the hydrolysis of TEOS, increases with temperature. This reduces the particle growth time and results in smaller particles due to shorter growth period. Secondly, high nucleation rate at higher temperature inhibits nuclei from growing into larger particles, leading to the formation of smaller particles. Researchers have observed a decrease in mean particle size with increased temperature, as well as reduced critical supersaturation at which nucleation takes place, resulting in fewer but larger nuclei. Therefore, careful control of temperature is necessary to achieve the desired particle size and morphology in the Stöber reaction (Bogush et al, 1988; Dabbaghian et al., 2010; Fouilloux et al., 2012). In 1988, Bogush et al. investigated the effect of temperature on the Stöber method within the range of 9–55°C and reported a clear decrease in mean particle size with an increase in temperature, leading to increased monodispersity (Bogush et al, 1988). In 2010, Dabbaghian et al. found that increasing the reaction temperature leads to the formation of smaller particles due to the increase in the nucleation rate and shorter growth period, ultimately resulting in smaller particle size (Dabbaghian et al., 2010). In 2012, Fouilloux et al. reported that increasing temperature increases solubility and reduces the critical supersaturation at which nucleation occurs, leading to fewer and larger nuclei (Fouilloux et al., 2012).

2.3.3 Effect of Presence of Seed Particles

Researchers have utilized the seed growth method to regulate the growth process by using smaller particles as seeds for the production of bigger particles with different size distributions via multi-step hydrolysis and condensation of TEOS. This technique has proven effective in producing large particles ($>1\mu\text{m}$) by condensing all TEOS directly onto the seeds. It has been observed that seed addition has a more direct impact on the final size distribution compared to the chemical composition of the reacting solution and the operational conditions (Huang & Pemberton, 2010). In 1996, researchers prepared large monodisperse silica particles using seed particles and found that secondary particle formation is influenced by the generation rate of supersaturation by the reaction and the consumption rate by particle growth. They observed that the early stages of growth of silica particles are controlled by diffusion of electrically charged condensed species onto the surface of the silica seeds against the electrostatic repulsion (Chen et al., 1996a; Chen et al., 1996b). Additionally, Chang et al. (2005) found that turbulent fluid motion promotes the growth of particles by lowering the hydrodynamic barrier against the transport of materials required for growth. They observed that secondary particle formation was inhibited and seed particle growth was promoted by agitation. At a mild agitation regime, a large population of tiny secondary particles (smaller than 100 nm) were formed, which decreased gradually as agitation speed increased. Eventually, this population disappeared completely at an agitation speed of 1500 rpm (Chang et al, 2005). Chou and Chen (2008) proposed that secondary nucleation is related to the distance between seed particles. When the distance between seed particles exceeds a critical value, secondary nucleation is likely to occur, while shorter distances result in simple growth. A higher generation rate corresponds to a shorter distance between seed particles, as reaction intermediates have limited time to find a seed surface for precipitation. Chou and Chen's results indicated that larger seed sizes require a higher specific seed surface area (i.e., higher seed concentration) to inhibit the production of new particles (Chou & Chen, 2008).

CHAPTER 3

MATERIALS AND METHOD

This chapter provides details about the experimental methodology for synthesizing monosize silica nanoparticles and bi-modal silica particles. It includes information on the materials used in the synthesis and a detailed description of the synthesis methods. Addition to synthesis, it contains explanation of the mechanical tests including MEK, impact resistance, T bent, pencil hardness, adhesion tests and characterization methods such as particle size distribution, SEM, AFM, FTIR and contact angle measurements.

3.1 Materials

3.1.1 Synthesis of SNPs

The synthesis of SNPs involved the use of TEOS (Sigma-Aldrich, 99.99%) as the silica source, while ethanol (Tekkim, 96%) served as the solvent and ammonium hydroxide (NH₄OH) (Merck, 25%) acted as the basic catalyst. Ultrapure water (18.2 MΩ) was utilized in all experimental procedures. All chemicals were utilized as received without any further modifications.

3.1.2 Silica Added Coatings Studies

This section explores the impact of silica in coil coatings by comparing systems with and without the addition of pigments and fillers. Initially, a clear coat system (free of pigments and fillers) obtained from AkzoNobel Kemipol was used, and silica particles

were incorporated into it. Subsequently, a white polyester topcoat loaded with TiO₂ pigment, filler and commercial silica (as a matting agent with a size of 7-9 μm) was supplied from AkzoNobel Kemipol to create hydrophobic surfaces. Coatings were applied to primed aluminium metal substrates with film thicknesses of 10 and 20 microns. The wet coating properties are listed below:

Table 2. Wet coating properties of polyester topcoat

Properties	Specs for Clear Coat	Specs for Topcoat
Viscosity (DIN 53211, DIN4, 23°C)	95 – 110 seconds	95 – 110 seconds
Solid Content by Weight (DIN 532156)	52.00 - 56.00 %	63.90 – 67.90 %
Solid Content by Volume (DIN 532156)	45.00 -49.00 %	47.50 – 51.50 %
Density (ASTM D 1475, 23°C)	0.98 – 1.08 g/cm ³	1,32 – 1,42 g/cm ³

3.2 Methods

The synthesis of SNPs was carried out through the base-catalysed Classic Stöber method, which involves the hydrolysis and condensation of tetraethyl orthosilicate in an alcoholic medium in the presence of a base catalyst (ammonia). The experimental details of the synthesis of SNPs process were provided in the subsequent sections. In addition to this, external parameters such as the addition of seed particles, which were also produced using the Stöber method were also incorporated into the Classic Stöber method. In the synthesis phase, both monosize particles (ranging from 500-550 nm) and bi-modal particles (consisting of multisize particles, with sizes of 1.2 μm and 550 nm) were produced for addition into the coil coating. The effects of different particle sizes and size distributions of silica were investigated in coil coating applications. The silica added coating studies section elaborated on the characterization and mechanical test controls conducted on the coil-coated panels.

3.2.1 SNP Synthesis Using Stöber Method

The synthesis of silica nanoparticles using Stöber method involves the hydrolysis and condensation of tetraethyl orthosilicate (TEOS) in the presence of ammonium hydroxide as a base catalyst. This method produces particles with spherical morphology and uniform size distribution. In the Classic Stöber method, a mixture of ammonium hydroxide (1.09 M) and water (11.67 M) was stirred with ethanol (12.14 M) at room temperature ($\sim 20^{\circ}\text{C}$) by creating a vortex during the mixing process. Mixing rate which was generally between the 800-1000 rpm was selected to amount of total solution. TEOS (0.25 M) was added to the solution in pulses to initiate silica synthesis. The reaction was allowed to proceed for 24 hours before the particles were separated from the solution using centrifugation. Since Stöber mentioned the reaction time of 2 hours is sufficient, the reaction results after 2 and 24 hours were followed (Stöber et al, 1968). The resulting solution was centrifuged (Eppendorf Centrifuge 5804, Hamburg) at 6500 rpm for 5 minutes to collect the silica nanoparticles. The resulting particles were then washed with water and ethanol to remove any unreacted reagents and dried at room temperature for further characterization.

Firstly, effect of TEOS loading amount on the particle size were investigated. Additionally, it was aimed to observe how the different concentration amounts of each reacting component together with TEOS affect the system. These studies were performed to investigate the effects of the followings:

- i. TEOS concentrations
- ii. TEOS & ethanol, TEOS & water, TEOS & ammonium hydroxide concentrations

In order to investigate the impact of varying TEOS concentration on the particle size, shape and morphology of silica produced, the quantities of other components including ethanol, ammonium hydroxide, and water were kept constant following the Classic Stöber method as shown in Table 3. 5 different concentrations of TEOS were introduced to the system as pulse and totally 5 different samples were obtained and mixed 24 hours. Then representative samples were taken from the suspensions in the end of 2 & 24 hours and sizes of particles were determined by Scanning Electron Microscopy (SEM).

Table 3. Effect of TEOS concentrations experimental values

Parameters	Value
TEOS (mol/L)	0.0625M, 0.125M, 0.25 M, 0.50 M, 1 M
Ethanol (mol/L)	12.14 M
H ₂ O (mol/L)	11.67 M
NH ₃ (mol/L)	1.09 M

After this experiment, classic Stöber method was indicated as silica C (including TEOS 0.25 M) and 0.50 M TEOS used method was remarked as silica D.

In this part, the amount of TEOS and each component in the Stöber method (Silica C) were doubled sequentially to investigate particle shape and size distribution as shown in Table 4. Obtained particle size range and shape analysis were performed using SEM.

Table 4. Effect of TEOS & Other Components Concentrations for Silica C

Components	Classic Stöber	Experiment 1	Experiment 2	Experiment 3
	Method (Silica C Method)			
TEOS	0.25 M	0.50 M	0.50 M	0.50 M
Ethanol	12.14 M	24.28 M	12.14 M	12.14 M
H₂O	11.67 M	11.67 M	23.34 M	11.67 M
NH₃	1.09 M	1.09 M	1.09 M	2.18 M

Amount of TEOS and each component in the Silica D method were doubled in order as listed in Table 5. SEM analysis was used to compare results.

Table 5. Effect of TEOS & Other Components Concentrations for Silica D

Components	Silica D Method	Experiment 1	Experiment 2	Experiment 3
TEOS	0.50 M	1.00 M	1.00 M	1.00 M
Ethanol	12.14 M	24.28 M	12.14 M	12.14 M
H₂O	11.67 M	11.67 M	23.34 M	11.67 M
NH₃	1.09 M	1.09 M	1.09 M	2.18 M

3.2.2 SNP Synthesis by Seed Addition (Seeded Growth)

Seeded growth experiments were performed by introducing a predetermined amount of monodispersed silica particles into the solution containing ammonium, water, and ethanol before the addition of TEOS. The experiments involved the synthesis of seed particles followed by their growth.

The purpose of these studies was to investigate the effects of various parameters such as different seed size, different seed amount, different TEOS amount and TEOS addition ratio on the final shape, size and distribution of SNPs by using SEM analysis.

To investigate the effect of different seed sizes on the synthesized silica particles, a modified formula was prepared initially. Synthesizing seed procedure, TEOS amount in the reaction were increased from 0.25 M to 0.50 M and 1 M respectively as shown in Table 6. Then the particles were redispersed in fresh TEOS-free Stöber solution (NH₃/H₂O/EtOH), in other words growth solution, so as to use as seed solution.

Table 6. Different Seed Formulas

Components	Classic Stöber Method	Seed 1 Formula	Seed 2 Formula
TEOS	0.25 M	0.50 M	1.00 M
Ethanol	12.14 M	24.28 M	12.14 M
H₂O	11.67 M	11.67 M	11.67 M
NH₃	1.09 M	1.09 M	1.09 M

After adding different amounts of TEOS into the mixture, the solution was mixed for 2 hours and SEM pictures were taken to observe the synthesized particles. After redispersed seed 1 in fresh TEOS-free Stöber solution (NH₃/H₂O/EtOH), two different TEOS concentrations (1.75 M and 3 M) were pulse added to the system in pulses as shown in Figure 16.

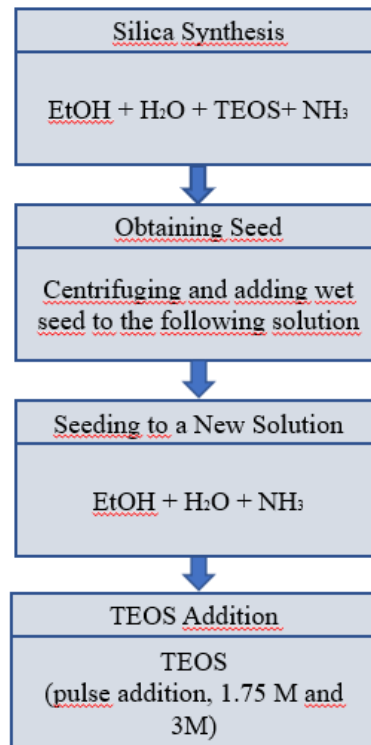


Figure 16. Flowsheet for the different seed and their growth solution, pulse addition

After redispersing seed 2 in a fresh TEOS-free Stöber solution ($\text{NH}_3/\text{H}_2\text{O}/\text{EtOH}$), the system was supplemented with 1.75 M TEOS. Furthermore, to compare pulse and continuous addition methods, another batch was prepared using seed 2. In this solution, TEOS with a concentration of 0.50 M was introduced to the system at a rate of 5 ml/min, following the specified schedule.

To observe the effect of different combinations of TEOS additions on the resulting silica particles, three different TEOS addition methods were planned. In the continuous addition phase, a TEOS concentration of 0.5 M was continuously added to the TEOS-free Stöber solution at a rate of 5 ml/min. Secondly, TEOS, ammonium hydroxide, and water were added to the medium containing only EtOH at the same addition rate of 5 ml/min. Lastly, TEOS, ammonium hydroxide, and water were simultaneously added to the medium containing both EtOH and ammonium hydroxide, also at a rate of 5 ml/min as listed in Figure 17.

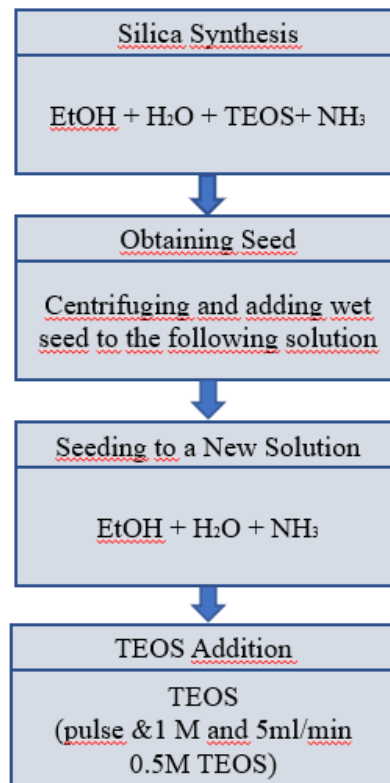


Figure 17. Flowsheet for the different seed and their growth solution, continuous addition

In this part, 4 different seed were obtained and different Stöber reaction combinations were applied to obtain bi-modal SNPs. After obtaining indicating data from 3.2.1 part, Silica D, Modified Silica D, Classic Stöber (Silica C) and Modified Classic Stöber (Modified Silica C), synthesis methods were used to obtain seed particles. Subsequently, TEOS-free growth solutions were prepared by combining various components, and different amounts of TEOS were directly added to the solution. After evaluating the best results obtained from the trials conducted in the experiment, the continuous addition of TEOS was further explored in the subsequent phase of experiments. General experiment schedule and each experiment details were listed in Figure 18.

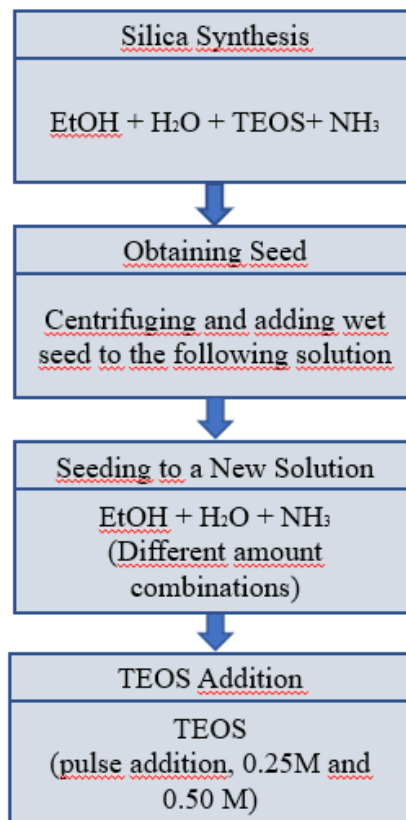


Figure 18. Flowsheet for the effect of TEOS amounts on growth solution

Firstly, silica D was used as seed and same formula which indicated in the Table 7 was used to growth SNPs.

Table 7. Silica D and growth solution study

Components	Seed: Silica D	Growth Solution 1
TEOS	0.50 M	0.50 M
Ethanol	12.14 M	12.14 M
H₂O	11.67 M	11.67 M
NH₃	1.09 M	1.09 M

Secondly, doubled TEOS and EtOH amount in Silica D Method were followed to form seed. Silica D formula was used as a growth solution as seen in Table 8.

Table 8. Modified Silica D and growth solution study

Components	Seed: Modified Silica D	Growth Solution 1
TEOS	1.00 M	0.50 M
Ethanol	28.28 M	12.14 M
H₂O	11.67 M	11.67 M
NH₃	1.09 M	1.09 M

After that, silica C were synthesized and used as seed in three different growth solutions as seen in Table 9.

Table 9. Seed: Silica C (Classic Stöber Method) and different growth solution studies

Components	Seed: Classic Stöber Method (Silica C)	Growth Solution 1	Growth Solution 2	Growth Solution 3
TEOS	0.25 M	0.50 M	0.50 M	0.50 M
Ethanol	12.14 M	12.14 M	12.14 M	24.28 M
H₂O	11.67 M	23.34 M	11.67 M	11.67 M
NH₃	1.09 M	1.09 M	1.09 M	2.18 M

Lastly, doubled TEOS and water amount in Classic Stöber Method were used to obtain seed in three different growth solutions as seen in Table 10.

Table 10. Seed: Modified Silica C and different growth solution studies

Components	Seed: Modified Classic Stöber Method (Modified Silica C)	Growth Solution 1	Growth Solution 2	Growth Solution 3
TEOS	0.50 M	0.50 M	0.50 M	0.50 M
Ethanol	12.14 M	12.14 M	12.14 M	24.28 M
H₂O	23.34 M	23.34 M	11.67 M	11.67 M
NH₃	1.09 M	1.09 M	1.09 M	2.18 M

The seeds formed were collected by centrifuging, washed and diluted with deionized water to stop residual reactions and stored as a stock solution of 15 g/L solid concentration assuming complete conversion of TEOS into silica. Both short and long term stability of this stock solution was controlled after prepared solution of 2h, 5h, 2 weeks and 2 months by using SEM. After obtained stable the seed stock, seed amounts of 75 and 150 mg were transferred into TEOS free Stöber solutions containing EtOH/H₂O/NH₃.

Firstly, 150 mg seed was used and TEOS (same amount as the Stöber solution) was added to the solution with a rate of 0.7 ml/min as summarized in Table 11. After that, the solution was stirred for 4 hours and 24 hours, with samples taken for SEM analysis.

Table 11. Seed from Stöber Method and its growth solution

Components	Seed: Stöber Method	Growth Solution 1
TEOS	0.25 M	0.25 M
Ethanol	12.14 M	12.14 M
H₂O	11.67 M	11.67 M
NH₃	1.09 M	1.09 M

To reduce the rate at which TEOS was added to the growth solution, TEOS and EtOH were mixed, and a TEOS/EtOH ratio of 1/10 was incorporated into the solution by syringa. TEOS/EtOH addition rate in the growth solution was arranged as 1, 2, 4, and 8 ml/min. In this part of experiment, 75 mg of seed was added to growth solution. After reaction was started, SEM analysis were investigated at the end of 4 and 24 hours as seen in Figure 19.

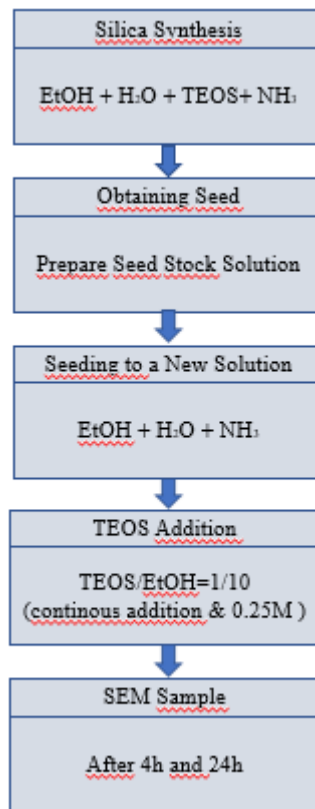


Figure 19. Flowsheet for effect of different seed amount and TEOS addition ratio

To investigate the effect of using different seed amount on the size of synthesized silica particles, the minimum (1 ml/min) and maximum (8 ml/min) TEOS & EtOH addition rate tests were repeated for 150 mg seed.

Lastly, particle size distribution of synthesized monosilica (500-550 nm) and multisize (1.2 μ + 500-550 nm) silica particles were controlled in Mastersizer 3000 (Malvern).

3.2.3 Coating Studies

Synthesized SNPs with different particle size were added into the coil coating mixture at high shear rates around 1200 rpm. After this mixing step, around both monosize and bi-modal 40% SNPs included coil coating mixture were prepared separately and particle size was measured. Since it had broad particle size distribution

(PSD), extra ball mill/shaker process were needed. The primary goal of using a shaker is to ensure that the coating materials are thoroughly mixed, preventing any inconsistencies or separation that may affect the quality of the final coating. When activated, the shaker creates a shaking or stirring action, causing the coating materials to blend together. 150 gram coating was put in a small jar with zirconium balls which around 0.8 – 1 mm. After 2 hour mixing process, coating applied to the primed aluminium metal and cured. Coating application parameters were summarized in Table 12.

Table 12. Coating application values

Layer	Value
Primer	5 micron
Topcoat	10 & 20 micron

The loading of 40% both monosize and bi-modal SNPs in the coatings was varied at concentrations of 35%, 30%, 25%, 20%, 15%, 10%, and 5%. All different percentages were applied to primed metal and cured. To compare the effect of SNPs loading, a blank sample (control sample) was also applied at two different film thicknesses: 10 and 20 microns.

3.2.3.1 Mechanical Tests

Coil coating mechanical tests (according to EN13523) general standard are conducted to evaluate the mechanical properties and performance of coated metal coils. These tests help ensure that the coatings meet the required quality standards and exhibit the desired mechanical characteristics. While specific standards may vary depending on the industry and application, there are some commonly followed standards for coil coating mechanical testing.

In order to analyse the degree of curing in the coated metal, solvent resistance rub test according to ASTM D4752 were applied by using methyl ethyl ketone as a solvent.

In this test, results were compared in 50 rubbing by using DJH Design (MEK 2110).



Figure 20. MEK test (Tunçgenç, 2004)

Another test is impact resistance (EN13523-11, ASTM D2794) test which test assesses the coating's ability to resist impact and deformation. It simulates scenarios where the coated coil may be subjected to impacts or collisions during handling, transportation, or in-service conditions. It was expected that no cracking in 10 J for galvanised steel and 4 J for aluminium steel by using Erichsen (508).



Figure 21. Impact Resistance Test (Tunçgenç, 2004)

T bending test (EN13523-7) is another important test which evaluates the flexibility and adhesion of the coating when the coil is bent or formed into different shapes. It helps determine the coating's ability to withstand bending without cracking or delaminating. Generally, it is expected that 1.5 T OK for topcoats.



Figure 22. T Bent Test, OT image (Tunçgenç, 2004)

Additionally, the hardness of the coating can be measured using various methods such as pencil hardness or indentation tests. This test assesses the coating's resistance to surface scratches, abrasion, and wear. Generally, pencil hardness test (EN13523-4) is used to determine the hardness of the coated panel and general spec is between the F-4H when using Mitsubishi Uni Hi-Uni pencil set.



Figure 23. Pencil Hardness Test (Tunçgenç, 2004)

Adhesion test is another important test to evaluate the ability of the coating to adhere to the substrate and is important for assessing the coating's durability and long-term performance. It involves preparing the coated sample, applying adhesive tape to the surface, removing the tape after a specific time, and visually assessing the tape for any coating damage. No peeling is expected.


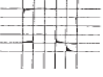



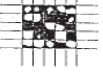
5B	0% None	
4B	Less than 5%	
3B	5 - 15%	
2B	15 - 35%	
1B	35 - 65%	
0B	Greater than 65%	

Figure 24. Adhesion Test Evaluation Specs (Tunçgenç, 2004)

Moreover, in the Clemen scratch test, a sharp or pointed tool is drawn across the coated surface with a specified load and speed. The test aims to evaluate the coating's ability to resist scratches and maintain adhesion to the substrate under mechanical stress. It helps assess the durability and quality of the coating system. The resulting scratch is typically examined visually or using microscopy to assess the adhesion of the coating to the substrate and to determine the coating's scratch resistance by using Elcometer (3000 Motorised). Various factors, such as the length and depth of the scratch, as well as any delamination or detachment of the coating, are considered during evaluation.

3.2.3.2 Coating Characterization

The in-situ size and morphology of the particles were measured by SEM Scanning Electron Microscopy (SEM) (Quanta 250 FEG) at present time intervals. A drop of colloidal suspension from the reaction solution was placed on an aluminium foil and dried in air; the sample was then coated by gold (Au) film before analysis. Also, the chemical structures of the samples were determined using Fourier Transform Infrared Spectroscopy (FTIR) (Perkin Elmer Spectrum One) in the wavenumber range of 4000-450 cm^{-1} . The

pellets for samples were prepared for the analysis. First, certain amount of silica particle was mixed with potassium bromide (KBr) (3 mg sample in 150 mg KBr-silica sample). Then, the samples were grounded in a mortar and pressing. The zeta (ζ) potentials were determined by Malvern (Zetasizer NanoZS). Additionally, Mastersizer was used to obtain particle size distributions.

The contact angle with water was measured by dropping 2 microliter water droplets on the NSPs added coated films by The Krüss (DSA100) which is a contact angle measuring instrument developed by Krüss GmbH. Rheometer (Anton Paar MCR 302) was used to analyse the rheology of the coating mixtures. Also, topography of surface was analysed by using AFM (Bruker-MMSPM Nanoscope 8).

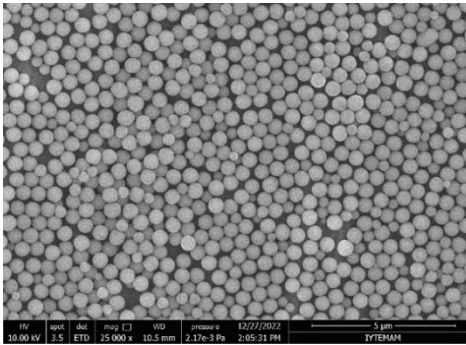
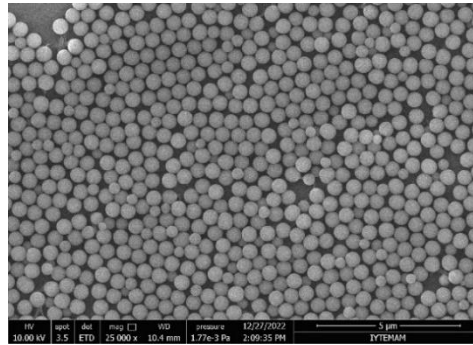
CHAPTER 4

RESULT AND DISCUSSION

4.1 Characterization of Stöber Silica SNPs

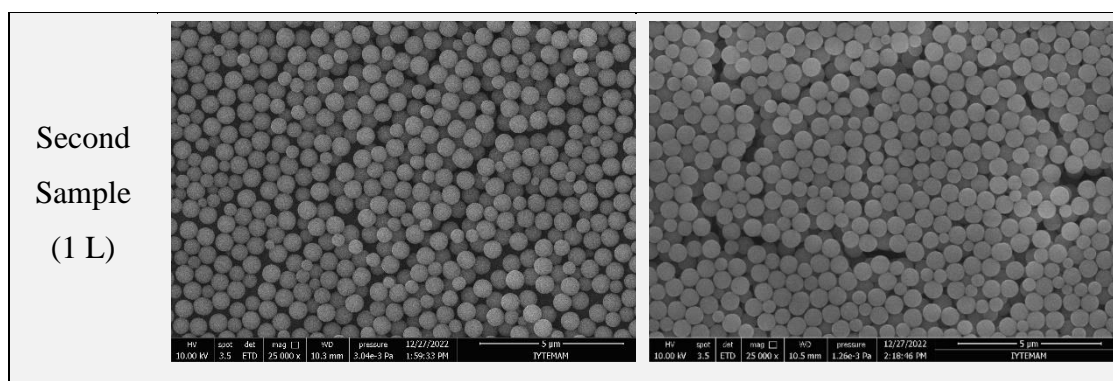
In a typical synthesis, the Classic Stöber method was employed, using a mixture of 0.25 M TEOS, 1.09 M NH₃, 12.14 M EtOH, and 11.67 M H₂O. This synthesis yielded solid silica particles that were perfectly spherical and exhibited monodisperse characteristics. The size and size distributions of these particles were analysed after 2 and 24 hours of the synthesis, and the results are presented in Table 13. Two different samples were prepared solutions of 100 ml and 1L, aiming to assess reproducibility and repeatability across small and large scales. The SEM images illustrated that the particles had an average size of 500-550 nm and displayed a uniform size distribution. This result was also supported by the particle size distribution as shown in Figure 25 in the following pages.

Table 13. SEM images of SNPs with different batches after 2 and 24 hours of synthesis

Sample	After 2 h	After 24 h
First Sample (100 ml)		

(cont. on next page)

Table 13 (cont.)



It was observed that the SNPs obtained after 2 hours and 24 hours at the beginning of the reaction were identical to each other. It was seen that average particle size of synthesized particles was 500-550 nm in SEM images. In addition, no differences were observed between the small- and large-scale samples.

It was observed that the SNPs obtained after 2 hours and 24 hours at the beginning of the reaction were identical to each other. In addition, no differences were observed between the small- and large-scale samples. It was seen that average particle size of synthesized particles were 500-550 nm in SEM images. This data was also verified from the particle size distribution measurements.

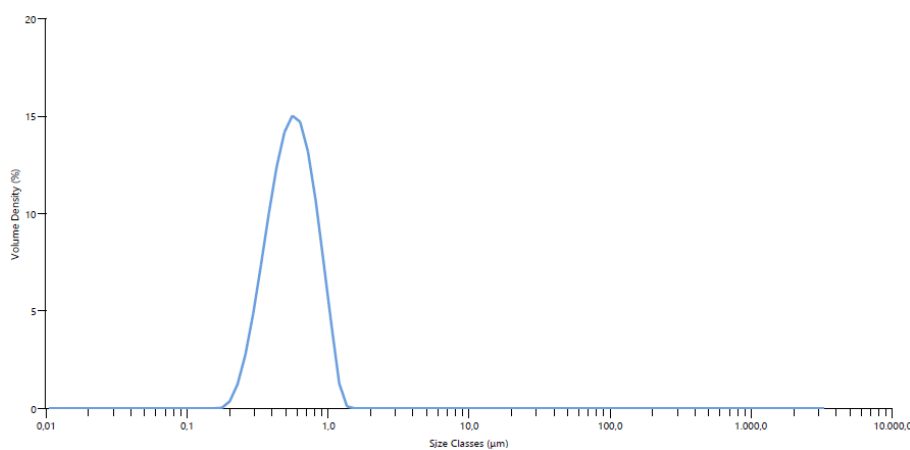


Figure 25. Particle Size Distribution of Stober Silica Particles

Particle size distribution in powders is commonly characterized by three values, denoted as "D" for distribution. D10 represents the size below which 10% of the particles

in the powders are smaller. D50 or DV(0.5) indicates that 50% of the total particles are smaller than this size. D90 or DV(0.9) signifies that 90% of the total particles are smaller than this size. This data can be presented in the form of a graph or table. Both sets of data are provided below.

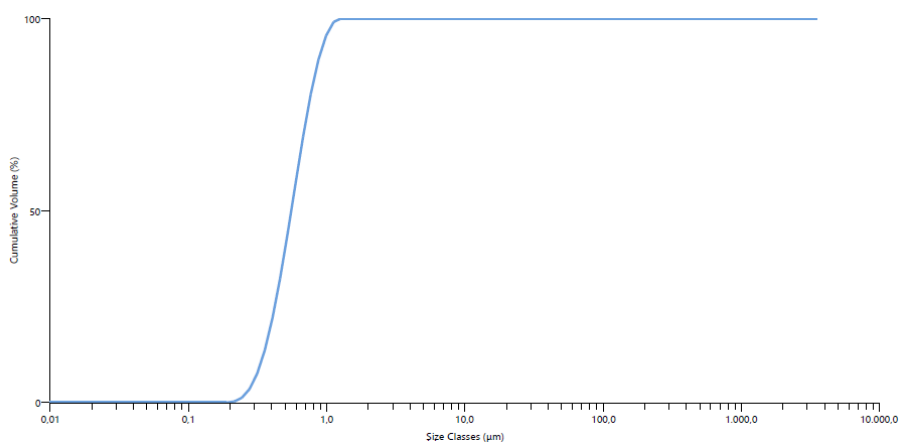


Figure 26. Cumulative Volume (%) vs Size Classes (μm)

Average particle size was obtained as 550 nm which also showed in D_x (50) μm of particle size distribution in the Table 14.

Table 14. Particle Size Distribution and Specific Surface Area of SPNs

Sample	D_x (10) (μm)	D_x (50) (μm)	D_x (90) (μm)	Specific Surface Area (m^2/g)
Stöber SNPs	0.331	0.554	1.12	11.75

Additionally, the zeta potential of these particles' distribution graph is shown in Figure 27.

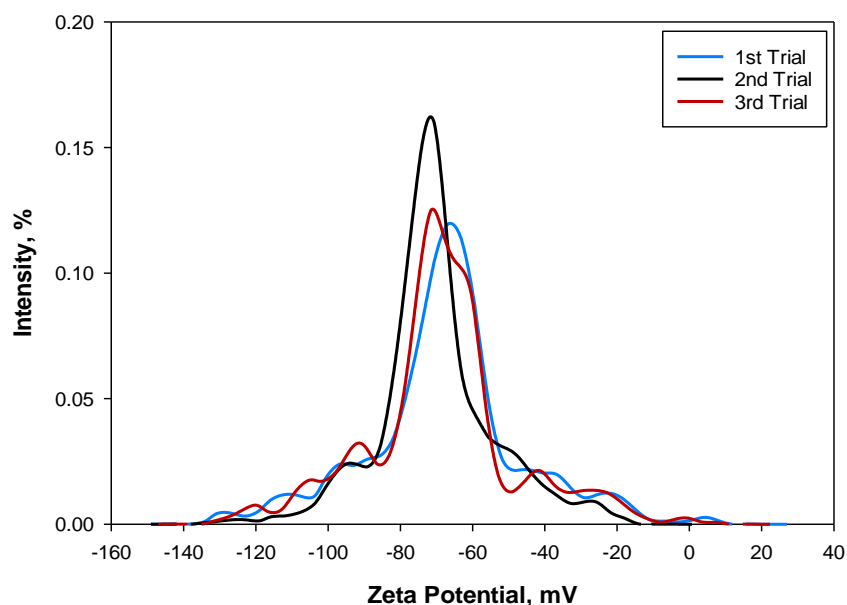


Figure 27. The zeta potential of Stöber Silica Particles

In the Stöber synthesis, firstly only TEOS amount, then different combinations of concentrations of water, ammonium hydroxide, TEOS and ethanol were changed and additionally different modes of TEOS addition were studied, and the results were given.

4.1.1 Effect of TEOS Concentration

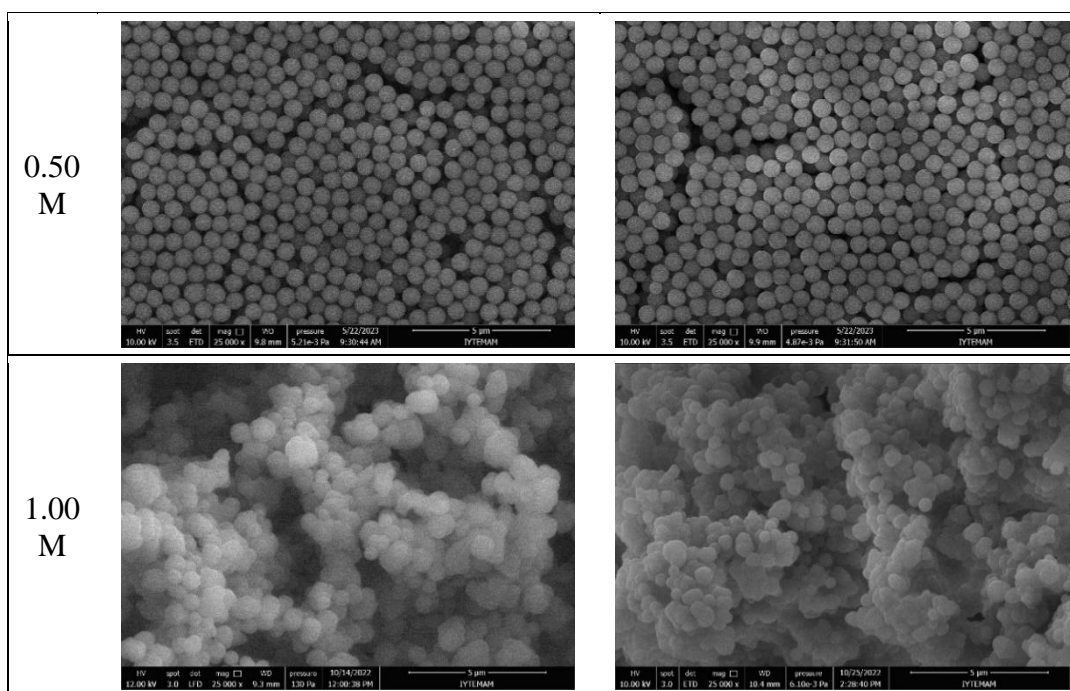
In this part, concentration of water, ammonium hydroxide and ethanol were kept constant. To observe the effect of TEOS concentration on the size and shape of the synthesized SNPs, the TEOS concentration was altered to 0.0625 M, 0.125 M, 0.25 M, 0.50 M, and 1 M.

Table 15. SEM images of SNPs with different TEOS amounts (M) after 2 and 24 h

TEOS load	After 2 h	After 24 h
0.0625 M		
0.125 M		
0.25 M		

(cont. on next page)

Table 15 (cont.)



TEOS concentration of Stöber method was decreased in the first two samples. When TEOS amount was used as 0.0625 M, it was seen that SNPs with the size of 400-470 nm particle size were obtained. In case of TEOS amount was increased from 0.065 M to 0.125 M, particle size of SNPs was increased to 450-530 nm. Addition to these, TEOS concentration of Stöber method was also increased. When TEOS amount was increased from 0.25 M to 0.50 M, it was seen that particle size of synthesized SNPs were also increased up to 590-620 nm. Lastly, 1 M TEOS concentration was used in the reaction, resulting in the formation of particles that did not exhibit a spherical or monodisperse morphology. SEM pictures revealed the presence of a slime-like structure between the formed particles. Additionally, the particles exhibited a wide size distribution ranging from 400 to 700 nm. Upon further increasing the TEOS concentration, particle formation ceased. This observation indicates that the Stöber reaction method has a critical and optimized ratio between the ingredients.

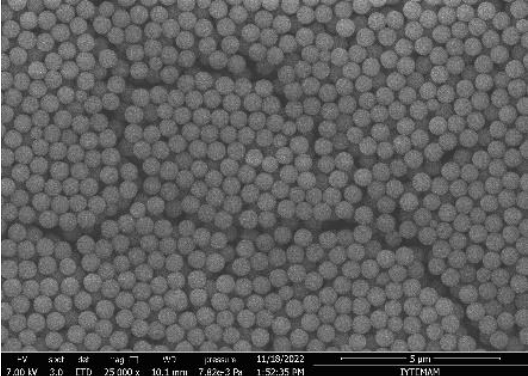
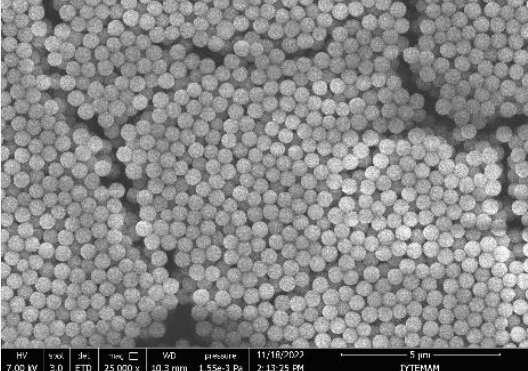
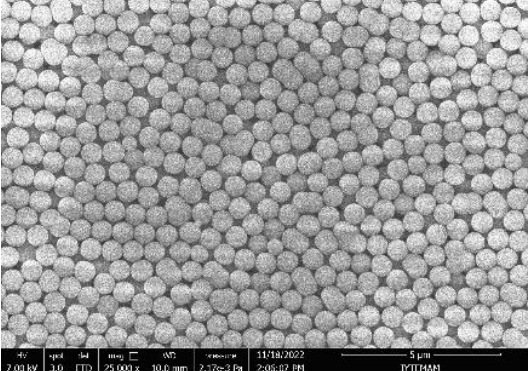
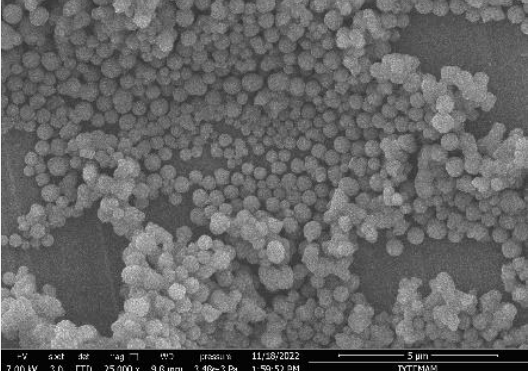
All in all, 0.25 M (Classic Stöber: Silica C) and 0.50 M (Silica D) TEOS produced larger, spherical, and monodisperse particles. As a result, these two formulations were used for the remaining experiments. Also, in all samples, it was determined that the SEM photo taken after 2 hours was identical to the one taken after 24 h. Hence, it can be concluded that waiting for 24 h is unnecessary for the completion of the reaction.

4.1.2 Effect of TEOS & Other Components Concentrations

In this phase of the study, a sequential doubling of TEOS and each component in the Silica C and Silica D Methods was carried out to examine the particle shape and size distribution. In accordance with the information provided in the preceding section, investigations were undertaken on these formulations due to the known capability of the silica C and silica D methods to produce larger and more uniform particles.

The research began by conducting experiments using the Classic Stöber method. Initially, the quantity of TEOS and ethanol was doubled to assess its impact. Additionally, a separate batch involved doubling the TEOS and water amounts. Lastly, by doubling the TEOS and ammonium hydroxide, the study examined how variations in TEOS concentration and other ingredients affected the size, shape, and morphology of the resulting particles.

Table 16. SEM images of SNPs with different concentration (M) combinations after 2 h

Method	After 2 h
<p>Stöber Method (Silica C) (500-550 nm)</p>	
<p>Doubled TEOS & EtOH loading (470-500 nm)</p>	
<p>Doubled TEOS & Water loading (650-670 nm)</p>	
<p>Doubled TEOS & Ammonium hydroxide loading (470-480 nm)</p>	

The Stöber process involves the hydrolysis of TEOS in the presence of water and a catalyst, typically ammonium hydroxide, resulting in the formation of silanol groups. A higher TEOS concentration provides more precursor molecules for hydrolysis and condensation reactions. These silanol groups then undergo condensation reactions, forming siloxane bonds and facilitating the growth of silica particles.

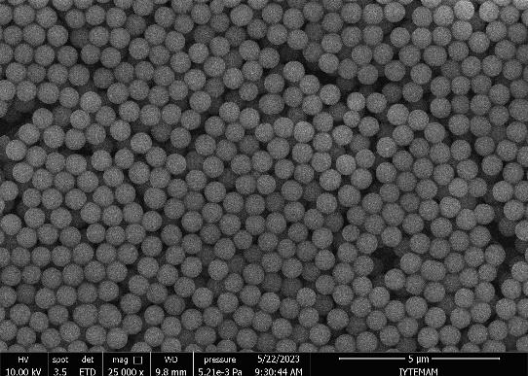
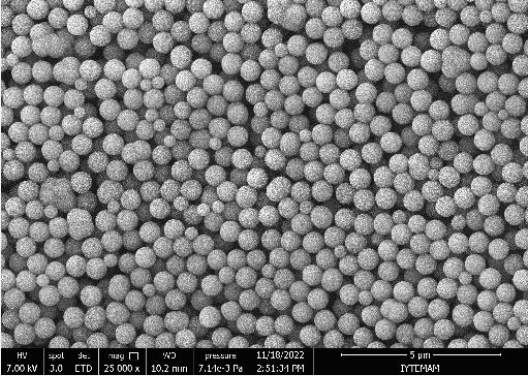
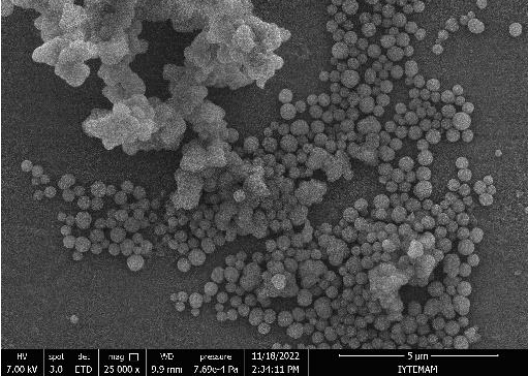
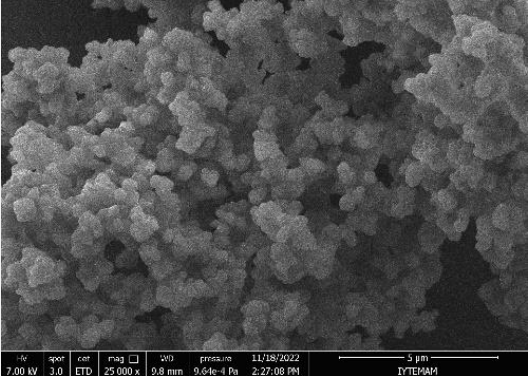
An interesting observation was made when both TEOS and EtOH concentrations were doubled, leading to a slight decrease in particle size from 500-550 nm to approximately 470-500 nm. Remarkably, despite this reduction, the particles maintained their original spherical shape, demonstrating their impressive stability. EtOH, functioning as a solvent in the Stöber reaction, plays a crucial role in controlling particle growth and aggregation by acting as a steric stabilizer. The smaller size of the obtained nanoparticles can be attributed to the steric stabilizing effect of EtOH, which prevents particle clumping and the formation of larger structures. It means that TEOS concentration provides more precursor molecules for hydrolysis and condensation reactions, while an increased EtOH concentration ensures system stability and prevents excessive particle growth or agglomeration.

Additionally, doubling the amounts of TEOS and water resulted in the formation of the largest spheres, measuring 650-670 nm. Increasing the water content in the reaction promotes faster hydrolysis of TEOS and the formation of more reactive silanol groups. These additional silanol groups accelerate the condensation reactions and may contribute to the growth of larger silica particles.

On the other hand, doubling both the TEOS and ammonium hydroxide amounts resulted in the formation of agglomerates and prevented the particles from assuming a spherical shape, even though they achieved similar particle sizes as in the experiment where TEOS and EtOH amounts were increased. The higher concentration of ammonium hydroxide in the reaction promotes the hydrolysis of TEOS and subsequent condensation reactions. The increased TEOS concentration allows for a more efficient conversion of TEOS into silanol groups and subsequent condensation, potentially resulting in the formation of smaller silica particles.

The same set of experiments was also conducted using the silica D method, which resulted in larger particles compared to those obtained in the Stöber method. Thus, in the silica D method, where twice the amount of TEOS is used compared to the Stöber method, it was observed how doubling the TEOS amount, along with other ingredients, impacts the structure, shape, and size of the synthesized nanoparticles.

Table 17. SEM images of SNPs with different concentration (M) combinations after 2 h

Method	After 2 h
<p>Silica D (590-620 nm)</p>	 <p>Technical data: HV 10.00 kV, spot 3.5, det ETD, mag 25 000 x, WD 9.8 mm, pressure 5.21e-3 Pa, 5/22/2023 9:30:44 AM, 5 µm scale bar, ITEM48</p>
<p>Doubled TEOS & EtOH loading (650-680 nm)</p>	 <p>Technical data: HV 7.00 kV, spot 3.0, det ETD, mag 25 000 x, WD 10.2 mm, pressure 7.11e-3 Pa, 11/18/2022 2:51:31 PM, 5 µm scale bar, ITEM49</p>
<p>Doubled TEOS & Water loading (380 - 400 nm)</p>	 <p>Technical data: HV 7.00 kV, spot 3.0, det ETD, mag 25 000 x, WD 9.9 mm, pressure 7.66e-4 Pa, 11/18/2022 2:34:11 PM, 5 µm scale bar, ITEM49</p>
<p>Doubled TEOS & Ammonium hydroxide loading (280 - 300nm)</p>	 <p>Technical data: HV 7.00 kV, spot 3.0, det ETD, mag 25 000 x, WD 9.8 mm, pressure 9.64e-4 Pa, 11/18/2022 2:27:08 PM, 5 µm scale bar, ITEM49</p>

The particles synthesized using the silica D method exhibit similarities to the TEOS doubled version in the silica C method. These particles have dimensions ranging from 590-620 nm, as indicated in Table 17.

By doubling the concentrations of TEOS and EtOH, slightly smaller particles were obtained compared to the Stöber particle sizes in the previous study. However, in this study, contrary to the previous findings, it was observed that perfectly spherical particles measuring approximately 650-680 nm were produced using the silica D method. This difference can be attributed to the steric stabilizing effect of EtOH, which prevented agglomeration and allowed for controlled growth of larger nanoparticles, with the use of Teos approximately 4 times higher than in the Stöber method.

Moreover, in the scenario where both the amount of TEOS and water is doubled, it was anticipated that the nanoparticle sizes would increase, consistent with previous results. The increased quantity of water in the reaction is expected to enhance the hydrolysis of TEOS. However, due to insufficient water in the medium relative to the amount of TEOS involved in the hydrolysis reaction, the particles likely did not fully form, resulting in agglomeration and the inability to achieve a monosize distribution.

The previous results confirm that doubling both the TEOS and ammonium hydroxide amounts led to the formation of agglomerates, preventing the particles from maintaining a spherical shape. Similar outcomes, characterized by the presence of agglomerated nanoparticles, were observed, and are illustrated in Table 15.

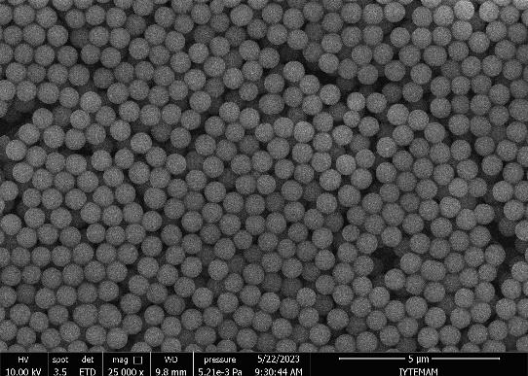
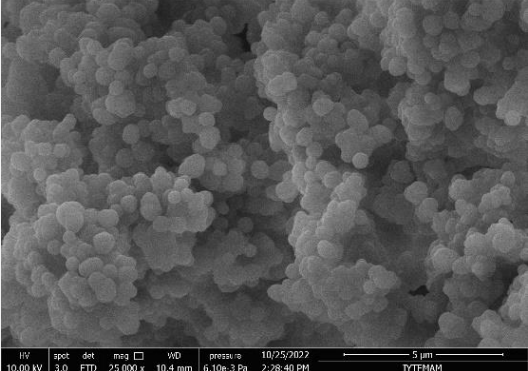
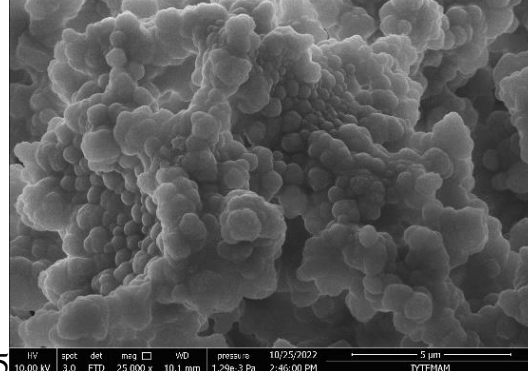
4.1.3 Seed Addition (Seeded Growth)

The addition of seeds to the Classic Stöber method introduces variations in particle size distribution, depending on the concentration of seeds and the mode of TEOS addition. TEOS, can either precipitate on the surface of existing seeds, leading to an increase in their diameter, or precipitate as new nuclei. Based on this understanding, the mechanisms behind the formation of colloidal silica in the presence of high seed concentrations are discussed in this study. Effect of different seed particle size, seed amount and TEOS addition rate parameters on obtained silica particles were investigated in this part of experiment.

4.1.3.1 Effect of Different Seed Size

In this phase of the experiment, two distinct seeds were synthesized using different concentrations of TEOS, namely 0.5 M and 1 M. The SEM analysis revealed that the seed prepared with 0.5 M TEOS exhibited excellent dispersion, while the sample prepared with 1 M TEOS showed a tendency towards agglomeration. The objective of selecting these seeds was to investigate their ability to maintain their properties and form perfect spheres during the growth process, despite their differing morphologies. Initially, the 0.5 M TEOS method, known as silica D, was employed to prepare the seeds. Subsequently, a TEOS-free Stöber reaction solution was utilized for the growth process. The growth was achieved by introducing pulses of 1.75 M and 3 M TEOS into the solution. After 2 hours of the reaction initiation, SEM samples were collected and analyzed, as depicted below:

Table 18. Effect of using silica D as seed and their different growth solutions

Method	After 2 h
Seed: Silica D (590-620 nm)	
1.75 M TEOS used in growth solution	
3 M TEOS used in growth solution	

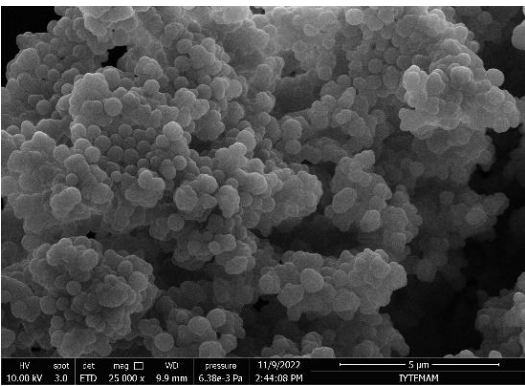
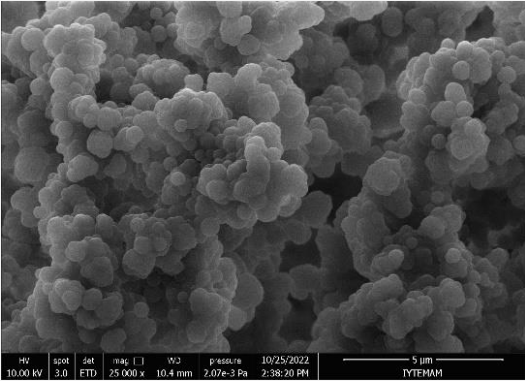
Upon examining the results, it becomes evident that attempting to grow spherical nanoparticles using an excessive amount of TEOS in an alternative Stöber solution led to the formation of agglomerated particles. This outcome aligns with the agglomerated particles observed in the findings presented in Table 16. The hindered formation of spherical particles can be attributed to the lack of sufficient other components for TEOS in the environment. Further details regarding the experiment, which involve entering the appropriate amount of TEOS in the Stöber reaction, will be discussed in the subsequent

experiments.

After perfect particles were employed as seeds, resulting in the formation of agglomerated grains. Subsequently, the focus shifted to investigating the process of obtaining grains by utilizing agglomerated particles as seeds.

In the second part of the experiment, seeds obtained using a 1 M TEOS concentration displayed clear agglomeration, as observed in their SEM images presented in Table 15. To facilitate the growth process, a TEOS-free Stöber reaction solution was employed. The growth was initiated by introducing pulses of 1.75 M TEOS into the solution. Following the same procedure, SEM samples were collected and analyzed after 2 hours of the reaction initiation, as depicted in Table 19.

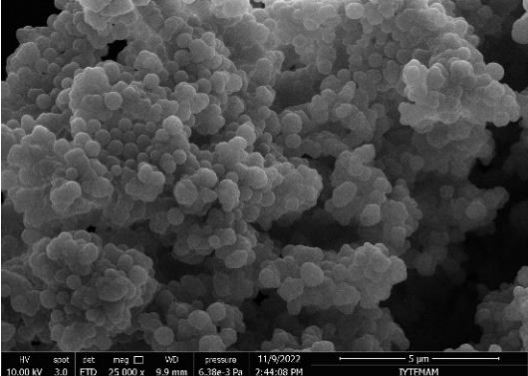
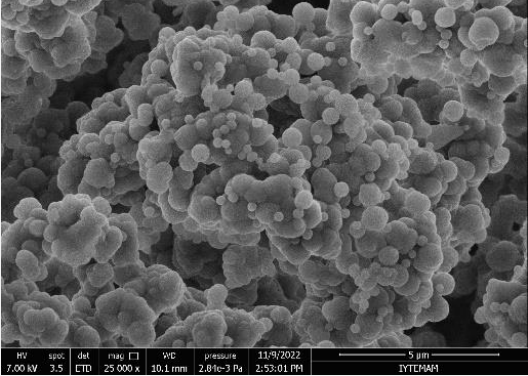

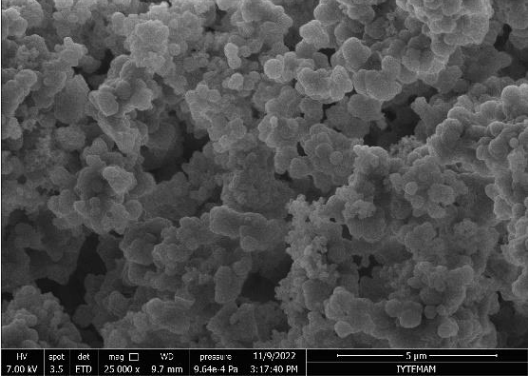
Table 19. Seed synthesis by using 1 M TEOS & 1.75 M TEOS in growth solutions

Method	After 2 h
Seed: 1 M TEOS concentration (350-450 nm)	
1.75 M TEOS used in growth solution	

After conducting the initial concentration trial of TEOS in this part, a significant increase in agglomeration was observed. Additionally, the particles lost their spherical shape and became more elongated. As a result, further increases in TEOS and other components were not considered for this study. Instead of pulse addition, the continuous addition mode was analyzed. Continuous TEOS addition to the solution, along with continuous addition of different component combinations, was also investigated.

During the continuous addition phase, a steady stream of TEOS with a concentration of 0.5 M was introduced to the TEOS-free Stöber solution at a constant rate of 5 ml/min. The concentrations of ammonium hydroxide, water, and EtOH in the Stöber reaction were the same. In the next step, TEOS, ammonium hydroxide, and water were simultaneously added to the medium containing only EtOH, maintaining the same addition rate of 5 ml/min. Lastly, a coordinated addition of TEOS, ammonium hydroxide, and water took place in the medium containing both EtOH and ammonium hydroxide, also at a rate of 5 ml/min.

Table 20. Seed synthesis by using 0.5 M TEOS and their different growth solutions

Method	After 2 h
<p>Seed: 1 M TEOS concentration (350-450 nm)</p>	
<p>0.50 M of TEOS was added with a rate of 5 ml/min</p>	
<p>TEOS, ammonium hydroxide and water were added to medium containing only EtOH with 5ml/min</p>	
<p>TEOS, ammonium hydroxide, and water were added to medium containing EtOH and ammonium hydroxide with 5ml/min</p>	

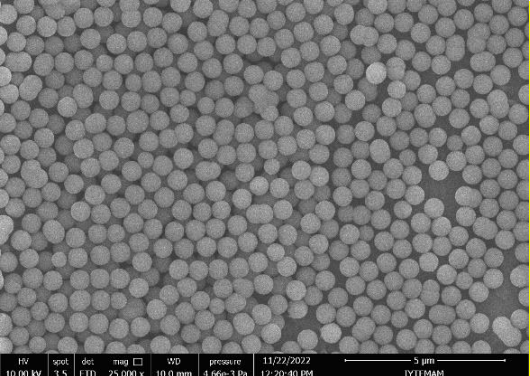
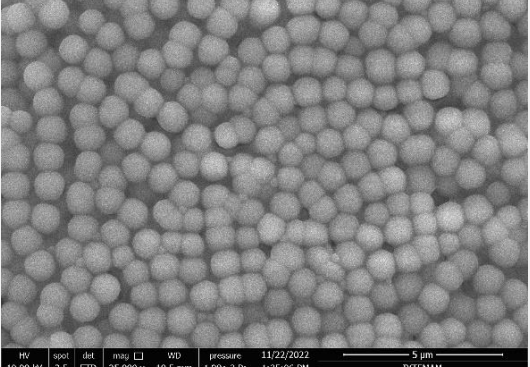
The continuous addition of TEOS in the Stöber method offers several advantages, including improved reaction control, enhanced mixing, and reduced supersaturation due to the time required for diffusion. Accordingly, TEOS was introduced gradually into the solution. However, it was noted that using agglomerated seed particles did not produce superior results compared to trials using spherical and larger particles. The experimental process involved dispersing the seed particles in EtOH initially, followed by the addition of TEOS, ammonium hydroxide, and water to the solution. Subsequently, ammonium hydroxide was incorporated into the growth solution, both in conjunction with TEOS in a syringe and in the TEOS-free medium. Across all experimental setups, it was observed that the use of agglomerated seeds hindered the formation of spherical silica nanoparticles in the final growth solution.

After analyzing the findings from the previous results, it was determined that conducting new experiments using four distinct methods as seed sources would be beneficial. These methods comprised the only silica D method and the silica D method with doubled TEOS and EtOH concentrations, resulting in 650-680 nm particles. Additionally, the only Classic Stöber method and the Classic Stöber method producing 650-670 nm particles were utilized in the experiments.

4.1.3.2 Effect of TEOS Amounts on Growth Solution

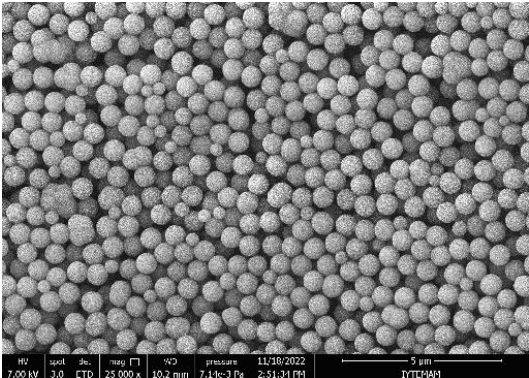
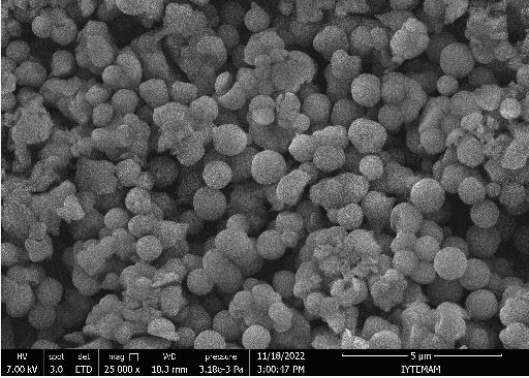
In this phase of the experiment, four different seeds were employed for the growth process. Initially, the Silica D Method with a TEOS concentration of 0.50 M was utilized to synthesize the first set of seeds. Subsequently, the same formulation was employed for the growth process. Initially, EtOH, water, and ammonium hydroxide were combined in a separate batch, followed by the addition of seeds to the solution. Once thorough dispersion was achieved, 0.5 M TEOS was added directly to the solution.

Table 21. Seed Silica D and covering with same formula, pulse TEOS 0.5 M addition

Method	After 2 h
Seed: Silica D (590-620 nm)	
0.50 M TEOS added directly in the growth solution (Obtained particles: 800-950 nm)	

The study yielded grains measuring 800-900 nm in size. During SEM analysis, random spots were examined, revealing newly synthesized particles in the range of 500-600 nm. These particles exhibited a distinct spherical shape. Intriguingly, a gel-like or mud-like structure was observed enveloping the surface of the formed grains. This observation implies that the quantity of EtOH, responsible for stabilizing the formulation, might have been inadequate. Therefore, in the subsequent investigation, a modified silica D formulation was synthesized as a seed, featuring doubled amounts of EtOH and TEOS. With the same procedure, another seed was synthesized using 1 M TEOS, 24.28 M EtOH, 11.67 M water, and 1.09 M ammonium hydroxide. These concentrations corresponded to the doubled amount of EtOH and TEOS in the silica D method. After obtaining these seeds, another batch was prepared using the silica D method without TEOS (12.14 M EtOH, 11.67 M water, and 1.09 M ammonium hydroxide), and the seeds were dispersed into the TEOS-free solution. After that, 0.5 M TEOS was added directly to the solution.

Table 22. Seed: doubled amount of TEOS and EtOH in Silica D and covering with silica D formula, pulse TEOS 0.5 M addition

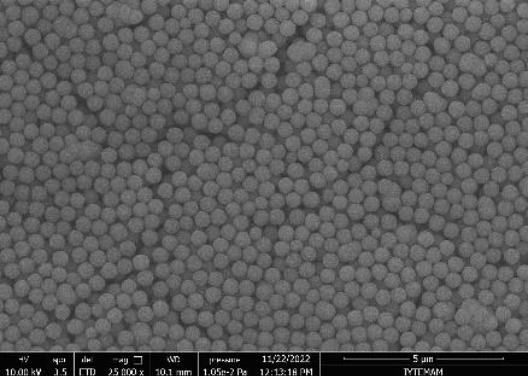
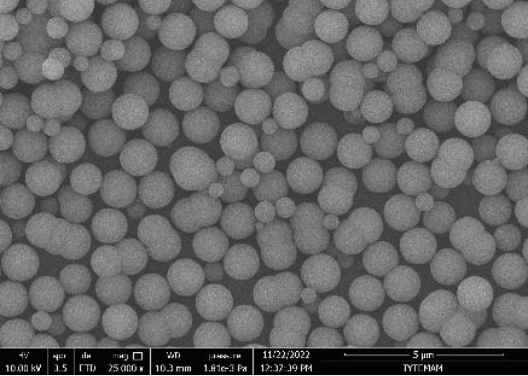
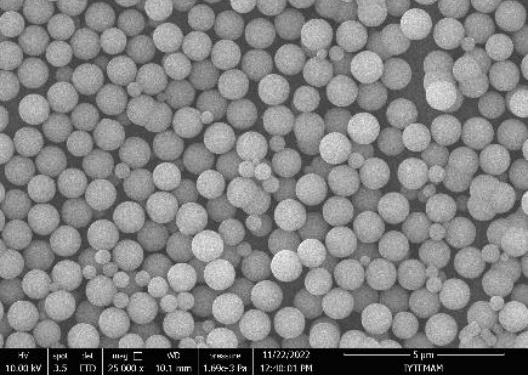
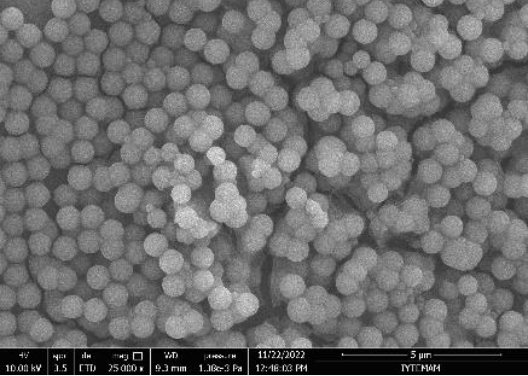
Method	After 2 h
Seed: doubled amount of EtOH and TEOS in the silica D method (650-680 nm)	
0.50 M TEOS added directly in the growth solution (Obtained particles: 1 μm + 450 -500 nm)	

In this phase of the experiment, nanoparticles of different sizes, approximately 1 μm plus 450-500 nm, were successfully obtained. It is noteworthy that this is the first observation of nanoparticles around 1 μm in size using the Stöber method. However, it was observed that these particles tended to agglomerate and did not possess a spherical shape. These findings, combined with previous results, indicate that it is indeed possible to synthesize larger particles using the Stöber method; however, further optimization of the ingredient proportions is required.

Based on these findings, seeds were synthesized using the Classic Stöber method. This phase of the experiment involved three different groups of growth solutions: doubled amount of TEOS & water classic Stöber growth solution, the silica D Method, and a modified silica D Method with doubled amounts of TEOS and EtOH. Initially, the seeds were obtained through the Classic Stöber reaction. Subsequently, the obtained seeds were re-dispersed in a separate first batch that lacked TEOS but contained the same values as the Classic Stöber reaction, namely 12.14 M EtOH, 23.34 M water, and 1.09 M

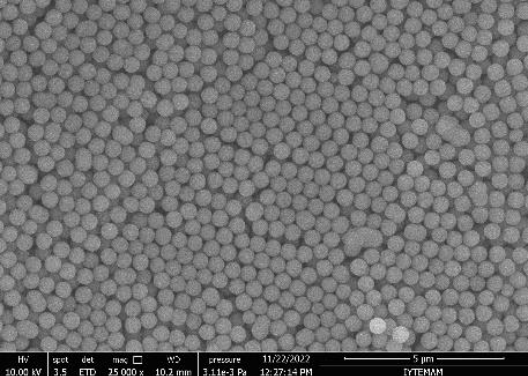
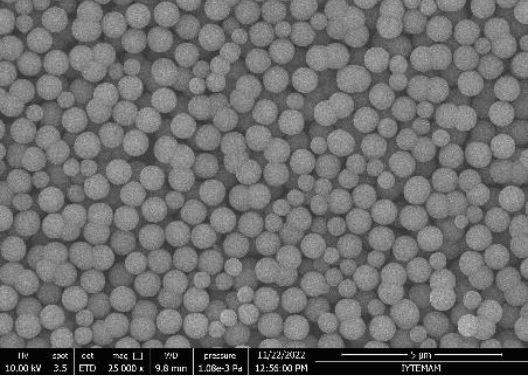
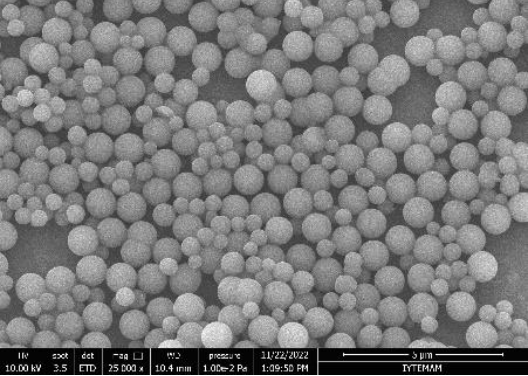
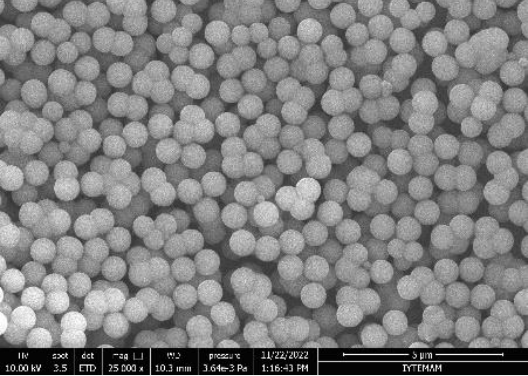
ammonium hydroxide. Following this, a direct addition of 0.5 M TEOS was made to the reaction. Additionally, a second batch was prepared, which was TEOS-free but had the same concentrations of 12.14 M EtOH, 11.67 M water, and 1.09 M ammonium hydroxide as the first batch. However, this time 0.5 M TEOS was added directly instead of 0.25 M. In the last batch, the seed was dispersed in a mixture of 24.28 M EtOH, 11.67 M water, and 1.09 M ammonium hydroxide. Subsequently, 0.5 M TEOS was directly added to the mixture. After allowing the reaction to proceed for 2 hours, an SEM sample was taken from the solution.

Table 23. Seed: Silica C and their different growth solutions

Method	After 2 h
<p>Seed: Stöber Method (Silica C) (500-550 nm)</p>	
<p>1st batch – Classic Stöber Method with doubled TEOS and water concentrations (Obtained particles: 900 nm + 500-600 nm)</p>	
<p>2nd batch - Silica D Method (Obtained particles: 1.1 μm + 200 nm)</p>	
<p>3rd batch - Silica D method with doubled TEOS and EtOH concentrations (Obtained particles: 650 – 750 nm)</p>	

In this study, it was observed that all the particles synthesized from the growth solution exhibited a perfect spherical shape without any agglomeration. However, when the seed obtained from the Classic Stöber method was grown using the silica D method, which involved doubling the amount of TEOS compared to the Stöber method, larger and more perfectly spherical particles were obtained. The resulting particle sizes were 1.2 microns and 200 nm, which were significantly smaller than the initial seed size. This indicates that new reactions were still ongoing, and a gradual addition of TEOS was necessary instead of a pulse addition. Furthermore, it can be concluded that there was insufficient time for the diffusion of silica molecules to the seed particles for their growth. Subsequently, the seed obtained from the Classic Stöber Method, which consisted of doubled amounts of TEOS and water, was used in the growth solution, following the same experimental procedure as before.

Table 24. Doubled amount of TEOS and water in Silica C and their different growths

Method	After 2 h
<p>Seed: Doubled amount of TEOS and water in the Classic Stöber Method (500-520 nm)</p>	
<p>1st batch – Doubled amount of TEOS and water in the Classic Stöber Method (Obtained particles: 650 – 750 nm)</p>	
<p>2nd batch - Silica D Method (Obtained particles: 650 – 750 nm)</p>	
<p>3rd batch - Silica D method with doubled TEOS and EtOH concentrations (Obtained particles: 650 – 750 nm)</p>	

The observation was made that particles in the micron size range could not be obtained in this instance. The likely reason for this is the excessive amounts of TEOS and water used in comparison to the Classic Stöber Method. Following the synthesis of the seed using this formula, the formation of particles in the growth solution may be adversely affected by the pulse addition of TEOS. Consequently, the decision was made to continue using the seed obtained from the Classic Stöber Method and gradually introduce TEOS, allowing ample time for the silica molecules to diffuse through the seed particles. To avoid preparing new seed for each set of experiments and minimize the potential for experimental error, it became necessary to prepare a stable stock seed solution, if feasible. The following section explains the preparation of the seed stock solution and the controls implemented to ensure its stability.

4.1.3.3 Effect of Different Seed Amount and TEOS Addition Rate

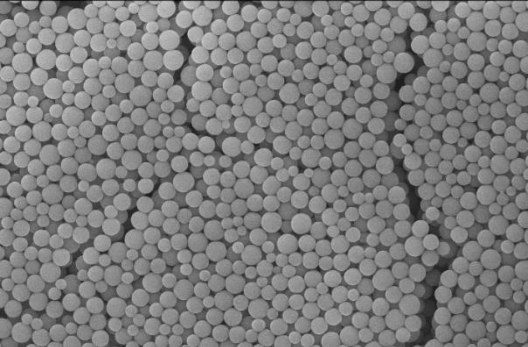
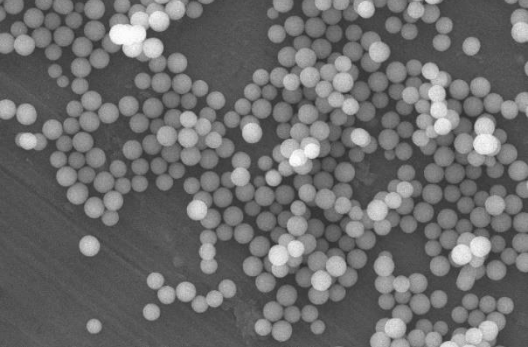
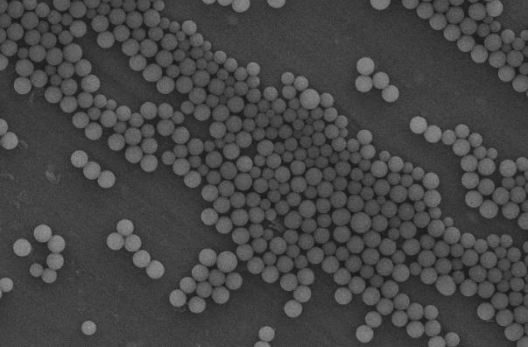
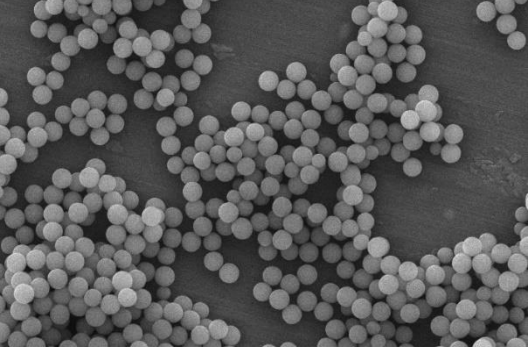
The stock solution of seed plays a crucial role in the Stöber reaction, offering multiple advantages. Firstly, it serves as a source of pre-formed silica nanoparticles that act as nuclei for the growth of larger particles during the synthesis process. These seed particles act as templates, facilitating the formation of uniform and controlled-size silica particles. By adjusting the concentration of the seed solution, researchers can manipulate the rates of nucleation and growth, granting them further control over the synthesis.

Moreover, the stock solution of seed enables enhanced control over the final particle size distribution. Careful adjustment of the seed solution concentration allows researchers to influence the rates of nucleation and growth, resulting in the desired particle sizes. This level of control is essential for achieving monodispersity, which refers to particles of similar sizes without significant variation. Furthermore, employing a consistent and well-characterized stock solution ensures that the same seed material is utilized in multiple synthesis batches, leading to more reliable and comparable outcomes. Overall, the stock solution of seed significantly enhances the reproducibility and control of the Stöber growth reaction.

To obtain the seed solution, a Classic Stöber solution was prepared, and the reaction was initiated for a duration of 2 hours. The resulting seeds were then collected through centrifugation. These nanosilica particles were subsequently dispersed in water.

This process effectively halted residual reactions and yielded a stock solution with a solid concentration of 15 g/L, assuming complete conversion of TEOS into silica. The stability of this stock solution was evaluated using scanning electron microscopy (SEM). Samples were taken for SEM analysis at 2 hours and 5 hours after the start of dispersion. Additionally, to assess long-term stability, new samples were collected from the stock solution after 2 weeks and 2 months, allowing for a comparison of both short-term and long-term stability.

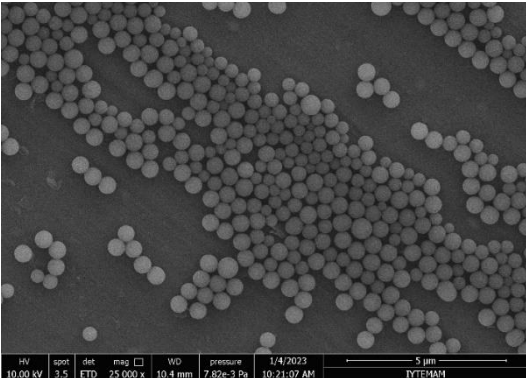
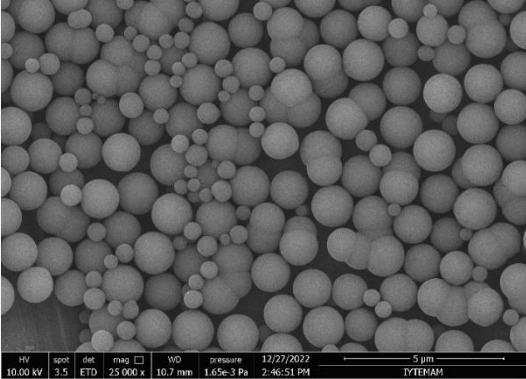
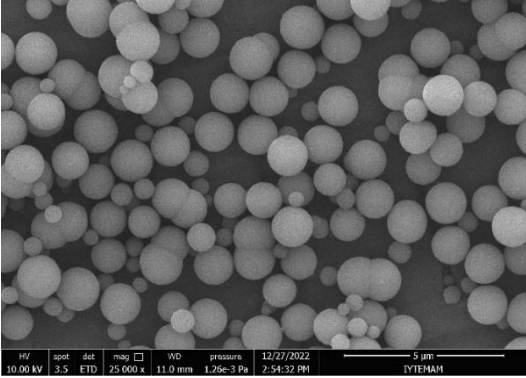
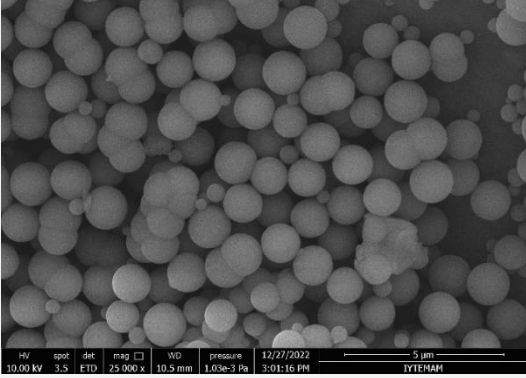
Table 25. Seed Stock Stability Control SEM images

Seed Stock Stability	SEM Images
After 2 hours	 <p>Technical data for SEM image (After 2 hours): HV: 10.00 kV, spot: 3.5, det: ETD, mag: 25 000 x, WD: 10.6 mm, pressure: 3.48e-3 Pa, 12/27/2022 2:36:02 PM, 5 µm scale bar, IYTEMAM.</p>
After 5 hours	 <p>Technical data for SEM image (After 5 hours): HV: 10.00 kV, spot: 3.5, det: ETD, mag: 25 000 x, WD: 10.7 mm, pressure: 2.17e-3 Pa, 12/27/2022 2:42:05 PM, 5 µm scale bar, IYTEMAM.</p>
After 2 weeks	 <p>Technical data for SEM image (After 2 weeks): HV: 10.00 kV, spot: 3.5, det: ETD, mag: 25 000 x, WD: 10.4 mm, pressure: 7.82e-3 Pa, 1/4/2023 10:21:07 AM, 5 µm scale bar, IYTEMAM.</p>
After 2 months	 <p>Technical data for SEM image (After 2 months): HV: 10.00 kV, spot: 3.5, det: ETD, mag: 25 000 x, WD: 10.3 mm, pressure: 1.77e-3 Pa, 1/4/2023 10:38:18 AM, 5 µm scale bar, IYTEMAM.</p>

Silica nanoparticles with a size range of 500-550 nm were successfully synthesized using the Classic Stöber Method. Following centrifugation and the preparation of the seed solution, the stability of the particles was evaluated over both short and long periods. Remarkably, the shape, size, and morphology of the synthesized particles remained unchanged throughout the duration of the study, indicating the robustness and reliability of the stock seed solution as a crucial and practical approach for growth solutions.

After the seed stock solutions were prepared, a seed quantity of 150 mg was selected to initiate the trials for the growth solution. Initially, a TEOS-free Stöber solution was prepared, and the 150 mg seed was dispersed into this solution. Following that, 0.25 M TEOS was gradually added to the solution at a rate of 0.7 ml/min. Previous research has emphasized the critical importance of allowing enough time for TEOS diffusion and the subsequent growth of the seed particles. Therefore, further investigations were undertaken to explore and understand the time-dependent dynamics of this process. Samples were taken at 2 hours, 6 hours, and 24 hours after the initiation of the reaction to facilitate this exploration and gain deeper insights into the process.

Table 26. Using 150 mg seed and 0.25 M TEOS added at a rate of 0.7 ml/min for growth solution

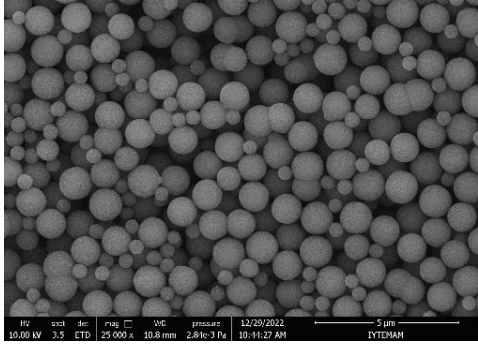
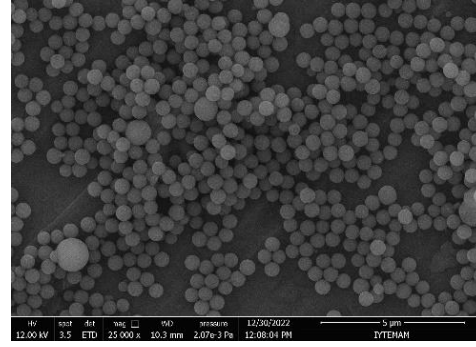
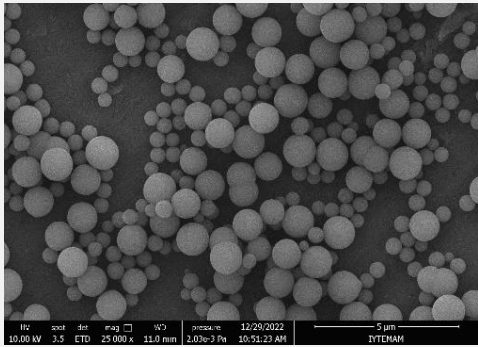
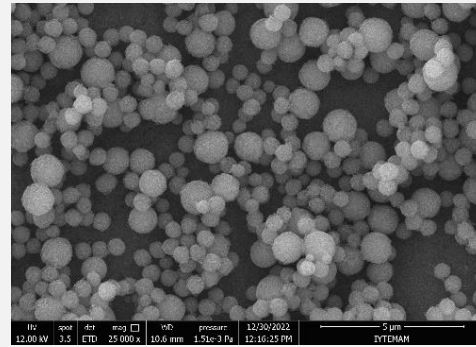
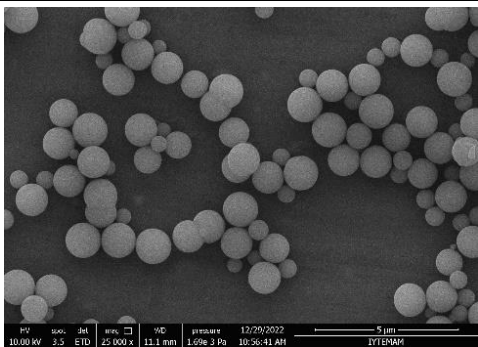
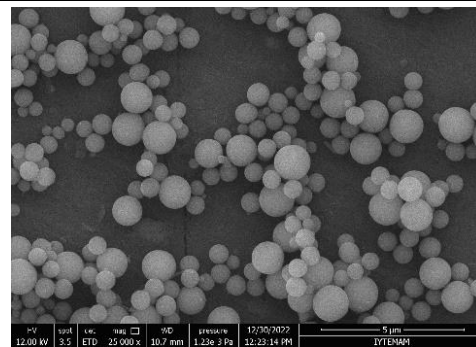
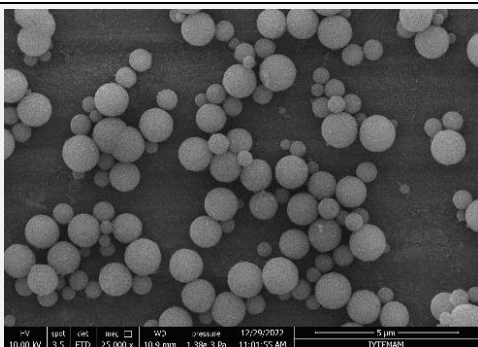
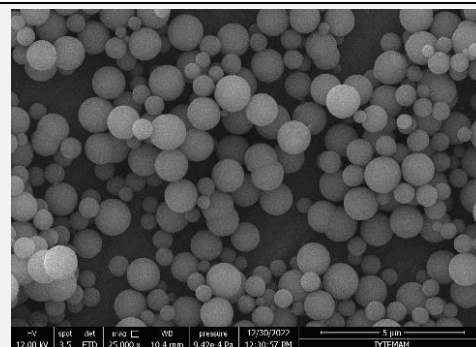
Seed Stock Stability	SEM Images
Seed	 <p>SEM image showing a distribution of spherical seed particles. The particles vary in size, with a concentration of smaller particles and some larger ones. Technical parameters: HV 10.00 kV, spot 3.5, det ETD, mag 25 000 x, WD 10.4 mm, pressure 7.82e-3 Pa, 1/4/2023 10:21:07 AM, 5 μm scale bar, TYTEHAM.</p>
After 2 hours	 <p>SEM image showing a dense population of spherical particles. The particles are more uniform in size compared to the seed. Technical parameters: HV 10.00 kV, spot 3.5, det ETD, mag 25 000 x, WD 10.7 mm, pressure 1.65e-3 Pa, 12/27/2022 2:46:51 PM, 5 μm scale bar, TYTEHAM.</p>
After 6 hours	 <p>SEM image showing a dense population of spherical particles. The particles appear slightly larger and more uniform than at 2 hours. Technical parameters: HV 10.00 kV, spot 3.5, det ETD, mag 25 000 x, WD 11.0 mm, pressure 1.25e-3 Pa, 12/27/2022 2:54:32 PM, 5 μm scale bar, TYTEHAM.</p>
After 24 hours	 <p>SEM image showing a dense population of spherical particles. The particles are very uniform in size and densely packed. Technical parameters: HV 10.00 kV, spot 3.5, det ETD, mag 25 000 x, WD 10.5 mm, pressure 1.03e-3 Pa, 12/27/2022 3:01:16 PM, 5 μm scale bar, TYTEHAM.</p>

After a 2-hour reaction period, it was observed that both larger and smaller particles started to form. The larger particles had an average size of approximately 1.2 microns, while the smaller particles measured around 450 nm. However, it was evident that these particles were not fully developed, and some remained combined. After 4 hours, it was noticed in random areas that the smaller particles had grown through the diffusion of silica molecules. Nevertheless, the previous observation regarding the incomplete formation of spherical particles still held true. At the end of 24 hours, smaller particles (500-600 nm) and larger particles (1.2 microns) reached a steady state, but there were still instances of particles attempting to combine observed in the SEM images. This outcome indicated the need for a slower addition rate of TEOS in the reaction to achieve separate spherical particles, as the diffusion of TEOS to the seed particles required more time.

Based on these results, it was necessary to reduce the addition rate of TEOS. To accomplish this, a decision was made to pump TEOS in conjunction with other ingredients. According to Section 4.1.3.1 and Table 20, the addition of TEOS with ammonium hydroxide and water resulted in the deformation of silica nanoparticles. As a solution, it was determined to pump TEOS and EtOH together to decrease the concentration of TEOS in the growth solution. Initially, EtOH and TEOS were mixed in a 1:1 ratio. However, when TEOS was mixed with water, a rapid hydrolysis reaction occurred, leading to the formation of silanol groups. This change was visually apparent as the color of the TEOS and EtOH mixture in the syringe transitioned from clear to white immediately. To prevent the hydrolysis reaction between TEOS and EtOH, they were mixed in a 1:10 ratio. Since TEOS acted as the limiting reagent, the amount of EtOH was calculated based on the quantity of TEOS, and any remaining EtOH was added to the solution at the beginning of the reaction.

In this experimental setup, EtOH, water, and ammonium hydroxide were initially combined according to the proportions outlined in the Stöber Method, and the seed was introduced to disperse in the solution. Subsequently, TEOS (0.25 M) and EtOH were added to the syringe and introduced into the solution. To monitor the addition rate of TEOS and EtOH, different rates of 1, 2, 4, and 8 ml/min were employed. After 4-hour and 24-hour period, samples were extracted from the solution to examine the synthesized silica particles. To investigate the impact of both the addition rate (1, 2, 4, and 8 ml/min) and the seed quantity (75 mg and 150 mg) on the morphology, size, and shape of the resulting silica particles, a seed amount of 75 mg was utilized in this phase of the experiment.

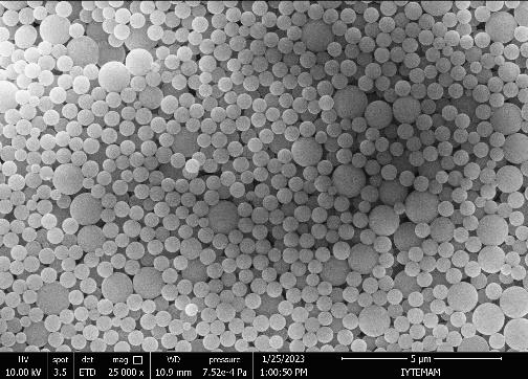
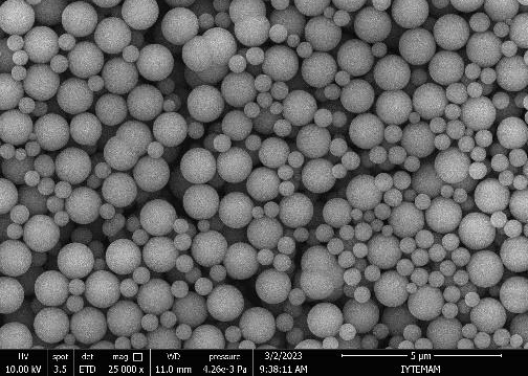
Table 27. After 4h and 24h of started reaction SEM images of silica particles by using 75 mg seed with different TEOS &EtOH (1/10) addition rates

TEOS &EtOH (1/10) addition rate	After 4 h	After 24 h
1 ml/min (Obtained particles: 1 μ + 200 nm)		
2 ml/min (Obtained particles: 1 μ + 350 nm)		
4 ml/min (Obtained particles: 1.1 μ + 400 nm)		
8 ml/min (Obtained particles: 1.2 μ + 200 nm)		

The duration of the necessary reaction was investigated in this section to determine the optimal timing. It was observed that the size of the obtained particles varied between the 4-hour and 24-hour marks after initiating the reaction. Specifically, larger silica particles were obtained after 4 hours. It was hypothesized that the diffusion of TEOS molecules to the seed particles primarily occurred during the initial stages of TEOS & EtOH dosing. However, at a certain point, it seemed that TEOS molecules started generating smaller nanoparticles around 500 nm instead of diffusing through the seed particles for growth. Furthermore, it was noted that an overnight duration was required to complete the reaction and diffusion processes fully.

When the TEOS & EtOH (1:10) mixture was pumped at a rate of 1 ml/min using 75 mg of seed, an imbalance was observed between the larger and smaller particles. Random sampling of SEM images confirmed an approximately equal percentage distribution between the larger and smaller particles. As a result, the subsequent experiments, which utilized 150 mg of seed, focused on investigating two distinct TEOS addition rates: the slowest rate of 1 ml/min and the fastest rate of 8 ml/min.

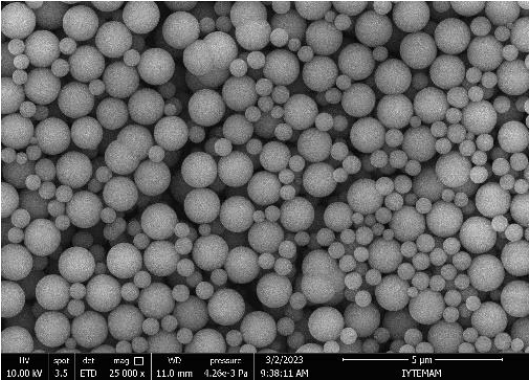
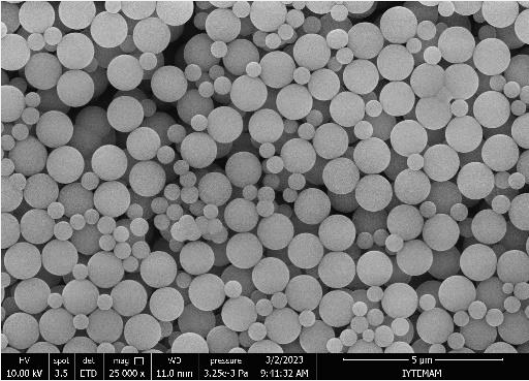
Table 28. After 24h of started reaction SEM images of silica particles by using 150 mg seed with different TEOS &EtOH (1/10) addition rates

TEOS&EtOH (1/10) addition rate	After 24 h
1 ml/min (Obtained particles: 1 μ + 300-500 nm)	
8 ml/min (Obtained particles: 1.2 μ + 550 nm)	

The comparison between the slowest TEOS addition rate of 1 ml/min and the fastest rate of 8 ml/min demonstrated that both rates achieved perfectly spherical particles with an equal percentage distribution of sizes between larger and smaller particles. Given the successful outcomes observed with the 8 ml/min addition rate in both cases, this formulation was selected.

The subsequent step involved producing a larger volume of the total solution, specifically 1.5 L. Before scaling up the production of bi-modal silica particles, a comparison was conducted between 100 ml and 1.5 L total solution, as illustrated in the following results.

Table 29. SEM images of 100 ml and 1.5 L total solution with 150 mg seed and 8 ml/min TEOS & EtOH addition rate

TEOS&EtOH (1/10) addition rate	After 24 h
8 ml/min 100 ml solution (Obtained particles: 1.2 μ + 550 nm)	 <p>SEM image showing spherical particles of varying sizes. The image includes technical data at the bottom: HV: 10.00 kV, spot: 3.5, det: ETD, mag: 25,000 x, WD: 11.0 mm, pressure: 3.25e-3 Pa, 3/2/2023, 9:38:11 AM, IYTEKAM, and a 5 μm scale bar.</p>
8 ml/min 1.5 L solution (Obtained particles: 1.2 μ + 550 nm)	 <p>SEM image showing spherical particles of varying sizes, similar to the 100 ml solution. The image includes technical data at the bottom: HV: 10.00 kV, spot: 3.5, det: ETD, mag: 25,000 x, WD: 11.0 mm, pressure: 3.25e-3 Pa, 3/2/2023, 9:11:32 AM, IYTEKAM, and a 5 μm scale bar.</p>

The observation was made that the growth solution could be effectively simulated in both small and large-scale quantities, leading to consistent and reproducible results. Additionally, particle size distribution graphs shown in below were also supported this SEM images.

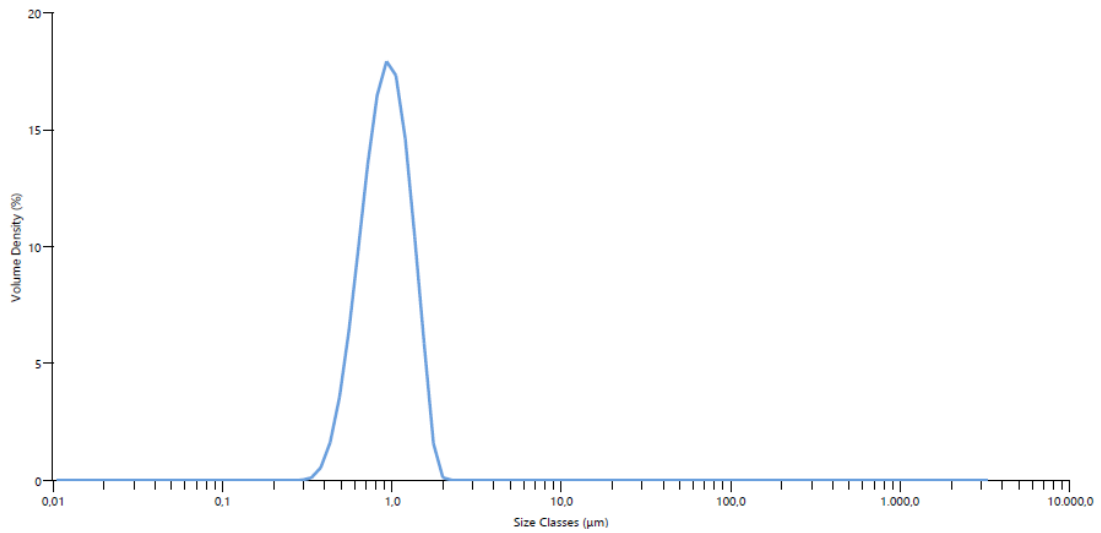


Figure 28. Particle Size Distribution of bi-modal silica particles

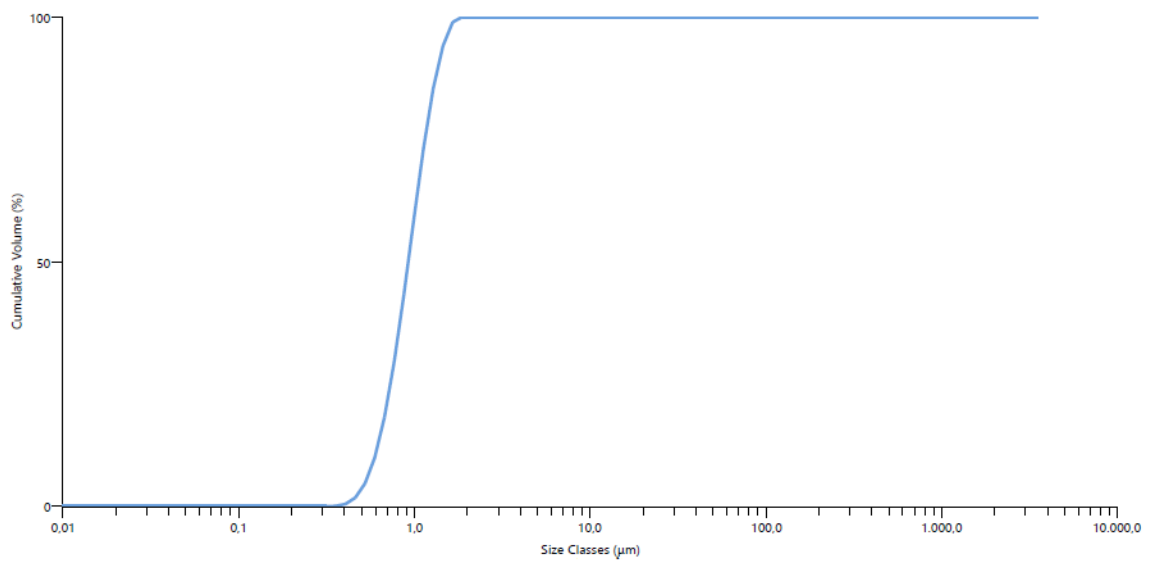


Figure 29. Cumulative Volume (%) vs Size Classes (μm)

Since the synthesized silica particles were a mixture of 1.2 μm and 500-550 nm silica particles, the average particle size was determined to be 922 nm, as indicated in the Dx (50) column of the particle size distribution table.

Table 30. Particle Size Distribution and Specific Surface Area of SPNs

Sample	Dx (10) (μm)	Dx (50) (μm)	Dx (90) (μm)	Specific Surface Area (m^2/g)
Stöber SNPs	0.595	0.992	1.67	6.9

Additionally, the zeta potential of these particles' distribution graph is shown in Figure 30.

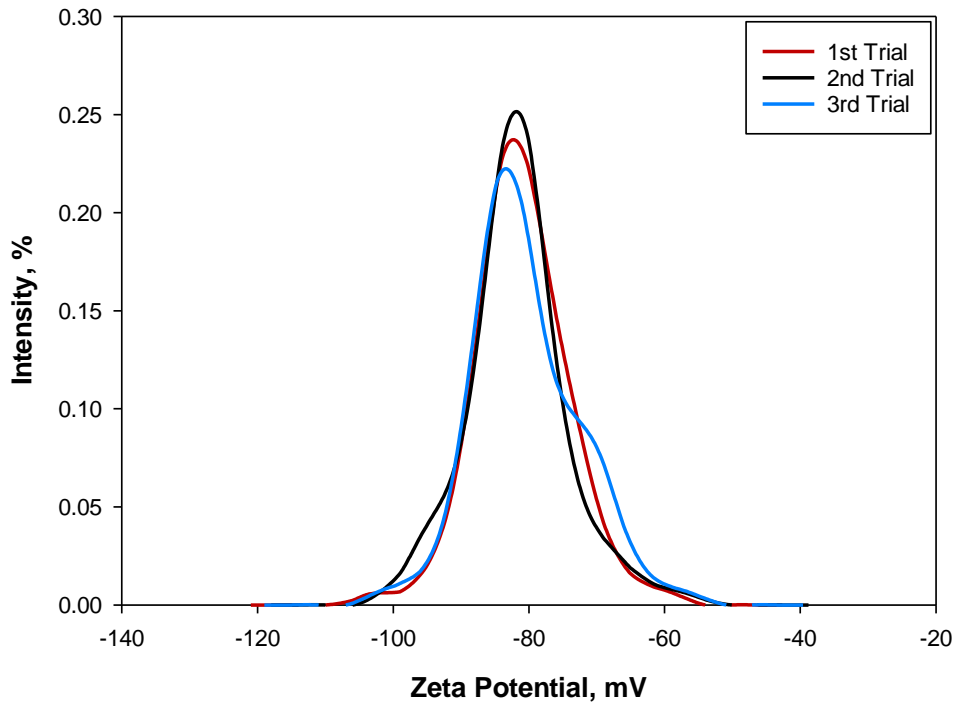


Figure 30. The zeta potential of Bi-Modal Silica Particles

Building on these reliable findings, larger batches of bi-modal silica particles were synthesized and made ready for subsequent coating studies.

Separate analyses of particle size distribution were conducted for both monosize and bi-modal silica particles. Additionally, a comparative study was performed by examining the particle size distribution graphs of both types of particles together.

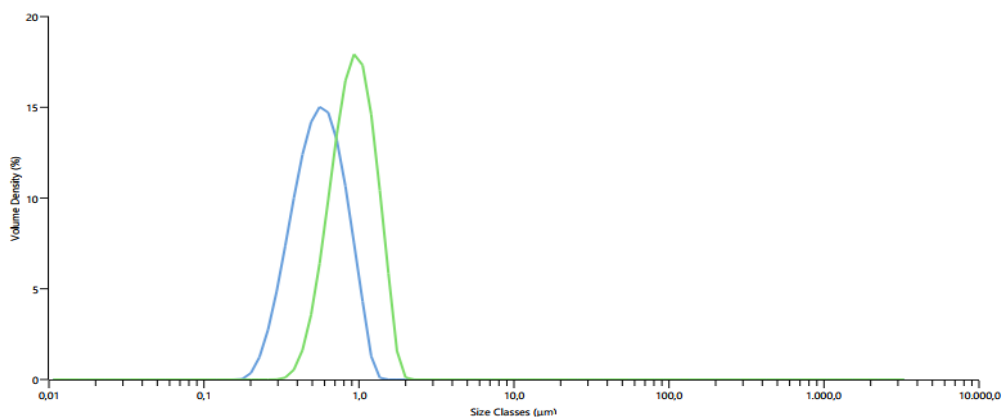


Figure 31. Cumulative Volume (%) vs Size Classes (μm) (Blue: monosize silica; green: bi-modal silica particles)

Addition to particle size distribution graph, FTIR spectrum was also observed for both monosize and bi-modal silica particles as shown in below.

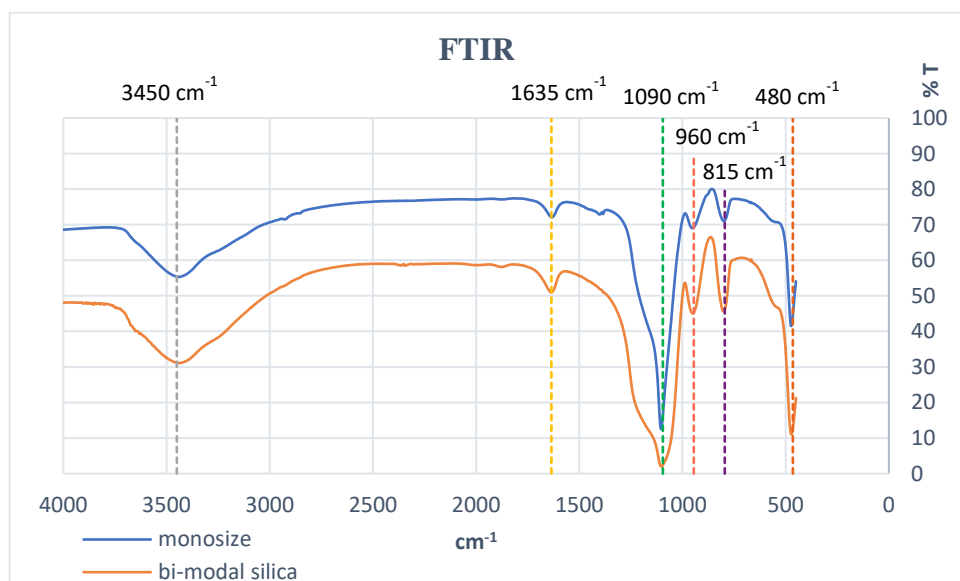


Figure 32. FTIR spectrum of monosize and bi-modal silica particles (transmittance vs wavenumber)

The FTIR spectrum displays bands ranging from 800 to 1200 cm^{-1} , which can be attributed to a combination of multiple SiO_2 peaks, Si-OH bonding, and residual organic group peaks. Silica particles show transmittance bands originated from asymmetric

vibration of Si–O (1090 cm^{-1}), asymmetric vibration of Si–OH (960 cm^{-1}), and symmetric vibration of Si–O (815 cm^{-1}). Water shows a common absorption peak between 3300 cm^{-1} and 3500 cm^{-1} due to O–H stretching in hydrogen bonded water. Also, this band can be controlled from the 1635 cm^{-1} band due to scissor bending vibration of molecular water. The absence of peaks at 2980 cm^{-1} (CH_3) and 2930 cm^{-1} (CH_2) indicates that TEOS was utilized during the synthesis process of the silica particles.

4.2 Coating Studies

This section can be divided into two categories: coating studies involving monosize nanosilica addition and coating studies involving bi-modal silica particle addition. The objective is to compare the impact of different silica particle sizes and size distributions on coating applications.

For the synthesis of monosize nanosilica particles, the Silica D Method (giving 590-620 nm particles) was utilized, which involved using double the amount of TEOS compared to the Classic Stöber Method. Given that coil coatings are typically applied with a thickness of 20 microns, both monosize and larger particles may be suitable for incorporation into the coil coating mixture to generate nano roughness on the surface.

In the second part of the coating studies, the seed obtained from the Classic Stöber Method was utilized in the growth solution, which also employed the same Stöber Method. Following the synthesis of bi-modal silica particles ($1.2\text{ }\mu\text{m} + 500\text{ nm}$), they were added to the coil coating to investigate mechanical tests, including surface hardness, as well as characterization studies involving contact angle measurements with water.

4.2.1 Monosize Silica-Added Coating Studies

In this part, firstly 70 gram of 590-620 nm silica particles were obtained by using Silica D Method. After that, this synthesized silica was added into clear coat (free of pigment & filler) and TiO_2 pigmented topcoat.

4.2.1.1 Adding SNPs into the Clear Coat System

A clear coat weighing 200 grams was prepared, and 10 grams of nanosilica particles, produced using the Silica D Method, were added to the clear coat. Initially, the particle size distribution of the coating mixture was measured as 100 μm using BYK GARDNER equipment. However, it was necessary to reduce the particle size distribution to 20 μm . To achieve this, a shaker with zirconium balls was employed, effectively decreasing the particle size distribution to a maximum of 20 μm .

To compare the rheology, characterization, and mechanical properties of the nanosilica added coating, a commercial silica commonly used in coating formulas was included in the blank coating. In total, three different coating samples were prepared: standard, 5% commercial silica added, and 5% nanosilica added. Before initiating the coating application, the rheological properties of the samples were evaluated.

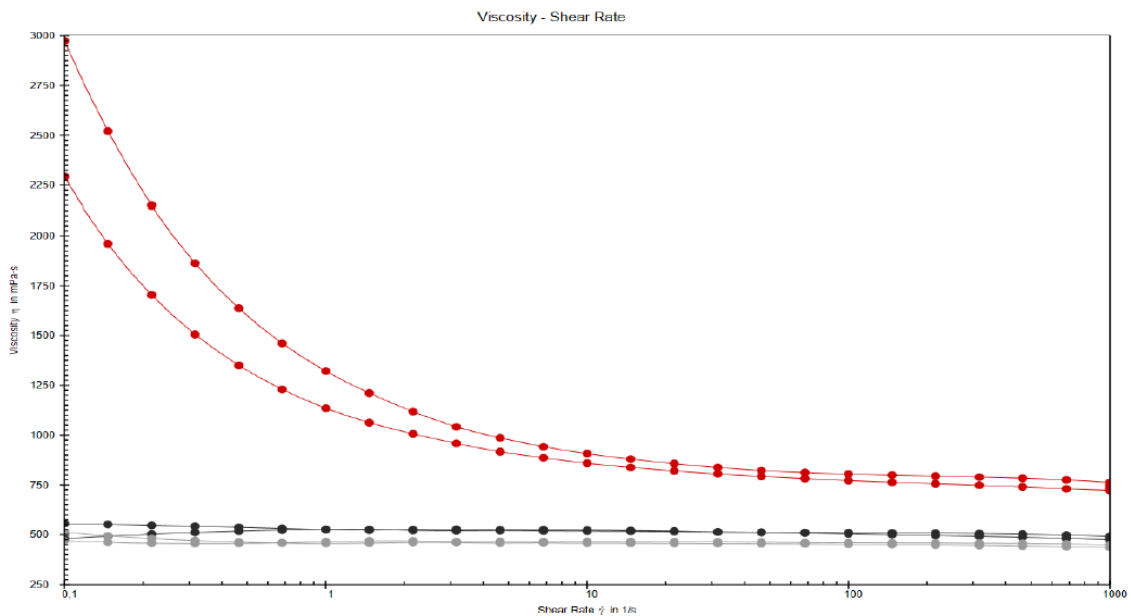


Figure 33. Viscosity vs Shear Rate Graph (Black: Standard Clear Coat, Grey: 5% SNP added coating, red: 5% commercial silica added coating)

In the viscosity vs shear rate graph, it was observed that the commercial silica loaded had a different rheology when same amount of commercial and nanosilica loaded separately.

Notably, as the shear rate increased, the viscosity of the commercial silica added sample exhibited a corresponding decrease, whereas the standard and nanosilica added samples showed negligible changes in viscosity. This observation prompted further investigation into the thixotropic behavior, which was analyzed using the viscosity vs shear rate graph.

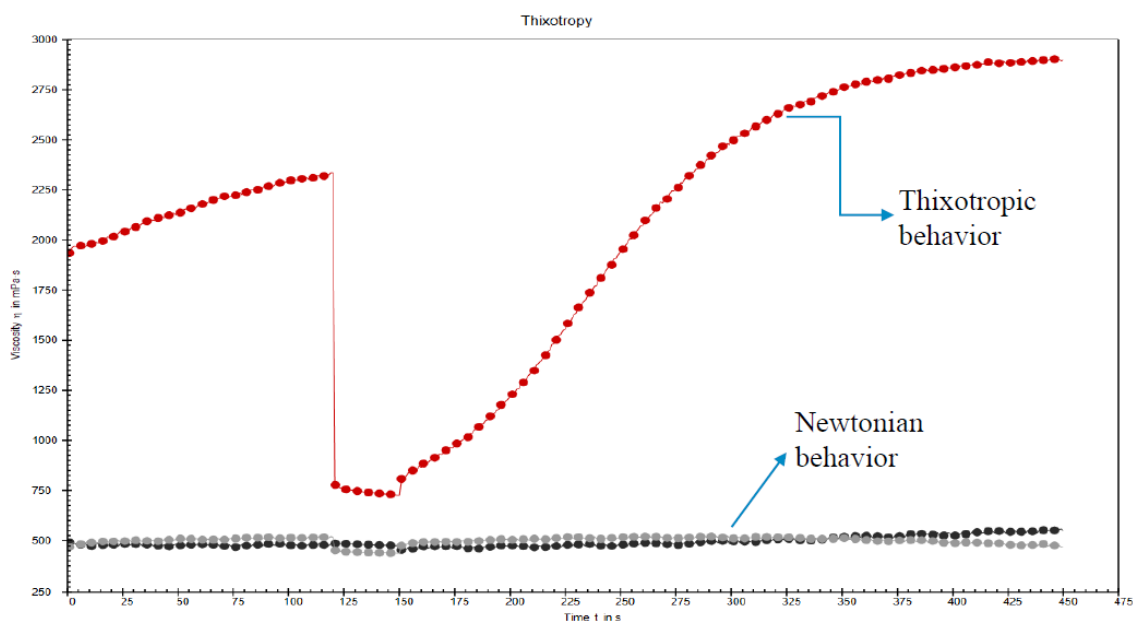


Figure 34. Viscosity vs Time Graph (Black: Standard Clear Coat, Grey: 5% SNP added coating, red: 5% commercial silica added coating)

The same observation was also evident in the thixotropy graph. During the study, a high shear rate was applied to the samples 120 seconds after initiation. It was noted that the sample with the addition of commercial silica exhibited a distinct behavior compared to the other samples. When the shear rate was removed, it took some time for the commercial silica sample to return to its original state. When this behavior is amplified, it has the potential to negatively impact line coating applications. Furthermore, it was observed that the addition of nanosilica particles to the coating did not alter the rheological behavior of the standard coating.

Afterwards, the coating application process was carried out as seen in Figure 35. Initially, applications were made with a 20 micron clear coat, but due to operational issues, it was not possible to apply a 10 micron film. Consequently, only the 20 micron coating was applied, and curing was followed. These obtained coating films underwent mechanical and characterization tests.

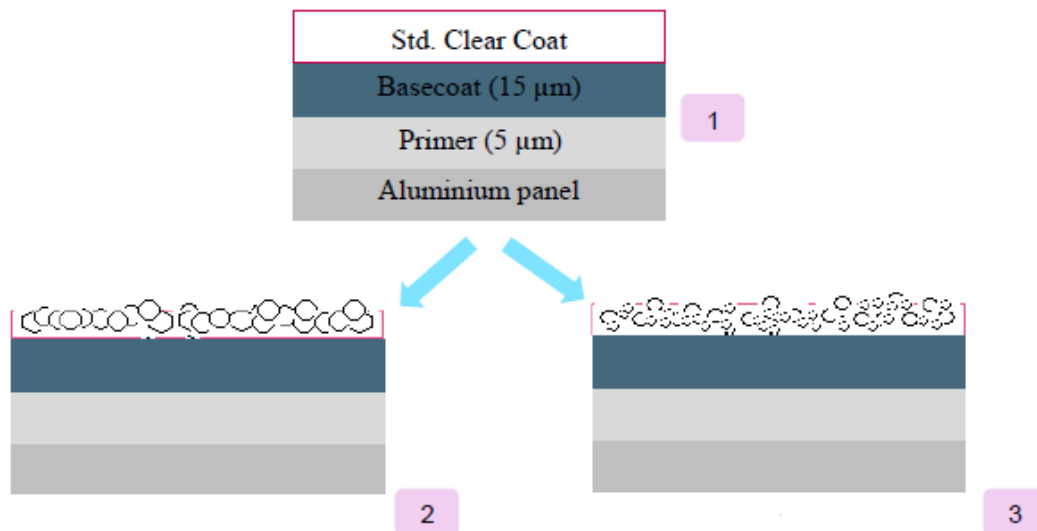
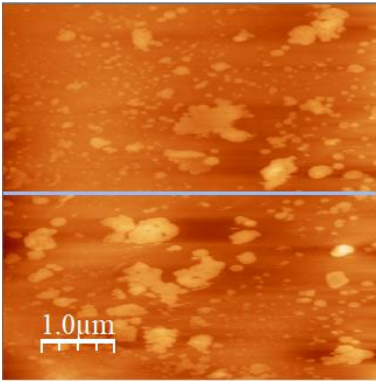
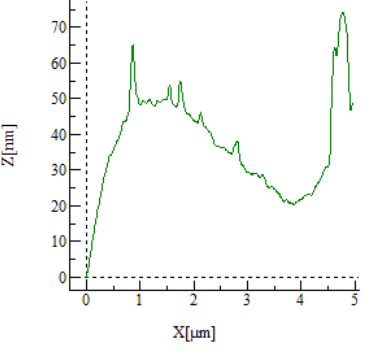
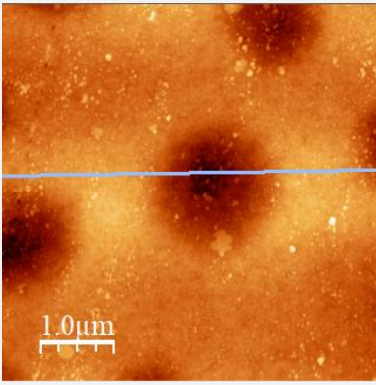
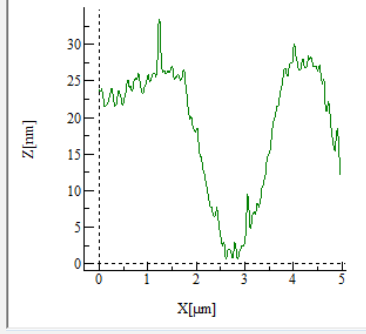


Figure 35. Standard clear coat system (1), commercial silica added coating (2) and nanosilica added coating (3)

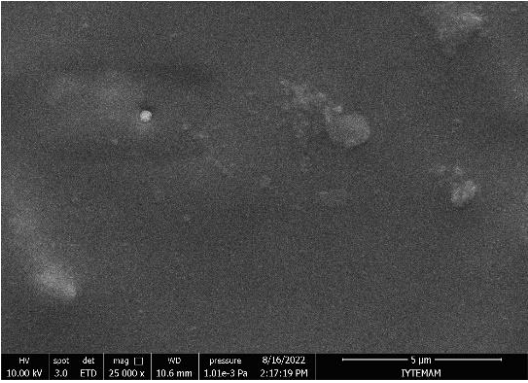
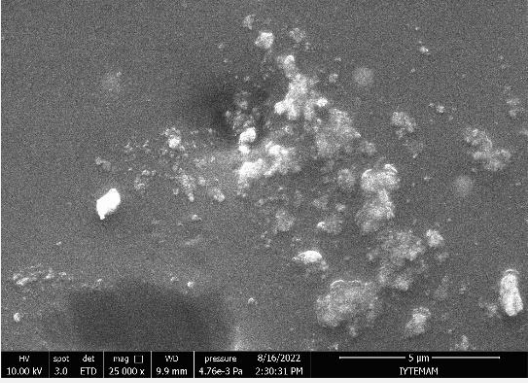
The topography of coatings with the addition of commercial silica and SNPs was examined using AFM. A line was scanned across the surface, and the resulting line profile graph displayed variations in surface height, as evidenced by the presence of maximum and minimum points. Notably, the SNPs-added coating exhibited larger differences between the minimum and maximum points compared to the commercial silica-added coating. These differences can be attributed to the uneven distribution of SNPs and the formation of agglomerates on the surface. Furthermore, it was observed that the SNPs were embedded within the film.

Table 31. AFM results of 5% of commercial and 5% of SNP added coated film

Sample	Surface Line	Line Profile
5% Commercial Silica Added		
5% SNPs Added		

To gain further insight into the agglomeration pattern on the surface, SEM images were analyzed.

Table 32. SEM Images of 5% commercial and SNPs added samples

Sample	SEM Images
5% of Commercial Silica Added	 <p>Technical data for the top SEM image: HV: 10.00 kV, spot: 3.0, det: ETD, mag: 1.1, WD: 10.6 mm, pressure: 1.01e-3 Pa, 8/16/2022, 2:17:19 PM, 5 μm scale bar, TYTEMAM.</p>
5% of SNPs Added	 <p>Technical data for the bottom SEM image: HV: 10.00 kV, spot: 3.0, det: ETD, mag: 1.1, WD: 9.9 mm, pressure: 4.76e-3 Pa, 8/16/2022, 2:30:31 PM, 5 μm scale bar, TYTEMAM.</p>

SEM images confirmed the observations made with AFM, showing the presence of agglomeration formations in the coatings with added SNPs. In contrast, the images of the coatings with commercial silica matched the expected results, as commercial silica is commonly used in existing productions. The roughness parameters were determined for the coating surfaces with the addition of 5% commercial silica and 5% SNPs. The calculated roughness parameter values were 1.060 for the commercial silica-added coating and 1.011 for the SNPs-added coating. In contrast, the blank sample had a roughness parameter value of 1.

To determine whether the SNPs remained embedded within the coating film or were located on its surface, contact angle with water measurements were performed. However, it is important to note that the contact angle measurement equipment assumes a smooth surface, leading to an automatic application of a roughness parameter value of 1. The standard blank sample demonstrated a contact angle value of 82.15°. In all experiments, the confidence interval was observed to range between 0.3° and 2.26°. Upon

the addition of commercial silica and SNPs into the coating film, the contact angle values increased to 84.62° and 83.01°, respectively. Although the coating surfaces exhibited inherent roughness, these contact angle values were obtained assuming a smooth surface. To obtain the actual contact angle, the roughness parameters representing the ratio of textured surface area to projected surface area were determined using the AFM results. Subsequently, the actual contact angle value was calculated as outlined in the introduction part.

Table 33. Roughness parameters and Contact Angle Measurements for blank, 5% commercial silica and 5% SNPs added coating

Sample	Projected Surface Area (μm^2)	Textured Surface Area (μm^2)	Roughness Parameter	Measured Contact Angle ($^\circ$)	Actual Contact Angle ($^\circ$)
Blank Clear Coat	25	25.00	1.000	82.15	82.18
5% Commercial silica added	25	26.51	1.060	84.62	84.83
5% SNPs added	25	25.27	1.011	83.01	83.85

During the characterization of the coating films with 5% addition of commercial silica and SNPs, it was observed that the nanosilica particles were embedded within the coating matrix, and the formation of agglomerates was evident. As the desired results were not achieved in this regard, the mechanical tests of the clear coats were not investigated further.

As a next step, the focus shifted to studying the effects of adding SNPs and commercial silica to the topcoat formulation containing pigments and fillers. This investigation aimed to assess the impact of these additives on the overall performance of the coated system.

4.2.1.2 Adding SNPs into the Topcoat System

The same experimental procedure as the previous section was followed to incorporate commercial silica and SNPs into the topcoat system, which contained pigments and fillers. A polyester topcoat weighing 150 grams was prepared, and to achieve a 45% addition of SNPs, 67.5 grams of nanosilica particles produced using the Silica D Method were added to the topcoat. Since the particle size distribution exceeded 20 μm , a shaker was utilized to reduce the distribution to a maximum of 20 μm .

Initially, a lower percentage of SNPs, specifically 1.2%, was added to the coating by mixing the standard polyester topcoat with the 45% SNPs-added coating. Rheological behaviors were assessed as the primary focus. Subsequently, three different coating samples were prepared: standard, 1.2 % commercial silica added, and 1.2 % nanosilica added. Before commencing the coating application, the rheological properties of the samples were examined.

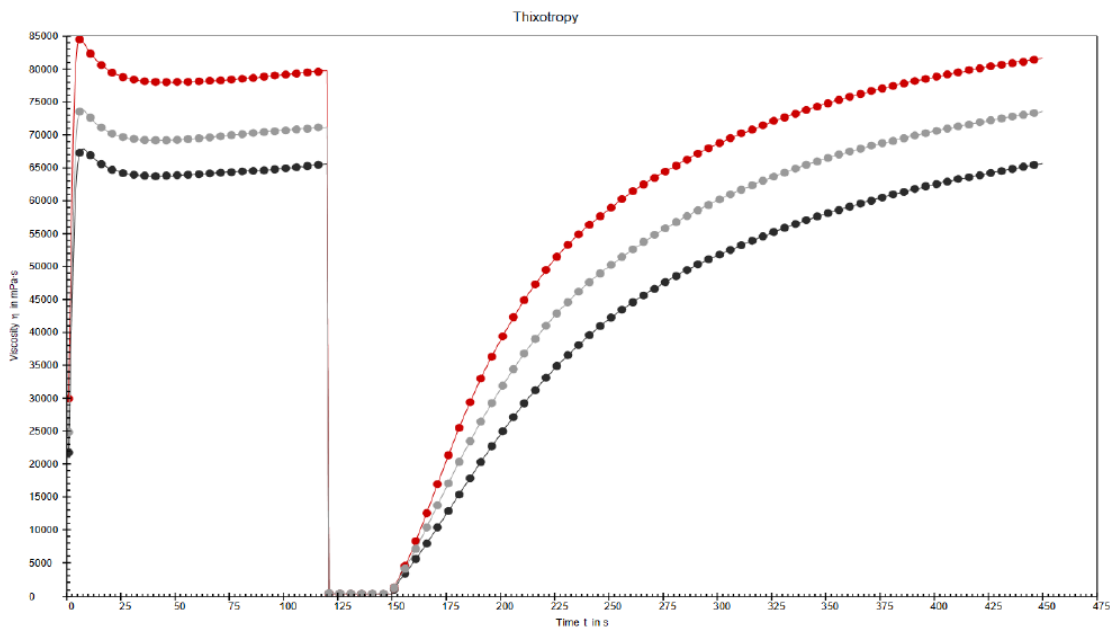


Figure 36. Viscosity vs Time Graph (Black: Standard Clear Coat, Grey: 1.2 % SNP added coating, red: 1.2 % commercial silica added coating)

The thixotropy graph revealed that all samples demonstrated similar behavior. Notably, the loading amounts of silica were relatively low, providing an insight into the expected trends. The rheological behavior of the SNPs-added sample was found to lie between that of the blank sample and the commercial silica-added samples. This suggests that the addition of SNPs to the topcoat did not lead to a significant alteration in the coating's rheology, consistent with the findings from the previous section.

After conducting checks on the rheology and particle size distribution, coating applications were performed following the outlined procedure. Coatings with film thicknesses of 20 μm and 10 μm were applied to investigate the influence of film thickness on the results of roughness and water contact angle measurements.

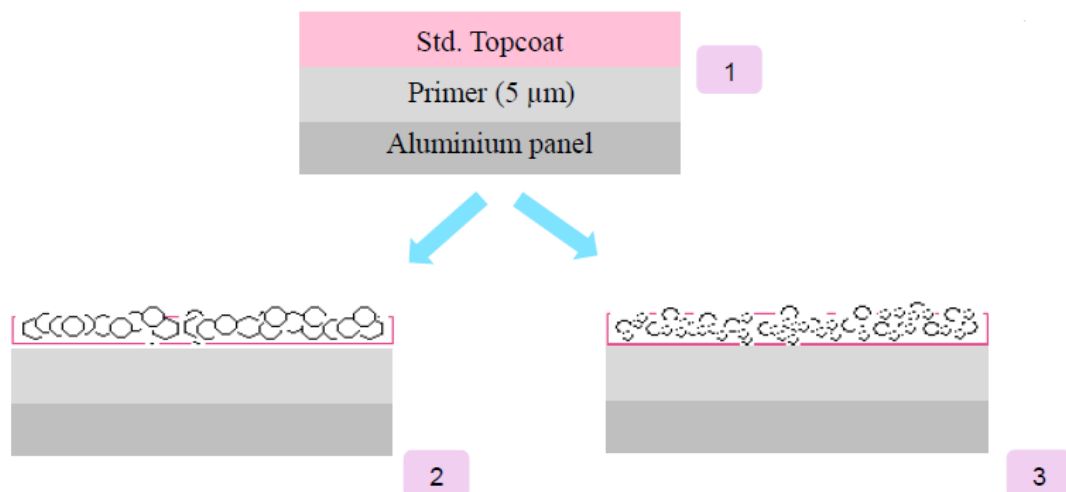
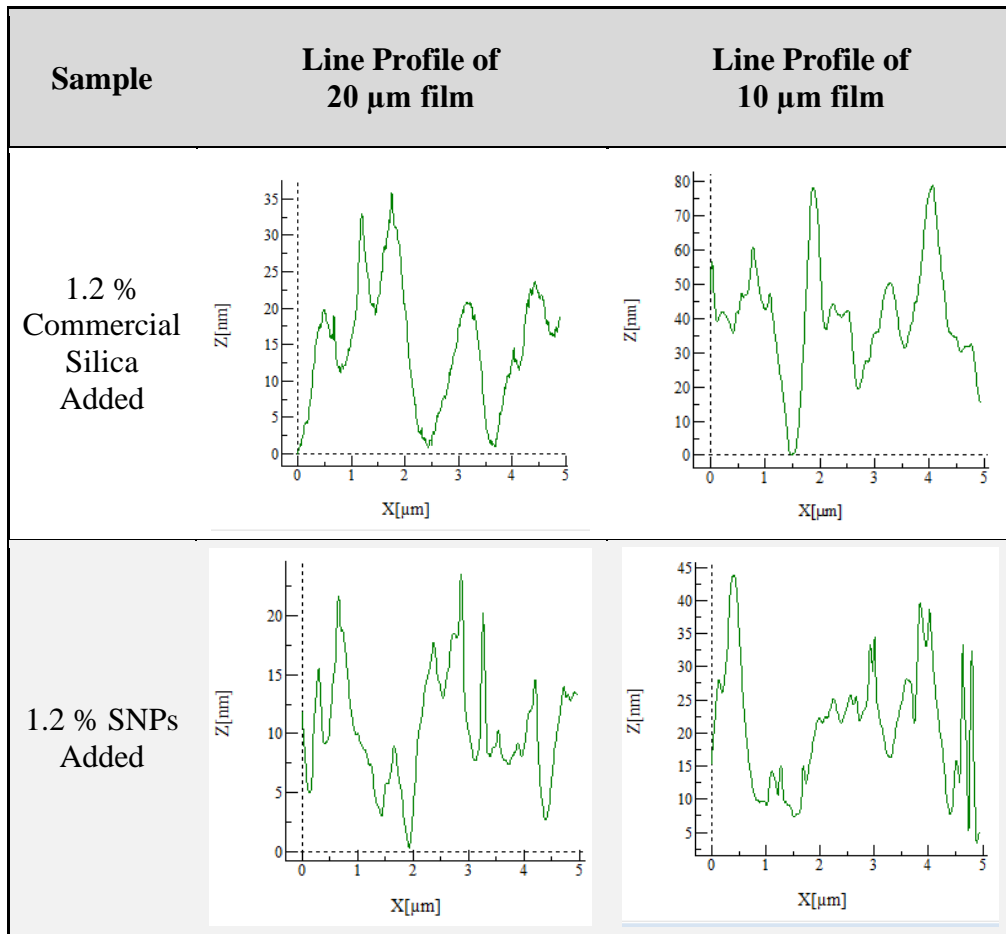


Figure 37. Standard clear coat system (1), commercial silica added coating (2) and nanosilica added coating (3)

The topography of coatings with the addition of commercial silica and SNPs was examined using AFM.

Table 34. AFM results of 1.2 % monosize SNP and 1.2 % commercial silica added coating



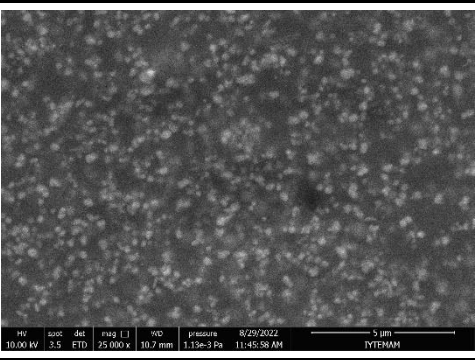
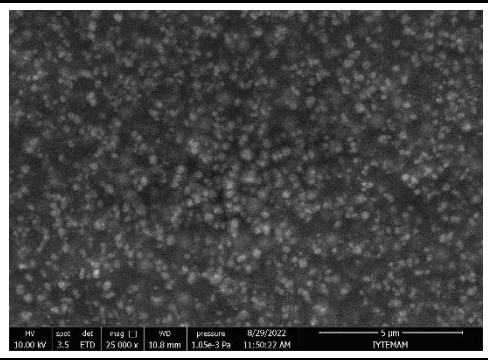
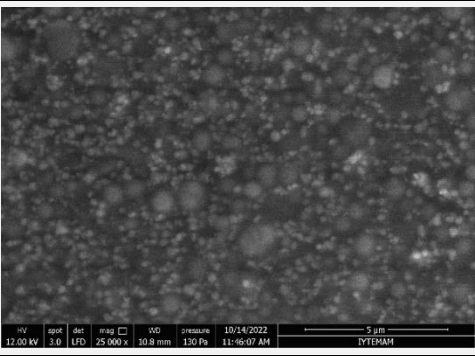
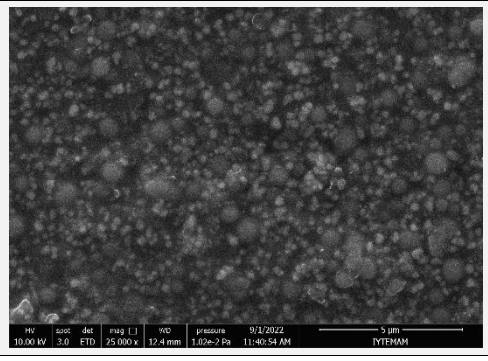
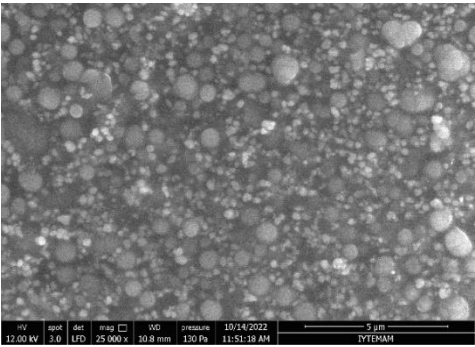
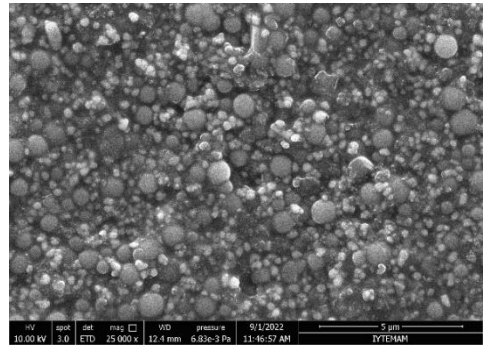
The coatings with added SNPs showed higher surface roughness compared to the coatings with the same amount of commercial silica, regardless of the film thicknesses tested. Moreover, reducing the film thickness from 20 μm to 10 μm resulted in an increased frequency of surface roughness within each sample. These findings suggest that the 10 μm film applications may achieve a higher contact angle with water.

Another implication is that the SNPs in the coatings may reside on the surface rather than being fully embedded within the film matrix. This behavior could be attributed to the presence of fillers and pigments in the coating, which help fill the system and prevent complete embedding of the nanoparticles into the film.

Based on the findings of these investigations, it was determined to incorporate nanosilica particles into the film matrix at varying concentrations ranging from 5% to 45%.

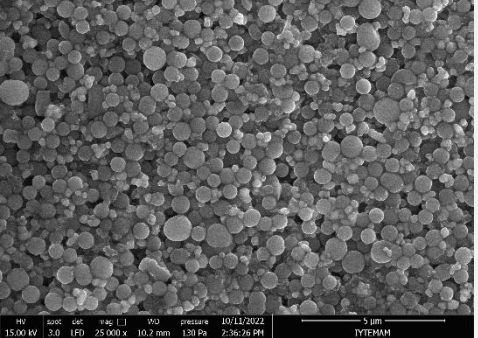
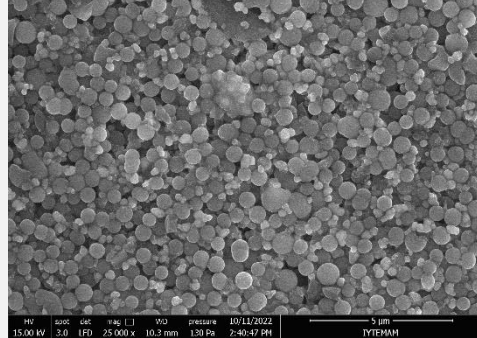
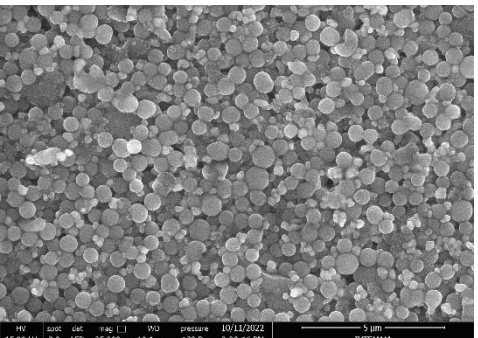
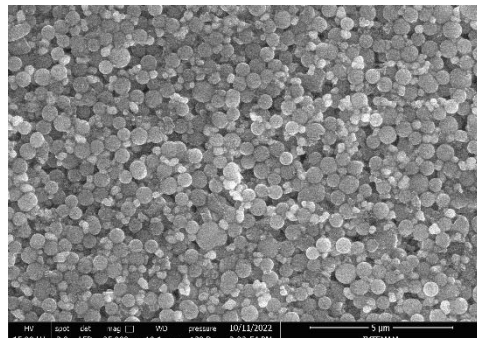
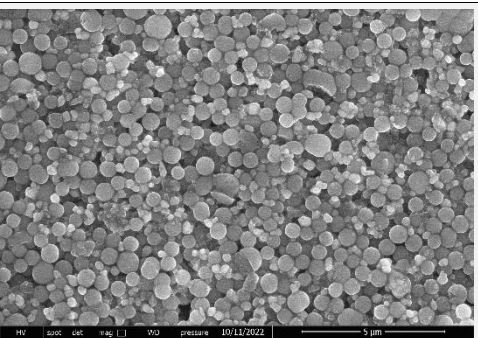
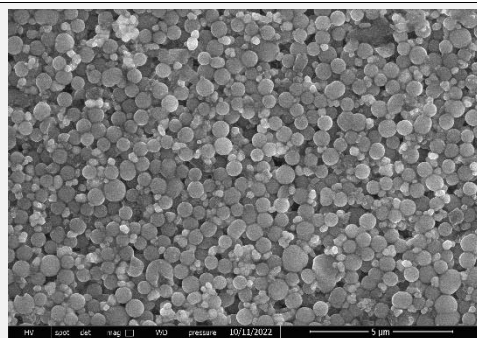
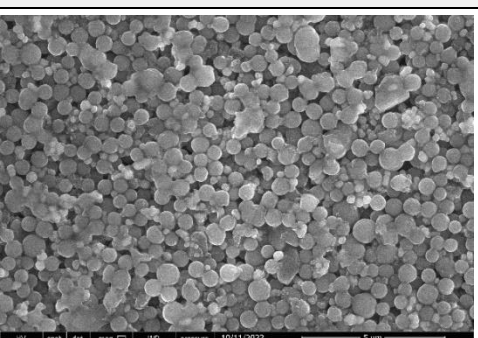
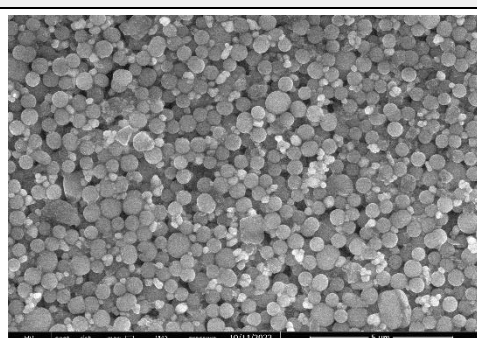
The experiment revealed that the presence of nanoparticles on the surface led to a noticeable increase in roughness within the range of 5% to 30% loading. However, loading 30% of NSPs did not yield a significant effect.

Table 35. SEM images different % of monosize SNPs added coating film

Sample	SEM images for 20 μm film	SEM images for 10 μm film
5% Added SNPs	 <p>SEM image showing a surface with a fine, granular texture. The image includes technical data at the bottom: HV 10.00 kV, spot 3.5, det ETD, mag 25,000 x, WD 10.7 mm, pressure 1.13e-3 Pa, 8/29/2022 11:45:38 AM, 5 μm scale bar, IYTEMAM.</p>	 <p>SEM image showing a surface with a fine, granular texture. The image includes technical data at the bottom: HV 10.00 kV, spot 3.5, det ETD, mag 25,000 x, WD 10.8 mm, pressure 1.05e-3 Pa, 8/29/2022 11:50:22 AM, 5 μm scale bar, IYTEMAM.</p>
15% Added SNPs	 <p>SEM image showing a surface with a fine, granular texture. The image includes technical data at the bottom: HV 12.00 kV, spot 3.0, det LFD, mag 25,000 x, WD 10.8 mm, pressure 130 Pa, 10/14/2022 11:46:07 AM, 5 μm scale bar, IYTEMAM.</p>	 <p>SEM image showing a surface with a fine, granular texture. The image includes technical data at the bottom: HV 10.00 kV, spot 3.0, det ETD, mag 25,000 x, WD 12.4 mm, pressure 1.02e-2 Pa, 9/1/2022 11:40:54 AM, 5 μm scale bar, IYTEMAM.</p>
20% Added SNPs	 <p>SEM image showing a surface with a fine, granular texture. The image includes technical data at the bottom: HV 12.00 kV, spot 3.0, det LFD, mag 25,000 x, WD 10.8 mm, pressure 130 Pa, 10/14/2022 11:51:18 AM, 5 μm scale bar, IYTEMAM.</p>	 <p>SEM image showing a surface with a fine, granular texture. The image includes technical data at the bottom: HV 10.00 kV, spot 3.0, det ETD, mag 25,000 x, WD 12.4 mm, pressure 6.83e-3 Pa, 9/1/2022 11:46:57 AM, 5 μm scale bar, IYTEMAM.</p>

(cont. on next page)

Table 35 (cont.)

Sample	SEM images for 20 μm film	SEM images for 10 μm film
25% Added SNPs	 <p>SEM image showing the morphology of a 20 μm film with 25% added SNPs. The surface is covered with numerous small, spherical particles. Technical parameters: HV 15.00 kV, spot 3.0, det LFD, mag 25,000 x, WD 10.2 mm, pressure 130 Pa, 10/11/2022 2:36:26 PM. Scale bar: 5 μm.</p>	 <p>SEM image showing the morphology of a 10 μm film with 25% added SNPs. The surface is covered with numerous small, spherical particles. Technical parameters: HV 15.00 kV, spot 3.0, det LFD, mag 25,000 x, WD 10.2 mm, pressure 130 Pa, 10/11/2022 2:40:47 PM. Scale bar: 5 μm.</p>
30% Added SNPs	 <p>SEM image showing the morphology of a 20 μm film with 30% added SNPs. The surface is covered with numerous small, spherical particles. Technical parameters: HV 15.00 kV, spot 3.0, det LFD, mag 25,000 x, WD 10.1 mm, pressure 130 Pa, 10/11/2022 2:29:16 PM. Scale bar: 5 μm.</p>	 <p>SEM image showing the morphology of a 10 μm film with 30% added SNPs. The surface is covered with numerous small, spherical particles. Technical parameters: HV 15.00 kV, spot 3.0, det LFD, mag 25,000 x, WD 10.1 mm, pressure 130 Pa, 10/11/2022 2:22:54 PM. Scale bar: 5 μm.</p>
40% Added SNPs	 <p>SEM image showing the morphology of a 20 μm film with 40% added SNPs. The surface is covered with numerous small, spherical particles. Technical parameters: HV 15.00 kV, spot 3.0, det LFD, mag 25,000 x, WD 10.1 mm, pressure 130 Pa, 10/11/2022 2:06:24 PM. Scale bar: 5 μm.</p>	 <p>SEM image showing the morphology of a 10 μm film with 40% added SNPs. The surface is covered with numerous small, spherical particles. Technical parameters: HV 15.00 kV, spot 3.0, det LFD, mag 25,000 x, WD 10.2 mm, pressure 130 Pa, 10/11/2022 2:12:18 PM. Scale bar: 5 μm.</p>
45% Added SNPs	 <p>SEM image showing the morphology of a 20 μm film with 45% added SNPs. The surface is covered with numerous small, spherical particles. Technical parameters: HV 15.00 kV, spot 3.0, det LFD, mag 25,000 x, WD 10.0 mm, pressure 130 Pa, 10/11/2022 1:56:30 PM. Scale bar: 5 μm.</p>	 <p>SEM image showing the morphology of a 10 μm film with 45% added SNPs. The surface is covered with numerous small, spherical particles. Technical parameters: HV 15.00 kV, spot 3.0, det LFD, mag 25,000 x, WD 10.0 mm, pressure 130 Pa, 10/11/2022 2:01:23 PM. Scale bar: 5 μm.</p>

As a result, it can be concluded that the increase in roughness stabilized and reached a steady state between 20% and 30% silica loading for both the 20 μm and 10 μm films. The findings obtained through AFM were further supported by SEM images.

Subsequently, contact angle measurements with water were conducted to explore the influence of topography and morphology on the hydrophobic behavior of the coating films with added SNPs.

Table 36. Contact Angle value of monosize SNPs added both 10 μm and 20 μm films

Loading	Monosize - 20 mikron	Monosize - 10 mikron
45%	113.61	111.90
40%	113.54	110.80
35%	112.00	109.50
30%	110.50	105.42
25%	107.60	107.34
20%	92.00	92.71
15%	87.66	87.25
10%	86.32	84.2
5%	85.45	83.50
0%	82.20	82.20

The presence of SNPs in the coil coating films was found to enhance their hydrophobic properties. Loading SNPs in the range of 15% to 20% resulted in the formation of a hydrophobic surface, exhibiting a contact angle of approximately 92° , which was higher than the baseline value of 90° . However, further increasing the SNP loading beyond 25% did not lead to a significant additional increase in the contact angle, as it remained around 113° . These findings were consistent with the results obtained from AFM and SEM analyses, which demonstrated that the addition of SNPs beyond 30% did

not have a notable impact on the hydrophobicity of the films.

As explained in the introduction part, roughness value was calculated by dividing the textured surface area, which was obtained from AFM results, to projected surface area. Since contact angle values were listed in Table 36 were taken from the contact angle measurement equipment which assumes the smooth surface. After contact angle measurement and calculation roughness parameter was found Eq 2 was applied to obtain actual contact angle as seen in below.

Table 37. Roughness parameter, Measured and Actual Contact Angle

Sample	Projected Surface Area (μ/m^2)	Textured Surface Area (μ/m^2)	Roughness Parameter	Measured Contact Angle ($^\circ$)	Actual Contact Angle ($^\circ$)
45%	25.00	28.81	1.15	113.61	117.49
40%	25	28.98	1.16	113.54	117.58
30%	25.00	29.35	1.17	110.5	114.28
20%	25.00	28.25	1.13	92.00	92.26
10%	25.00	25.52	1.02	86.32	86.24

Comparison of measured CA vs actual CA with respect to silica loading amount was plotted. By considering the roughness parameter was affected obtaining maximum CA with water.

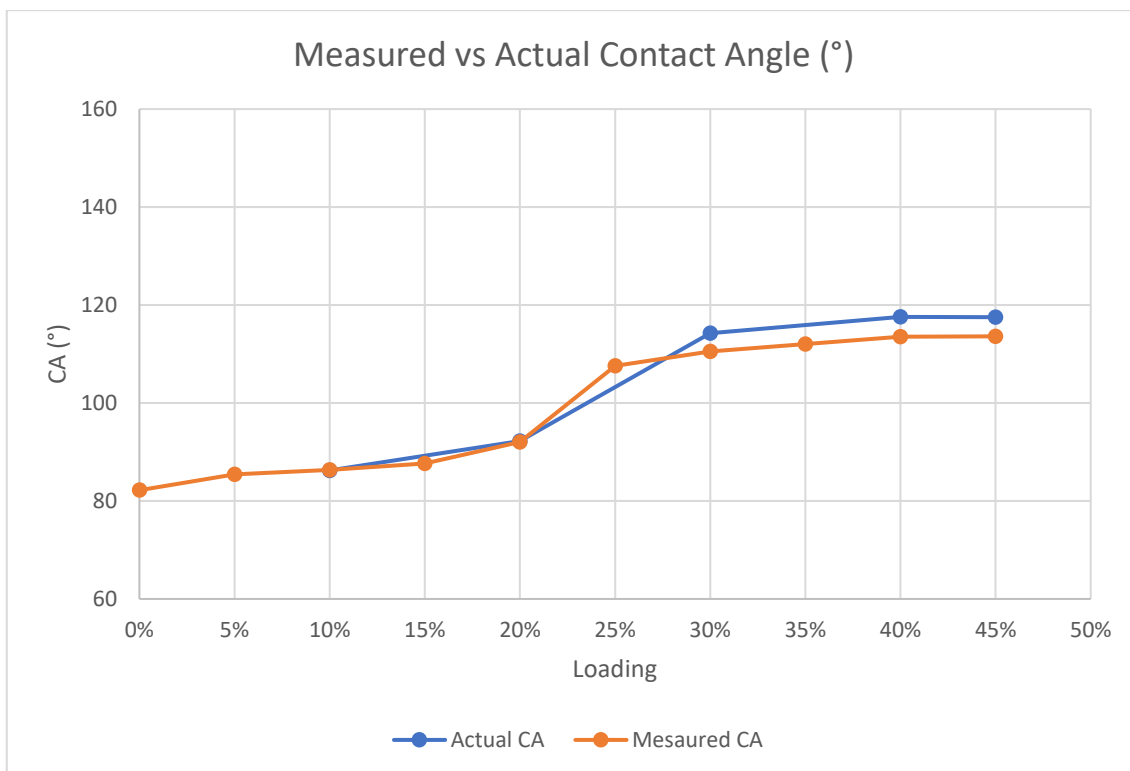


Figure 38. Comparison of measured vs actual CA with respect to silica loading amount

Additionally, mechanical tests of especially 20 μm films were conducted to further investigate the properties of the coil coating system. It was noted that an increase in the powder components within the coating system led to a reduction in overall flexibility. The results from flexibility test aligned with the anticipated outcomes. The sample with the highest silica loading, specifically 45%, demonstrated the lowest flexibility result of 2.5 T. To enable a comparative analysis, the flexibility of a topcoat containing 5% commercial silica was also evaluated. Interestingly, the 5% commercial silica topcoat exhibited a flexibility result of 3T, whereas the sample with nine times higher silica loading displayed superior flexibility. This disparity in flexibility may be attributed to variances in particle size distribution and morphology between the commercial and nanosilica particles. An adhesion test was conducted as well. The sample with the highest loading of SNPs exhibited a loss of adhesion ranging from 35% to 65%, indicating an adhesion rating of 1 B. In contrast, the sample with only 5% of commercial silica added showed a loss of adhesion higher than 65%, corresponding to an adhesion rating of 0 B. These findings suggest that consistent results were obtained in the adhesion tests. Additionally, pencil hardness test of samples was investigated as shown in below.

Table 38. Results of pencil hardness of monosize SNPs added coating

Sample	Results of 20 micron	Results of 10 micron
0 - 35 %	2H	2H
40 - 45 %	3H	3H

Observations revealed that loading SNPs up to 35% resulted in a surface hardness of 2H. However, further increasing the SNP loading up to 45% led to even harder surface properties, measuring 3H. The same relationship was valid for both film thicknesses. Thus, it can be concluded that an increase in the amount of nanosilica in the coating led to an enhancement in the surface hardness of the coating films. To observe the surface hardness, scratch resistance tests were also conducted as shown in below. Also, degree of curing test which was MEK were similar when compared to bi-modal added silica sample. Therefore, the result of MEK test was explained together in the following section.

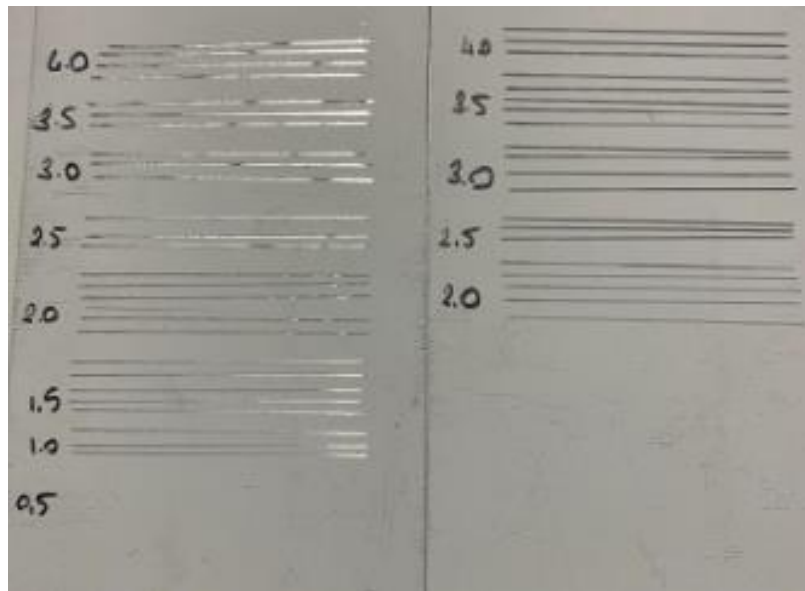


Figure 39. Scratch resistance results of 25 % and 30 % monosize silica added samples

On the left side of the figure, it was indicated that the monosize silica-added coated sample with a 25% content exhibited an approximate scratch resistance of 1 kg, whereas on the right side of the figure, the sample with 30% monosize silica showed a resistance of 2-2.5 kg. This suggests that an increase in the amount of silica results in a more hydrophobic and harder coating surface.

4.2.2 Bi-modal Silica-Added Coating Studies

In this section, the first step involved obtaining 60 grams of silica particles with sizes of 1.2 μm and 500-550 nm. These particles were synthesized using the Stöber Growth Solution method, with seeds obtained through the Stöber Method. As the silica particles were embedded into the coating matrix, the focus was solely on investigating the effect of adding SNPs on the surface of the topcoat, which already contained pigments and fillers. Subsequent sections included the characterization and mechanical testing of the coated panels.

The same experimental procedure as in the previous section was followed to incorporate commercial silica and SNPs into the topcoat system, which already contained pigments and fillers. A polyester topcoat weighing 150 grams was prepared, and to achieve a 40% addition of SNPs, 60 grams of silica were added. As the particle size distribution exceeded 20 μm , a shaker was used to reduce the distribution to a maximum of 20 μm . Since the rheological behavior of the SNPs-added sample showed similarities with the blank topcoat in previous sections, it was not necessary to investigate the rheology of the synthesized bi-modal silica-added samples. Other samples with different concentrations were prepared by mixing the standard polyester topcoat with the coating containing 40% SNPs. Coating applications were performed using two different film thicknesses, namely 20 μm and 10 μm .

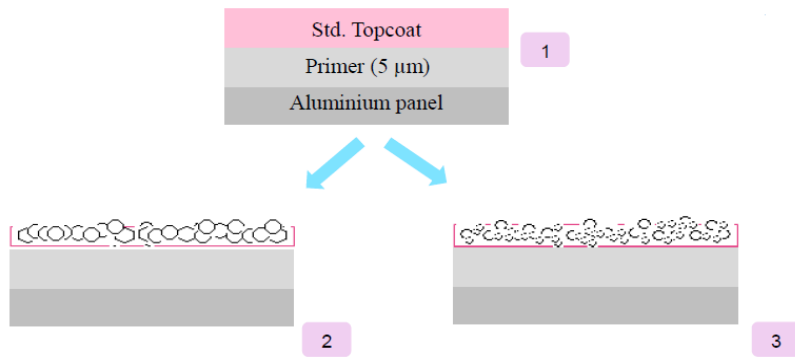


Figure 40. Standard clear coat (1), commercial silica added (2) and NSP added (3)

Table 39. AFM and SEM images different % of bi-modal SNPs added coating film

Sample	AFM	SEM
10%		
20%		
30%		
40%		

AFM and SEM results for addition of bi-modal silica to coil coating film were seen in Table 39. In the 1.2 μ + 500-550 nm silica particles were seen on the surface of coating film in SEM results, especially in the maximum loaded amount. These results were also supported with their AFM results that showed the topography of the surface. Also, it was clearly seen that the results of 30% and 40% silica loaded samples were similar while 20% silica loaded sample showed different surface topology. According to these results, it was expected that 30% and 40% silica loaded samples had similar contact angle value while 20% silica added sample had lower value than the others. To correlate these results, contact angle with water was also investigated. It was listed in Table 40.

Table 40. Contact Angle value of bi-modal SNPs added both 20 μ m and 10 μ m films

Loading	Bi-modal - 20 mikron	Bi-modal - 10 mikron
40%	116.70	111.50
35%	104.30	114.30
30%	108.40	110.50
25%	107.90	109.90
20%	106.10	106.40
15%	87.90	90.40
10%	88.30	88.50
5%	88.20	89.70
0%	82.20	82.20

In the case of 10 μ m applications, it was observed that the incorporation of 15% SNPs resulted in the achievement of hydrophobic surfaces. The addition of 20% monosize SNPs led to a contact angle of 92°. However, when the same amount of bi-

modal silica particles was added to the coating, a significant increase in contact angle values was observed, reaching up to 106°. This finding suggests that the presence of multisize silica particles was more effective in enhancing the hydrophobicity of the coil coating. Moreover, the addition of 40% bi-modal silica particles resulted in the highest contact angle value of 116.7°, providing further evidence of the improved hydrophobic properties.

As explained in the monosize silica particle characterization part, roughness parameter, measured and actual CA values were also obtained in the characterization of bi-modal silica added coating part as seen in Table 41.

Table 41. Roughness parameter, Measured and Actual Contact Angle

Sample	Projected Surface Area (μ/m^2)	Textured Surface Area (μ/m^2)	Roughness Parameter	Measured Contact Angle (°)	Actual Contact Angle (°)
40%	25.00	44.13	1.77	116.70	142.48
30%	25.00	42.64	1.71	108.40	122.57
20%	25.00	38.85	1.55	106.10	115.53
10%	25.00	25.96	1.04	88.30	88.24

Comparison of measured CA vs actual CA with respect to silica loading amount was plotted. By considering the roughness parameter was affected obtaining maximum CA with water.

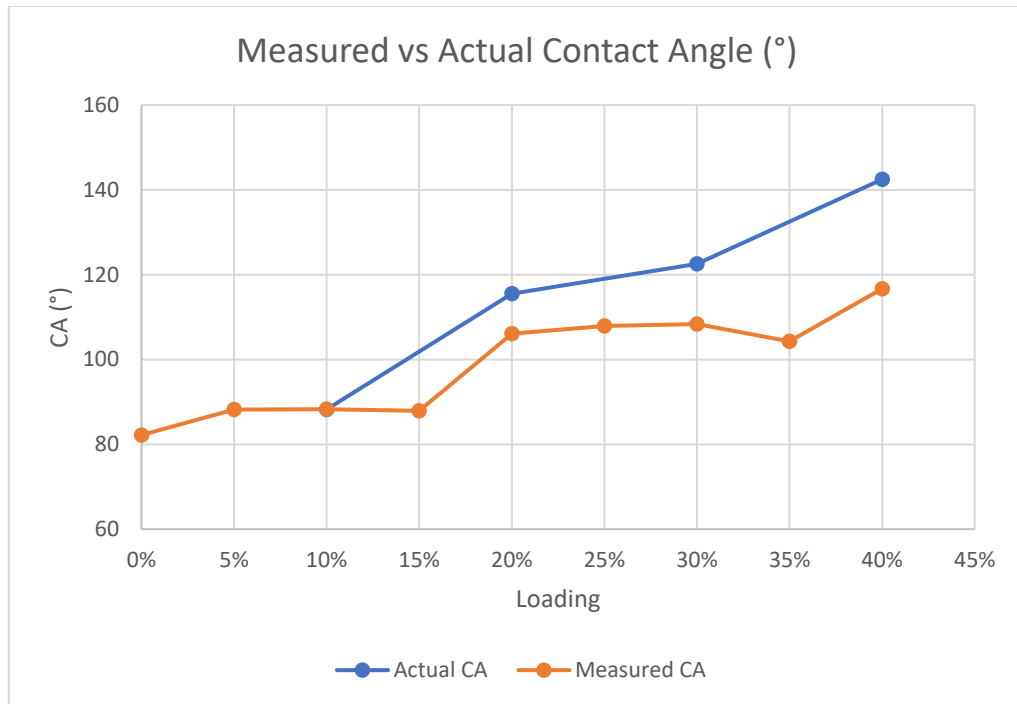


Figure 41. Comparison of measured vs actual CA with respect to silica loading amount

While there were lower differences between the measured and actual contact angle (CA) values in the monosize silica-added coating sample, significant differences were observed between the measured and actual CA values in the bi-modal silica-added coating sample, especially when the silica content exceeded 30%.

After the surface characterization stage, mechanical tests were performed, particularly on the 20 μm films, to further examine the properties of the coil coating system. As mentioned in the previous section, an increase in the powder components within the coating system resulted in decreased overall flexibility. Similar results were obtained for flexibility and adhesion tests. Loading 40% of silica demonstrated the lowest flexibility result of 2.5 T, aligning with expectations, and the adhesion test yielded a result of 1B, consistent with the monosize silica added experiments. To assess surface hardness, pencil hardness tests were conducted on the samples, as shown in Table 42.

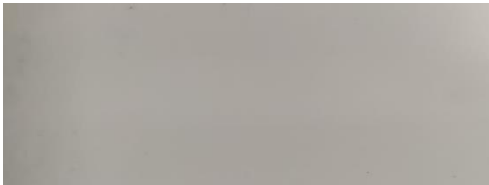
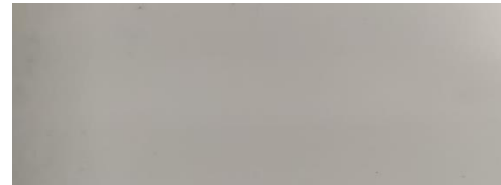
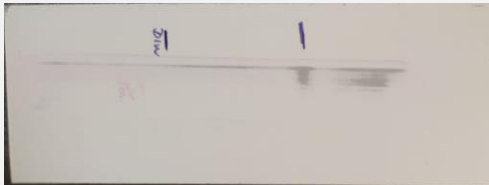
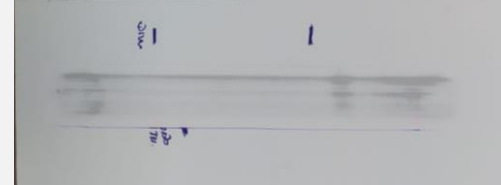
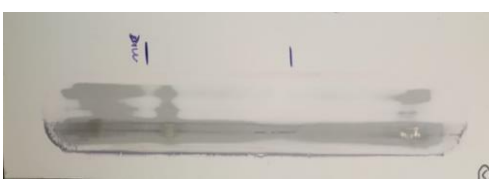

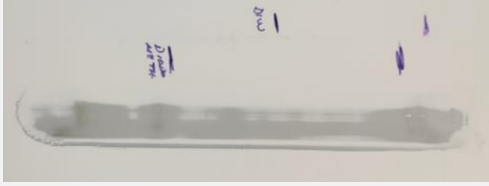
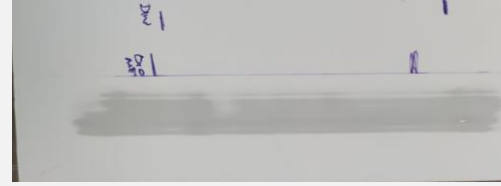

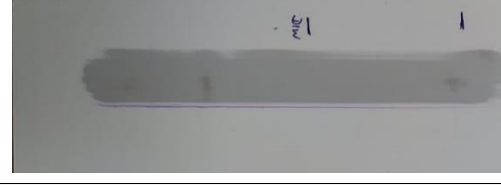
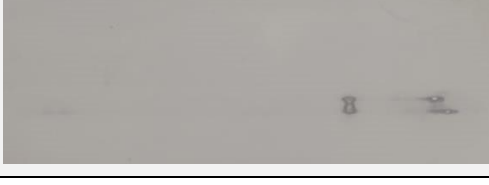
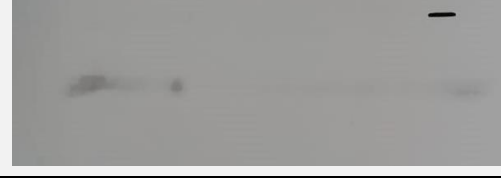

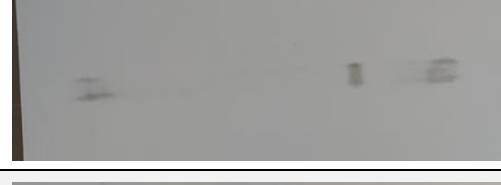
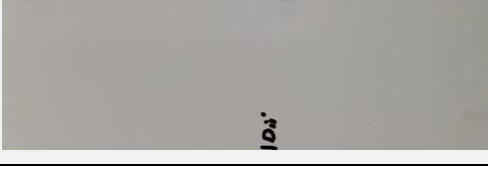
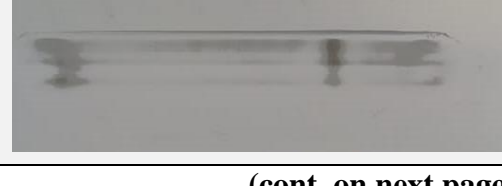
Table 42. Results of pencil hardness of bi-modal SNPs added coating

Sample	Results of 20 micron	Results of 10 micron
0 - 20 %	2H	2H
20 - 40 %	3H	3H

Achieving a pencil hardness of 3H required a 40% addition of silica, while a 20% addition of bi-modal silica particles was sufficient. This supports the notion that bi-modal silica particles were more effective in comparison to monosize silica in terms of performance.



Furthermore, the degree of curing test, specifically the MEK 50 test, was conducted. It should be noted that there were experimental errors in the results obtained from the 25% addition of bi-modal silica sample (10 μm).

Table 43. Results of MEK test of monosize SNPs added coating both 10 μm and 20 μm

%	Bi-modal-20 micron	Bi-modal-10 micron
std		
40 %		
35 %		
30 %		
25 %		
20 %		
15 %		
10 %		

(cont. on next page)

Table 43 (cont.)

%	Bi-modal-20 micron	Bi-modal-10 micron
5%		

Monosize and bi-modal silica particles performed similar MEK test results. Therefore, only bi-modal results were shown in Table 43. All results were performed better results when compared to MEK results of 5% commercial silica added sample which was performed 5B pencil hardness. For this reason, commercial silica is added to the coating formula by further processing and preparing a semi-product.

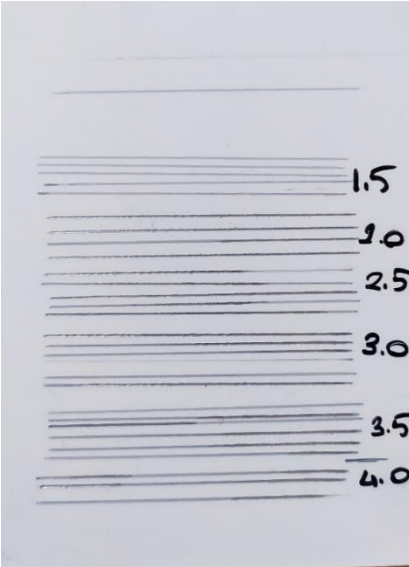
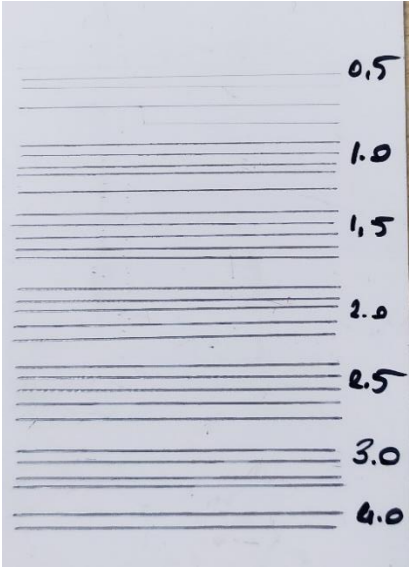
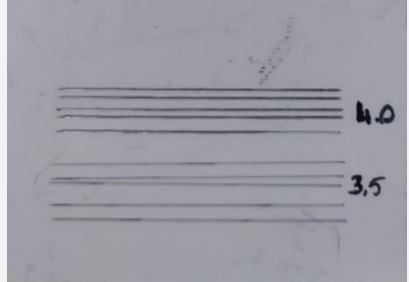
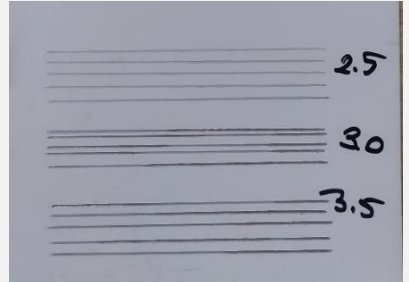


Figure 42. Test sample of 5% commercial silica added

The Clemen scratch test was conducted as the final step. In this test, the surface of the standard polyester topcoat (blank sample) was found to delaminate from the primer when subjected to a 1.5 kg application, resulting in a scratch resistance value of 1 kg for

the standard topcoat. However, an intriguing and significant finding emerged when 40% bi-modal silica particles were incorporated into the coating the scratch resistance remarkably increased to 3.5 kg. This outcome strongly suggests that the addition of bi-modal silica significantly enhances the coating's ability to withstand scratches. Similar results were observed when examining film thicknesses of 10 μm . Specifically, the standard topcoat with a 10 μm film thickness demonstrated a scratch resistance value of 0.5 kg. However, when 40% multi-size silica particles were introduced into the coating, the scratch resistance of the topcoat rose from 0.5 kg to 2.5 kg. Consequently, it can be concluded that multi-size silica particles exert a more pronounced effect on improving the scratch resistance of the surface when compared to mono-size silica particles.

Table 44. Result of scratch test for standard and 40% bi-modal silica added samples

%	20 micron application	10 micron application
std		
40%		

CHAPTER 5

CONCLUSION

Addition of nano-sized silica particles was observed to significantly improve the performance characteristics of coatings in this study. Due to their small size, nanosilica particles have a large surface area, which enhances their reinforcing, strengthening, and barrier properties. These properties led to increased surface hydrophobicity as well as improved mechanical properties, such as hardness and scratch resistance.

The study comprised of two main parts: the synthesis and characterization of monosize and multisize silica particles, and the subsequent coating test studies. Monosize nanosilica particles (500-550 nm) were synthesized using the Stöber Method, with production conducted on both large and small scales to ensure control over reproducibility and repeatability.

During the synthesis of silica particles within the 500-550 nm range, the TEOS concentration in the Stöber Method was investigated in detail. Lower amounts of TEOS led to the formation of agglomerated and smaller silica particles, whereas increasing the TEOS amount in the Silica D Method resulted in the production of larger silica particles ranging from 590-620 nm. However, further increases in TEOS concentration caused agglomeration and the formation of non-spherical particles. Additionally, the effects of doubling the amounts of TEOS and other ingredients in the Stöber reaction were examined to understand their influence on the morphology, size, and shape of silica particles. It was discovered that doubling the amounts of TEOS and water in the Stöber reaction led to the formation of perfectly spherical nanosilica particles with sizes of 650-670 nm. Similarly, using doubled concentrations of TEOS and EtOH in the Silica D Method resulted in the synthesis of silica particles ranging from 650-680 nm in size.

Furthermore, bi-modal (multisize) growth studies were conducted using different sizes and amounts of pre-manufactured Stöber seed particles. When seed particles produced using the Silica D Method were utilized in the growth solutions, the synthesized particles exhibited either agglomeration or smaller sizes, such as a combination of 650-750 nm. The optimal combination of multisize silica particles, with sizes of 1.1 μm + 200 nm, was achieved by utilizing seed particles produced using the classic Stöber Method in

the growth solution consisting of 0.5 M TEOS, 12.14 M Ethanol, 11.67 M water, and 1.09 M ammonium hydroxide. The formation of smaller particles indicated that additional time was required for the diffusion of silica molecules to the seed particles to facilitate their growth. Consequently, it was necessary to decrease the rate of TEOS addition to the growth solution, resulting in a mixture of TEOS and EtOH with a ratio of 1/10. The addition rates of TEOS & EtOH were tested at 1 ml/min, 2 ml/min, 4 ml/min, and 8 ml/min. Notably, an addition rate of 8 ml/min of TEOS to the growth solution, using the classic Stöber solution ingredients and seed particles synthesized via the classic Stöber Method, yielded the best combination of multisize particles with sizes of 1.2 μm and 550 nm.

The particle size distributions were investigated for monosize silica particles in the range of 500-550 nm, as well as multisize particles with measurements of 1.2 μm and 550 nm.

Following the synthesis of particles with mono and bi-modal size distributions, coating studies were conducted. Initially, monosize silica nanoparticles (SNPs) were introduced to a clear coat devoid of pigments and fillers. The AFM and SEM images confirmed the embedding of SNPs in the coating film, allowing the studies to progress with the topcoat containing pigments and fillers. Notably, when incorporating 15% of bi-modal silica particles into 10 μm applications, hydrophobic surfaces were successfully achieved. The addition of 25% monosize SNPs resulted in a contact angle of 92° , and further increasing the SNP loading beyond 25% did not yield a significant additional increase, as the contact angle remained around 113° . Conversely, the introduction of an equal amount of bi-modal silica particles led to a considerable rise in contact angle values, reaching up to 106° . This finding suggests that the presence of multisize silica particles more effectively enhances the hydrophobicity of the coil coating. Additionally, the highest contact angle value of 116.7° was obtained with the addition of 40% bi-modal silica particles by assuming smooth surfaces. When roughness parameter was considered, for bi-modal and monosize particles added coating film surfaces were performed 142.48° and 117.49° contact angle values with water, respectively.

In the mechanical tests, comparable results were observed for both monosize and bi-modal silica-added samples in terms of MEK resistance, flexibility, and adhesion. Furthermore, it was found that loading SNPs up to 35% resulted in a surface hardness of 2H. However, further increasing the SNP loading to 45% resulted in even greater surface hardness, measuring 3H. Notably, achieving a pencil hardness of 3H required the addition

of 40% monosize silica, while a 20% addition of bi-modal silica particles proved sufficient. These findings support the notion that bi-modal silica particles were more effective in enhancing performance compared to monosize silica.

In conclusion, the utilization of monosize and bi-modal silica particles successfully enhanced both the hydrophobicity and surface hardness of coil-coated panels.

This study on synthesized silica particles has the potential to contribute to various applications such as medicine, implants, bone cement, and antibacterial treatments. It aims to enhance mechanical strength, increase surface area, and more.

REFERENCES

- Alessi, A., Agnello, S., Buscarino, G., & Gelardi, F. M. (2013). Raman and IR investigation of silica nanoparticles structure. *Journal of Non-Crystalline Solids*, 362(1), 20–24. <https://doi.org/10.1016/j.jnoncrysol.2012.11.006>
- Bai, Y., Zhang, H., Shao, Y., Zhang, H., & Zhu, J. (2021). Recent progresses of superhydrophobic coatings in different application fields: An overview. *Coatings*, 11(2), 1–30. <https://doi.org/10.3390/coatings11020116>
- Bailey, J. K., & Mecartney, M. L. (1992). Formation of colloidal silica particles from alkoxides. *Colloids and Surfaces*, 63(1–2), 151–161. [https://doi.org/10.1016/0166-6622\(92\)80081-C](https://doi.org/10.1016/0166-6622(92)80081-C)
- Bari, A. H., Jundale, R. B., & Kulkarni, A. A. (2020). Understanding the role of solvent properties on reaction kinetics for synthesis of silica nanoparticles. *Chemical Engineering Journal*, 398(March), 125427. <https://doi.org/10.1016/j.cej.2020.125427>
- Branda, F., Silvestri, B., Luciani, G., & Costantini, A. (2007). The effect of mixing alkoxides on the Stöber particles size. *Colloids and Surfaces A: Physicochemical and Engineering Aspects*, 299(1–3), 252–255. <https://doi.org/10.1016/j.colsurfa.2006.11.048>
- Busquets, J., Peláez, N., Gil, M., Secanella, L., Ramos, E., Lladó, L., & Fabregat, J. (2016). Is Pancreaticoduodenectomy a Safe Procedure in the Cirrhotic Patient? *Cirugía Española (English Edition)*, 94(7), 385–391. <https://doi.org/10.1016/j.cireng.2016.01.002>
- Bogush, G., Tracy, M., & Zukoski, C. (1988). Preparation of monodisperse silica particles: Control of size and mass fraction. *Journal of Non-Crystalline Solids*, 104(1), 95–106. [https://doi.org/10.1016/0022-3093\(88\)90187-1](https://doi.org/10.1016/0022-3093(88)90187-1)
- Bogush, G., & Zukoski, C. (1991). Uniform silica particle precipitation: An aggregative growth model. *Journal of Colloid and Interface Science*, 142(1), 19–34. [https://doi.org/10.1016/0021-9797\(91\)90030-c](https://doi.org/10.1016/0021-9797(91)90030-c)
- Chakraborty, D., Dingari, N. N., & Chakraborty, S. (2012). Combined effects of surface roughness and wetting characteristics on the moving contact line in microchannel flows. *Langmuir*, 28(48), 16701–16710. <https://doi.org/10.1021/la303603c>
- Chang, S. M., Lee, M., & Kim, W. (2005). Preparation of large monodispersed

- spherical silica particles using seed particle growth. *Journal of Colloid and Interface Science*, 286(2), 536-542. <https://doi.org/10.1016/j.jcis.2005.01.059>
- Chen, S. L., Dong, P., Yang, G. H., & Yang, J. J. (1996a). Characteristic aspects of formation of new particles during the growth of monosize silica seeds. *Journal of Colloid and Interface Science*, 180(1), 237–241. <https://doi.org/10.1006/jcis.1996.0295>
- Chen, S. L., Dong, P., Yang, G. H., & Yang, J. J. (1996b). Kinetics of Formation of Monodisperse Colloidal Silica Particles through the Hydrolysis and Condensation of Tetraethylorthosilicate. *Industrial and Engineering Chemistry Research*, 35(12), 4487–4493. <https://doi.org/10.1021/ie9602217>
- Chou, K. Sen, & Chen, C. C. (2008). The critical conditions for secondary nucleation of silica colloids in a batch Stöber growth process. *Ceramics International*, 34(7), 1623–1627. <https://doi.org/10.1016/j.ceramint.2007.07.009>
- Dabbaghian, M., Babalou, A., Hadi, P., & Jannatdoust, E. (2010). A Parametric Study of the Synthesis of Silica Nanoparticles via Sol-Gel Precipitation Method. *International Journal of Nanoscience and Nanotechnology*, 6(2), 104–113.
- Finnie, K. S., Bartlett, J. R., Barbé, C. J. A., & Kong, L. (2007). Formation of silica nanoparticles in microemulsions. *Langmuir*, 23(6), 3017–3024. <https://doi.org/10.1021/la0624283>
- Fouilloux, S., Daillant, J., & Thill, A. (2012). Single step synthesis of 5-30nm monodisperse silica nanoparticles: Important experimental parameters and modeling. *Colloids and Surfaces A: Physicochemical and Engineering Aspects*, 393, 122–127. <https://doi.org/10.1016/j.colsurfa.2011.11.009>
- Ghimire, P. P., & Jaroniec, M. (2021). Renaissance of Stöber method for synthesis of colloidal particles: New developments and opportunities. *Journal of Colloid and Interface Science*, 584, 838–865. <https://doi.org/10.1016/j.jcis.2020.10.014>
- Hörnström, S. E., Hedlund, E. G., Klang, H., Nilsson, J. -O, Backlund, M., & Tegehall, P. -E. (1992). A surface study of the chemical pretreatment before coil coating of hot dip zinc-coated steel. *Surface and Interface Analysis*, 19(1–12), 121–126. <https://doi.org/10.1002/sia.740190124>
- Huang, Y., & Pemberton, J. E. (2010). Synthesis of uniform, spherical sub-100nm silica particles using a conceptual modification of the classic LaMer model. *Colloids and Surfaces A: Physicochemical and Engineering Aspects*, 360(1–3), 175–183. <https://doi.org/10.1016/j.colsurfa.2010.02.031>

- Hyde, E. D. E. R., Seyfaee, A., Neville, F., & Moreno-Atanasio, R. (2016). Colloidal Silica Particle Synthesis and Future Industrial Manufacturing Pathways: A Review. *Industrial and Engineering Chemistry Research*, 55(33), 8891–8913.
<https://doi.org/10.1021/acs.iecr.6b01839>
- Ibrahim, I. a. M., Zikry, a. a. F., & Sharaf, M. a. (2010). Preparation of spherical silica nanoparticles: Stober silica. *Journal of American Science*, 6(11), 985–989.
- Innocenzi, P. (2016). *The Sol to gel transition*. Springer.
- Jana, N. R., Gearheart, L., & Murphy, C. J. (2001). Seeding growth for size control of 5-40 nm diameter gold nanoparticles. *Langmuir*, 17(22), 6782–6786.
<https://doi.org/10.1021/la0104323>
- Jiang, X., Tang, X., Tang, L., Zhang, B., & Mao, H. (2019). Synthesis and formation mechanism of amorphous silica particles via sol–gel process with tetraethylorthosilicate. *Ceramics International*, 45(6), 7673–7680.
<https://doi.org/10.1016/j.ceramint.2019.01.067>
- Kim, S. S., Kim, H. S., Kim, S. G., & Kim, W. S. (2004). Effect of electrolyte additives on sol-precipitated nano silica particles. *Ceramics International*, 30(2), 171–175.
[https://doi.org/10.1016/S0272-8842\(03\)00085-3](https://doi.org/10.1016/S0272-8842(03)00085-3)
- Koch, B. M. L., Amirfazli, A., & Elliott, J. A. W. (2014). Wetting of rough surfaces by a low surface tension liquid. *Journal of Physical Chemistry C*, 118(41), 23777–23782. <https://doi.org/10.1021/jp5071117>
- Krasowska, M., Zawala, J., & Malysa, K. (2009). Air at hydrophobic surfaces and kinetics of three phase contact formation. *Advances in Colloid and Interface Science*, 147-148, 155-169. <https://doi.org/10.1016/j.cis.2008.10.003>
- LaMer, V. K., & Dinegar, R. H. (1950). Theory, production and mechanism of formation of Monodispersed Hydrosols. *Journal of the American Chemical Society*, 72(11), 4847-4854. <https://doi.org/10.1021/ja01167a001>
- Liang, T., Yuan, H., Li, C., Dong, S., Zhang, C., Cao, G., Fan, Y., Zhao, X., & Cao, X. (2021). Corrosion inhibition effect of nano-SiO₂ for galvanized steel superhydrophobic surface. *Surface and Coatings Technology*, 406(October), 126673. <https://doi.org/10.1016/j.surfcoat.2020.126673>
- Liu, X., Wang, R., Fan, Y., & Wei, M. (2017). Effect of SiO₂ nanoparticles on the hydrophobic properties of waterborne fluorine-containing epoxy coatings. *MATEC Web of Conferences*, 130. <https://doi.org/10.1051/mateconf/201713008005>
- Malay, O., Yilgor, I., & Menciloglu, Y. Z. (2013). Effects of solvent on TEOS

- hydrolysis kinetics and silica particle size under basic conditions. *Journal of Sol-Gel Science and Technology*, 67(2), 351–361. <https://doi.org/10.1007/s10971-013-3088-4>
- Marrion, A. (2004). *The chemistry and physics of coatings* (2nd ed.).
- Matsoukas, T., & Gulari, E. (1988). Dynamics of growth of silica particles from ammonia-catalyzed hydrolysis of tetra-ethyl-orthosilicate. *Journal of Colloid And Interface Science*, 124(1), 252–261. [https://doi.org/10.1016/0021-9797\(88\)90346-3](https://doi.org/10.1016/0021-9797(88)90346-3)
- Meier, M., Ungerer, J., Klinge, M., & Nirschl, H. (2018). Synthesis of nanometric silica particles via a modified Stöber synthesis route. *Colloids and Surfaces A: Physicochemical and Engineering Aspects*, 538(September 2017), 559–564. <https://doi.org/10.1016/j.colsurfa.2017.11.047>
- Mine, E., Nagao, D., Kobayashi, Y., & Konno, M. (2005). Solvent effects on particle formation in hydrolysis of tetraethyl orthosilicate. *Journal of Sol-Gel Science and Technology*, 35(3), 197–201. <https://doi.org/10.1007/s10971-005-2289-x>
- Momber, A. W., Irmer, M., & Marquardt, T. (2020). Effects of polymer hardness on the abrasive wear resistance of thick organic offshore coatings. *Progress in Organic Coatings*, 146(March), 105720. <https://doi.org/10.1016/j.porgcoat.2020.105720>
- Nguyen-Tri, P., Tran, H. N., Plamondon, C. O., Tuduri, L., Vo, D. V. N., Nanda, S., Mishra, A., Chao, H. P., & Bajpai, A. K. (2019). Recent progress in the preparation, properties and applications of superhydrophobic nano-based coatings and surfaces: A review. *Progress in Organic Coatings*, 132(April), 235–256. <https://doi.org/10.1016/j.porgcoat.2019.03.042>
- Rout. (2013). Sol-Gel Process for Anti-Corrosion Coatings. *Journal of Research Updates in Polymer Science*, January. <https://doi.org/10.6000/1929-5995.2013.02.04.4>
- Tunçgenç, M., (2004). *Boya Teknolojisine Giriş*
- Saarimaa, V., Markkula, A., Juhanaja, J., & Skrifvars, B. J. (2015). Improvement of barrier properties of Cr-free pretreatments for coil-coated products. *Journal of Coatings Technology and Research*, 12(4), 721–730. <https://doi.org/10.1007/s11998-015-9663-6>
- Sorce, F. S., Ngo, S., Lowe, C., & Taylor, A. C. (2019). The effect of HMMM crosslinker content on the thermal-mechanical properties of polyester coil coatings. *Progress in Organic Coatings*, 137(August), 105338. <https://doi.org/10.1016/j.porgcoat.2019.105338>

- Suh, K. Y., & Jon, S. (2005). Control over wettability of polyethylene glycol surfaces using capillary lithography. *Langmuir*, 21(15), 6836–6841.
<https://doi.org/10.1021/la050878+>
- Stöber, W., Fink, A., & Bohn, E. (1968). Controlled growth of monodisperse silica spheres in the micron size range. *Journal of Colloid and Interface Science*, 26(1), 62–69. [https://doi.org/10.1016/0021-9797\(68\)90272-5](https://doi.org/10.1016/0021-9797(68)90272-5)
- Völz, H. G. (2001). *Industrial color testing: Fundamentals and techniques*. Wiley-VCH Verlag GmbH.
- Wang, J., Wu, Y., Cao, Y., Li, G., & Liao, Y. (2020). Influence of surface roughness on contact angle hysteresis and spreading work. *Colloid and Polymer Science*, 298(8), 1107–1112. <https://doi.org/10.1007/s00396-020-04680-x>
- Wang, D., Zhao, A., Li, L., He, Q., Guo, H., Sun, H., & Gao, Q. (2015). Bioinspired ribbed hair arrays with robust superhydrophobicity fabricated by micro/nanosphere lithography and plasma etching. *RSC Advances*, 5(117), 96404–96411.
<https://doi.org/10.1039/c5ra18439h>
- Yang, Z., Xu, H., Shi, Y. L., Li, M. K., Huang, Y., & Li, H. L. (2005). The fabrication and corrosion behavior of electroless Ni-P-carbon nanotube composite coatings. *Materials Research Bulletin*, 40(6), 1001–1009.
<https://doi.org/10.1016/j.materresbull.2005.02.015>
- Yilgör, I., Lgor, S. Y., Lgor, E. Y., Yilgör, E., Soz, C. L., & Söz, Ç. K. (2016). Superhydrophobic polymer surfaces: Preparation, properties and applications.
- Zeno W. Wicks, J., Jones, F. N., Pappas, S. P., & Wicks, D. A. (2007). *Organic coatings: Science and technology*. John Wiley & Sons.
- Zhang, Y., Cao, M., Yao, Z., Wang, Z., Song, Z., Ullah, A., Hao, H., & Liu, H. (2015). Effects of silica coating on the microstructures and energy storage properties of BaTiO₃ ceramics. *Materials Research Bulletin*, 67, 70–76.
<https://doi.org/10.1016/j.materresbull.2015.01.056>